



Murdoch
UNIVERSITY

Unravelling the Lipidome of
Idiopathic Pulmonary Fibrosis and its
Spatial Distribution using High
Resolution Mass Spectrometry

by

Shabarinath Mathoosoothenen Nambiar

BSc. (Hons)

This thesis is presented for the degree of Doctor of Philosophy at
the School of Veterinary and Life Sciences, Murdoch University,
Perth, Western Australia

2018

A journey that took my breath away

Declaration

I declare that this thesis is my own account of my research and contains, as its main content, work that has not been previously submitted for a degree at any tertiary educational institution.

In addition, I claim the majority of authorship for each manuscript presented in this thesis. In doing so, I declare that the co-authors listed in the “Statement of Authorship” contributed by critically evaluating and commenting on the relevant manuscript.

Shabarinath Mathoosoothenen Nambiar

Statement of Authorship for Chapter 1

Title of Manuscript	Metabolomics in chronic lung diseases: <i>a practical review for clinicians</i>	
Manuscript Status	<input type="checkbox"/> Published <input type="checkbox"/> Accepted for publication	<input checked="" type="checkbox"/> Submitted for review <input type="checkbox"/> Ready for submission
Manuscript Details	The manuscript was submitted to Respirology (Impact factor: 4.407) and is included as Chapter 1 in this thesis.	


Principal Author

Name of Principal Author	Shabarinath Nambiar
Contribution to the Manuscript	Critically reviewed the literature, prepared the manuscript and acted as corresponding author.
Signature	
Date	29/11/2018

Co-Authors

By signing this Statement of Authorship, each co-author certifies that:

- the candidate's stated contribution to the manuscript is accurate (as detailed above);
- the co-author's stated contribution to the manuscript is accurate (as per below); and
- permission is granted for the candidate to include the manuscript in this thesis.

Name of Co-Author	Bong Sze How
Contribution to the Manuscript	Proposed the concept, critically reviewed and approved the final version of the manuscript.
Signature	
Date	29/11/2018

Name of Co-Author	Robert Trengove
Contribution to the Manuscript	Reviewed and evaluated the manuscript.
Signature	
Date	29/11/2018

Name of Co-Author	Joel Gummer
Contribution to the Manuscript	Reviewed and evaluated the manuscript.
Signature	
Date	23/11/2018

Name of Co-Author	Yuben Moodley
Contribution to the Manuscript	Proposed the review and evaluated the manuscript.
Signature	
Date	29/11/2018

Statement of Authorship for Chapter 2

Title of Manuscript	Untargeted metabolomics of human plasma reveals unique lipid markers in COPD and IPF patients	
Manuscript Status	<input type="checkbox"/> Published <input type="checkbox"/> Accepted for publication	<input type="checkbox"/> Submitted for review <input checked="" type="checkbox"/> Ready for submission
Manuscript Details	The manuscript will be submitted to Respirology (Impact factor: 4.407) and is included as Chapter 2 in this thesis.	

Principal Author

Name of Principal Author	Shabarinath Nambiar
Contribution to the Manuscript	Processed and interpreted the data. Prepared the manuscript.
Signature	
Date	29/11/2018

Co-Authors

By signing this Statement of Authorship, each co-author certifies that:

- d) the candidate's stated contribution to the manuscript is accurate (as detailed above);
- e) the co-author's stated contribution to the manuscript is accurate (as per below); and
- f) permission is granted for the candidate to include the manuscript in this thesis.

Name of Co-Author	Bong Sze How
Contribution to the Manuscript	Helped evaluate and critically reviewed the manuscript.
Signature	
Date	29/11/2018

Name of Co-Author	Catherine Rawlinson
Contribution to the Manuscript	Performed sample preparation and instrumental analysis on all samples.
Signature	
Date	26/11/2018

Name of Co-Author	Joel Gummer
Contribution to the Manuscript	Supervised the project and edited the manuscript.
Signature	
Date	23/11/2018

Name of Co-Author	Yuben Moodley
Contribution to the Manuscript	Provided the samples and supervised the development of work.
Signature	
Date	29/11/2018

Name of Co-Author	Robert Trengove
Contribution to the Manuscript	Supervised the project development, helped in data interpretation and manuscript evaluation.
Signature	
Date	29/11/2018

Statement of Authorship for Chapter 3

Title of Manuscript	SONAR enhances the specificity of unbiased lipid plasma profiling of idiopathic pulmonary fibrosis	
Manuscript Status	<input type="checkbox"/> Published <input type="checkbox"/> Accepted for publication	<input type="checkbox"/> Submitted for review <input checked="" type="checkbox"/> Ready for submission
Manuscript Details	The manuscript will be submitted to Journal of Lipid Research (Impact factor: 5.559) and is included as Chapter 3 in this thesis.	

Principal Author

Name of Principal Author	Shabarinath Nambiar
Contribution to the Manuscript	Performed sample preparation and analyses, processed and interpreted the data. Prepared the manuscript.
Signature	
Date	29/11/2018

Co-Authors

By signing this Statement of Authorship, each co-author certifies that:

- g) the candidate's stated contribution to the manuscript is accurate (as detailed above);
- h) the co-author's stated contribution to the manuscript is accurate (as per below); and
- i) permission is granted for the candidate to include the manuscript in this thesis.

Name of Co-Author	Robert Trengove
Contribution to the Manuscript	Evaluated and commented on the manuscript.
Signature	
Date	29/11/2018

Name of Co-Author	Adam King
Contribution to the Manuscript	Helped with the analytical and data processing workflows.
Signature	
Date	28/11/2018

Name of Co-Author	Yuben Moodley
Contribution to the Manuscript	Provided the samples and supervised the project.
Signature	
Date	29/11/2018

Name of Co-Author	Bong Sze How
Contribution to the Manuscript	Supervised the analytical workflow, critically reviewed the manuscript.
Signature	
Date	29/11/2018

Statement of Authorship for Chapter 4

Title of Manuscript	MALDI-mass spectrometry imaging by freeze-spot deposition of the matrix	
Manuscript Status	<input type="checkbox"/> Published <input type="checkbox"/> Accepted for publication	<input type="checkbox"/> Submitted for review <input checked="" type="checkbox"/> Ready for submission
Manuscript Details	The manuscript will be submitted to Analytical Chemistry (Impact factor: 6.042) and is included as Chapter 4 in this thesis.	

Principal Author

Name of Principal Author	Shabarinath Nambiar
Contribution to the Manuscript	Performed sample preparation and analyses, processed and interpreted the data. Prepared the manuscript.
Signature	
Date	29/11/2018

Co-Authors

By signing this Statement of Authorship, each co-author certifies that:

- j) the candidate's stated contribution to the manuscript is accurate (as detailed above);
- k) the co-author's stated contribution to the manuscript is accurate (as per below); and
- l) permission is granted for the candidate to include the manuscript in this thesis.

Name of Co-Author	Robert Trengove
Contribution to the Manuscript	Supervised project development and helped evaluate the manuscript.
Signature	
Date	29/11/2018

Name of Co-Author	Joel Gummer
Contribution to the Manuscript	Supervised the project concept and design. Critically reviewed the manuscript.
Signature	
Date	23/11/2018

Statement of Authorship for Chapter 5

Title of Manuscript	Optimisation of MALDI-MSI matrix improves spatial resolution of lipid species in fibrotic lung tissue	
Manuscript Status	<input type="checkbox"/> Published <input type="checkbox"/> Accepted for publication	<input type="checkbox"/> Submitted for review <input checked="" type="checkbox"/> Ready for submission
Manuscript Details	The manuscript will be submitted to Progress in Lipid Research (Impact factor: 8.435) and is included as Chapter 5 in this thesis.	

Principal Author

Name of Principal Author	Shabarinath Nambiar
Contribution to the Manuscript	Developed project concept and design, performed sample preparation and analyses, processed and interpreted the data. Prepared the manuscript.
Signature	
Date	29/11/2018

Co-Authors

By signing this Statement of Authorship, each co-author certifies that:

- m) the candidate's stated contribution to the manuscript is accurate (as detailed above);
- n) the co-author's stated contribution to the manuscript is accurate (as per below); and
- o) permission is granted for the candidate to include the manuscript in this thesis.

Name of Co-Author	Robert Trengove
Contribution to the Manuscript	Reviewed and evaluated the manuscript.
Signature	
Date	29/11/2018

Name of Co-Author	Joel Gummer
Contribution to the Manuscript	Reviewed and evaluated the manuscript.
Signature	
Date	23/11/2018

Name of Co-Author	Yuben Moodley
Contribution to the Manuscript	Provided the samples and supervised the development of the work
Signature	
Date	29/11/2018

Name of Co-Author	Bong Sze How
Contribution to the Manuscript	Critically reviewed and evaluated the manuscript.
Signature	
Date	29/11/2018

Abstract

Chronic lung diseases are complex, progressive disorders with increasing incidence and mortality. Chronic obstructive pulmonary disease (COPD), asthma and pulmonary fibrosis are examples of chronic lung conditions that can significantly impact the quality of life. Minimally-invasive diagnostic methods that eliminate bronchoscopic and surgical biopsy from patients are ideal; metabolomics therefore holds considerable promise for the discovery of biomarkers that can aid diagnosis and treatment with greater sensitivity, specificity and precision.

The main aim of this project was to employ ultra-performance liquid chromatography-quadrupole time-of-flight (UPLC-QTOF) high resolution mass spectrometry (HRMS) and matrix-assisted laser desorption ionisation (MALDI) mass spectral imaging (MSI) together with multivariate statistics-based metabolomics to identify and characterize potential lipid biomarkers of idiopathic pulmonary fibrosis (IPF). This dissertation consists of the following studies: (1) literature review of metabolomics in chronic lung diseases; (2) application of HRMS for untargeted metabolic profiling of chronic lung disease including COPD and IPF; (3) investigation of a novel data-independent acquisition (DIA) approach to augment untargeted approaches for lipid biomarker identification; (4) development of a novel matrix application technique to improve MALDI-MSI acquisitions of tissue sections whilst maintaining spatial localisation of endogenous metabolites; and (5) exploiting potassium adduct formation to resolve the spatial distribution of lipids in fibrotic tissues.

A total of 65 clinical plasma samples (from 20 healthy control subjects, 21 COPD and 24 IPF patients) were profiled using UHPLC-QTOF-MS. A fundamental challenge in using HRMS for untargeted profiling of complex, chronic lung diseases is the heterogeneity of the human samples. Various contaminations present in fibrotic tissues or adjacent non-

fibrotic constituents can confound characterization and encumber the discovery of reliable biomarkers. The results of this study revealed significant correlation between COPD and IPF clinical phenotypes and plasma metabolite profiles. The unbiased metabolomics workflow and deconvolution pipeline provided end-to-end analysis from peak picking and annotation through to metabolite identification.

Subsequently, the ability of the UPLC-QTOF-MS method to discriminate between lipid species was enhanced by the application of a DIA method to distinguish between “stable *versus* progressor” IPF patients. This DIA method is known as SONAR and uses a wide, continuously sliding precursor window for fragmentation, thereby allowing correlation of precursor and fragment ions. SONAR lipid data were processed using Progenesis QI and searched against LIPID MAPS for structural elucidation and metabolite confirmation. The lipids identified were found to be intermediates of key metabolic pathways such as the glycolytic/TCA cycle, mitochondrial-beta oxidation and lipid metabolism and hold considerable promise as biomarkers of disease.

The matrix deposition step in MALDI-MSI is crucial for simultaneous extraction of metabolites from tissue sections as well as maintaining the spatial dimensionality of the endogenous metabolites. A novel, efficient and cost-effective preparative method referred to as the “freeze-spot” method was developed using wheat seed sections to demonstrate extraction efficiency and reliability, whilst maintaining the spatial resolution of the acquired MALDI-MSI images. The technique was also found to be simple and robust, forming fine matrix crystals that enabled efficient ionisation of surface metabolites, further eliminating the need for sophisticated matrix application approaches.

In the final study, 10 healthy and 10 fibrotic tissues were compared using MALDI-MSI. The MSI technique developed uses potassium adduct formation to improve spatial resolution and dimensionality of lipid species such as triglycerides (TG), ceramides,

sphingolipids and glycerophospholipids. The results of this study showed changes in lipid composition of IPF tissues compared to healthy controls. This study identified lysophosphatidylcholine (LysoPC), phosphatidylcholine (PC) and phosphatidylethanolamine (PE) as potential lipid biomarkers of the disease and requires further study as targets of intervention and treatment. Both SONAR and MSI successfully identified similar classes of lipids (TG, PE, LysoPC and PC) which may play a role in the pathophysiology of the IPF lipidome.

This project highlighted the complementarity of HRMS and MSI based metabolomics for the characterization of unique lipid features in fibrotic tissue and plasma samples. The study also demonstrated the discriminative power of the unbiased DIA approach for the identification of lipids via fragment ion patterns that were indicative of specific lipid classes. In addition, the application of chemometric principal component analysis (PCA) and orthogonal partial least-squares to latent structures-direct analysis (OPLS-DA) proved useful for the identification of statistically significant lipids. This statistical approach allowed for the assessment of covariance and correlation between lipids and the modelled lung diseases, and further illustrated lipid compositional changes in chronic lung diseases.

Taken together, the experimental work presented in this thesis show the large potential for mass spectrometry-based metabolomics as a tool for discovery. The specificity of the novel methods outlined will be highly beneficial for compound identification and further confirmation of disease biomarkers.

Table of Contents

Declaration	iii
Statements of authorship	iv
Abstract	x
Table of Contents	xiii
List of Figures	xv
List of Tables	xviii
List of Units	xix
List of Abbreviations	xx
Milestones and Achievements	xxiii
Acknowledgements	xxvi
Chapter 1 Metabolomics in chronic lung diseases: a practical review for clinicians	
1.1 Abstract	1
1.2 Introduction	2
1.3 Metabolic pathways implicated in chronic lung diseases	3
1.3.1 Cellular energetics	3
1.3.1.1 Glycolysis and TCA cycle	4
1.3.1.2 Mitochondrial beta oxidation and fatty acid metabolism	7
1.3.1.3 Lipid metabolism	7
1.4 Metabolomics-an emerging ‘omic modality for clinical application	8
1.5 Analytical techniques in metabolomics	10
1.5.1 NMR spectroscopy	10
1.5.2 Mass spectrometry	11
1.6 Metabolomics-driven discovery of biomarkers	13
1.6.1 Metabolomics studies of COPD	19
1.6.2 Metabolomics studies of asthma	20
1.6.3 Metabolomics studies of IPF	21
1.7 Frontiers in metabolomic analysis of chronic lung diseases	23
1.8 Conclusion	25
1.9 References	27
Chapter 2 Untargeted metabolomics of human plasma reveals unique lipid markers in COPD and IPF patients	
2.1 Abstract	39
2.2 Introduction	40
2.3 Materials and Methods	42
2.3.1 Chemicals and reagents	42
2.3.2 Biological samples	42
2.3.3 Sample preparation	42
2.3.4 Mass spectrometry acquisition	43
2.3.5 Data processing and statistical analysis	44
2.4 Results and Discussion	45
2.5 Conclusion	59
2.6 References	60
Chapter 3 SONAR enhances the specificity of unbiased lipid plasma profiling of idiopathic pulmonary fibrosis	
3.1 Abstract	78

3.2	Introduction	79
3.3	Materials and Methods	81
3.3.1	Chemical and reagents	81
3.3.2	Biological samples	81
3.3.3	Sample preparation	81
3.3.4	UPLC configuration	82
3.3.5	Mass spectrometry acquisition	82
3.3.6	Data processing	83
3.3.7	Statistical analysis	84
3.4	Results and Discussion	85
3.4.1	Lipid markers correlated to IPF	99
3.5	Conclusion	103
3.6	References	104
Chapter 4	MALDI-mass spectrometry imaging by freeze-spot deposition of the matrix	
4.1	Abstract	120
4.2	Introduction	121
4.3	Experimental section	125
4.3.1	Chemicals	125
4.3.2	Sample preparation	125
4.3.3	Matrix application	126
4.3.4	Microscopy	127
4.3.5	MALDI-MSI acquisition	127
4.4	Results and Discussion	128
4.5	Conclusion	137
4.6	References	138
Chapter 5	Optimisation of MALDI-MSI matrix improves spatial resolution of lipid species in fibrotic lung tissue	
5.1	Abstract	143
5.2	Introduction	144
5.3	Materials and Method	147
5.3.1	Chemicals	147
5.3.2	Biological samples	147
5.3.3	Sample preparation	148
5.3.4	Freeze-spot matrix application	148
5.3.5	MALDI-MSI acquisition	149
5.4	Results and Discussion	150
5.4.1	Potassium adducts enhanced MALDI-MSI intensities of lipids	150
5.4.2	MALDI images of biopsied lung sections	157
5.5	Conclusion	163
5.6	References	164
Chapter 6	General discussion and Conclusion	
6.1	General Discussion	175
6.2	Current challenges	178
6.3	Future work	179
6.4	Conclusion	180
6.5	References	181

List of Figures

- Figure 1.1 An illustration of the metabolic pathways involved in cellular energetics: yellow, blue and red zones correspond to pathways affected in COPD, asthma and IPF, respectively. Sections in green (COPD and IPF) and purple (asthma and IPF) illustrates overlapping pathways in the aforementioned diseases. 6
- Figure 2.1 Principal component analysis scores plots using the first two principal components showing all samples analysed. (A) PCA plot was generated before background correction and (B) was generated after the corrections were applied. Black, blue, green and red squares represent pooled QC samples, IPF samples, healthy controls and COPD samples, respectively. 46
- Figure 2.2 Orthogonal Projection to Latent Structure-Discriminant Analysis (OPLS-DA) models between HC and COPD samples (A), and HC and IPF samples (B). The S-plots generated from the respective OPLS-DA scores plots were presented directly below. Blue, green and red squares represent the IPF samples, healthy controls and COPD samples, respectively. 49
- Figure 2.3 Orthogonal Projection to Latent Structure-Discriminant Analysis (OPLS-DA) models between COPD and IPF samples. The two observed outliers (COPD sample 6 and IPF sample 2) were removed and the OPLS-DA scores plot was fitted resulting in the model on the right. The S-plot generated from newly fitted OPLS-DA model was presented directly below. Red and blue squares represent the COPD and IPF samples, respectively. 50
- Figure 3.1 Overlaid total ion chromatograms of both TOF-MS (red) and SONAR (green) acquisitions in positive mode. The highlighted regions of the chromatogram illustrate the elution of lysophosphatidylethanolamine (LysoPE), phosphatidylcholine (PC), phosphatidylethanolamine (PE), phosphatidylserine (PS), phosphatidylinositol (PI), lysophosphatidylcholine (LysoPC), phosphatidic acid (PA), phosphatidylglycerol (PG), sphingomyelin (SM), diacylglycerol (DG), triglyceride (TG) and ceramide (Cer). 85
- Figure 3.2 Overlaid total ion chromatograms of both TOF-MS (red) and SONAR (green) acquisitions in negative mode. 86
- Figure 3.3 The extracted ion chromatograms of spiked deuterium-labelled SPLASH LipidoMix standards in positive mode showing peaks corresponding to 15:0-18:1(d7) PC, 15:0-18:1(d7) PE, 15:0-18:1(d7) PS, 15:0-18:1(d7) PG, 15:0-

	18:1(d7) PI, 15:0-18:1(d7) PA, 18:1(d7) LysoPC, 18:1(d7) LysoPE, 18:1(d7) Chol Ester, 18:1(d7) MG, 15:0-18:1(d7) DG, 15:0-18:1(d7)-15:0 TG, 18:1(d9) SM and cholesterol (d7).	87
Figure 3.4	The extracted ion chromatograms of spiked deuterium-labelled SPLASH LipidoMix standards in negative mode showing peaks corresponding to 15:0-18:1(d7) PC, 15:0-18:1(d7) PE, 15:0-18:1(d7) PS, 15:0-18:1(d7) PG, 15:0-18:1(d7) PI, 15:0-18:1(d7) PA, 18:1(d7) LysoPE, 18:1(d7) Chol Ester and 18:1(d9) SM.	88
Figure 3.5	PCA score plots generated from all stable (ST, black), progressor (PR, red) and QC (QC, green) samples in all four modes of acquisition. The clustering of the pooled QC samples in each acquisition modes were shown encircled in green.	90
Figure 3.6	Global sample projection of positive SONAR showing an overall intensity of uncorrected data for QCs 5 and 6, and normalised intensity post-correction using the MatrixAnalyzer tool. Correction lines (dotted blue) were fitted through the QCs and the samples and QCs were represented by the red and blue dots.	92
Figure 3.7	OPLS-DA and S-plots comparing stable versus progressors plasma samples in positive mode TOF-MS (A), negative mode TOF-MS (B), positive mode SONAR (C) and negative mode SONAR (D).	94
Figure 4.1	The different matrix application approaches using DHB prepared at 20 mg/mL. (A) Automatic sprayer; (B) manual spotting with an ambient dry-out step; (C) manual spotting on dry ice followed by a dry-out step; and (D) freeze-spotting technique.	129
Figure 4.2	Light microscopic images of the matrix crystals obtained by the different application approaches using DHB prepared at 20 mg/mL. (A) Automatic sprayer; (B) manual spotting with an ambient dry-out step; (C) manual spotting on dry ice followed by a dry-out step; and (D) freeze-spotting technique.	131
Figure 4.3	MALDI-MSI images comparing the signal intensity of m/z 585 ions found on seed sections when extracted using 3 μ L (left) and 5 μ L (right) of DHB solution at 20 mg/mL.	133
Figure 4.4	MALDI-MSI images comparing the signal intensities of sucrose (m/z 343, m/z 365 and m/z 381) when extracted with the different variations of matrix: DHB only (A), DHB+NaOAc (B), and DHB+KOAc (C). The ion maps illustrated in the top row are from controls whilst images	

	in the second row show a comparison with sections spotted with sucrose standard (1 mg/mL).	135
Figure 4.5	Wheat saccharide distribution across the surface of the cryo-sections using the developed MALDI-MSI method. The figure outlines the various sugars present with their associated adduct formation.	136
Figure 5.1	The total ion chromatograms (TIC) of the lipid standards mixture spotted on a glass slide at 1 $\mu\text{g/mL}$ and extracted with (A) DHB with NH_4OAc , (B) DHB with KOAc , (C) DHB with NaOAc and (D) DHB only.	151
Figure 5.2	Extracted ion chromatograms of the lipid adducts $[\text{M}+\text{NH}_4]^+$, $[\text{M}+\text{K}]^+$, $[\text{M}+\text{Na}]^+$ and $[\text{M}+\text{H}]^+$ denoted by A, B, C and D, respectively. All six lipid standards were extracted with DHB containing NaOAc .	155
Figure 5.3	Extracted ion chromatograms and ion intensity maps of the lipid adducts generated by Mass Lynx and HD Imaging software, respectively. All six lipid standards were extracted with DHB containing KOAc and their associated adducts $[\text{M}+\text{NH}_4]^+$, $[\text{M}+\text{K}]^+$, $[\text{M}+\text{Na}]^+$ and $[\text{M}+\text{H}]^+$ are denoted by A, B, C and D, respectively.	156
Figure 5.4	The optical images (A and C) of sectioned lung tissue obtained by light microscopy at 40x magnification with an auto exposure mode and the corresponding MALDI-MSI images generated at 20 μm resolution.	158
Figure 5.5	MALDI-MSI images showing decreased signal intensities of LysoPC, PC and PE ions in IPF tissues compared to healthy control samples.	159

List of Tables

Table 1.1	Summary of recent metabolomics studies reporting the metabolic pathways associated with COPD, asthma and IPF, samples assessed, and analytical techniques used. Ionisation modes are described as positive (+) and/or negative (-) electrospray (ESI) or electron impact (EI) while MS/MS and 1D-1H and stands for tandem MS technique and one-dimensional proton NMR experiment, respectively.	15
Table 1.2	Putative and candidate biomarkers of chronic lung diseases correlating to the glycolytic and TCA-cycle, mitochondrial beta-oxidation, fatty acid as well as lipid metabolism pathways.	18
Table 2.1	The m/z values, putative identification and fold changes of features of interest identified by multivariate statistics through database matching.	51
Supplementary Table 2.1	Patient demographics and clinical characteristics including sex, age, history of smoking as well as c-reactive protein (CRP), soluble tumour necrosis factor receptor-1 (sTNFR1), forced expiratory volume in 1 sec (FEV1) and forced vital capacity (FVC) levels.	71
Supplementary Table 2.2	The m/z values, chemical formulas, mass error, percentage isotopic similarities, ANOVA p-values as well as the mean abundances, relative standard deviations and fold changes of metabolite features annotated using LIPID MAPS, Biomolecules, ChEBI, HMDB and Drug Bank databases.	74
Table 3.1	Table showing the plasma lipids that were identified for stable and progressors of IPF through different acquisition modes and their associated fold changes.	97
Supplementary Table 3.1	Progenesis output of the features detected including m/z , chemical formula, mass error, putative identification (ID) as well as the calculated mean abundance, percentage relative standard deviation (%RSD), fold-changes and the relative concentrations based on the SPLASH LipidoMix standards.	114

List of Units

%	percentage
°C	degree Celsius
μL	microlitre
μm	micrometre
Da	dalton
g	centrifugal force
hrs	hours
Hz	hertz
J	joules
kV	kilovolt
mg/mL	milligram per millilitre
mins	minutes
mL	millilitre
mM	micromolar
mm	millimetre
mm/min	millimetre per minute
pg/μL	picogram per microlitre
ppm	parts per million
psi	pounds per square inch
rpm	revolutions per minute
s	second
V	volt
v/v	volume/volume concentration

List of Abbreviations

ACN	acetonitrile
ANOVA	analysis of variance
ARDS	acute respiratory distress syndrome
BALF	bronchoalveolar lavage fluid
Cer	ceramide
ChEBI	chemical entities of biological interest
COPD	chronic obstructive pulmonary disorder
CV	coefficient of variation
DESI	desorption electrospray ionisation
DG	diacylglycerol
DHB	2,5-dihydroxybenzoic acid
DIA	data independent acquisition
EBC	exhaled breath condensate
ESI	electrospray ionisation
FA	fatty acid
GC-MS	gas chromatography-mass spectrometry
H ₂ O	water
HC	healthy controls
HILIC	hydrophilic interaction liquid chromatography
HMDB	human metabolome database
IPA	isopropanol
IPF	idiopathic pulmonary fibrosis
KOAc	potassium acetate
LC-MS	liquid chromatography-mass spectrometry
LysoPA	lysophosphatidic acid
LysoPC	lysophosphatidylcholine
LysoPE	lysophosphatidylethanolamine
MALDI	matrix-assisted laser desorption ionisation
MeOH	methanol

MG	monoacylglycerol
MS	mass spectrometry
MS/MS	tandem mass spectrometry
MSI	mass spectrometry imaging
NaOAc	sodium acetate
NH ₄ OAc	ammonium acetate
NMR	nuclear magnetic resonance
OCT	optimal cutting temperature
OPLS-DA	orthogonal projections to latent structures-discriminant analysis
PA	phosphatidic acid
PC	phosphatidylcholine
PCA	principal component analysis
PE	phosphatidylethanolamine
PG	phosphatidylglycerol
PI	phosphatidylinositol
PPAR α	peroxisome proliferator-activated receptor alpha
PR	progressor
PS	phosphatidylserine
PUFA	polyunsaturated fatty acid
QC	quality control
Q-TOF	quadrupole time-of-flight
ROS	reactive oxygen species
RP	reversed-phase
SM	sphingomyelin
ST	stable
TCA	tricarboxylic acid
TFA	trifluoroacetic acid
TG	triglyceride
TGF- β	transforming growth factor-beta
TIC	total ion chromatogram

TOF	time-of-flight
UPLC	ultra-performance liquid chromatography
VIP	variable importance in projection
XIC	extracted ion chromatogram

Milestones and Achievements

Awards

North American Chemical Residue Workshop, Student Scholarship Winner (2018)

Mass Spectrometry: Applications to the Clinical Lab European Congress, Young Investigator Travel Grant (2017)

Telethon Kids Institute Rottneest Retreat, New Investigator Award (2016)

Murdoch International Post-graduate PhD Scholarship (2015)

Oral

Nambiar, S.; Trengove, R. D. and Bong, S. H. (2018). “Simultaneous extraction and clean-up using solubilized extractants—a miniaturized approach.” North American Chemical Residue Workshop in Naples, Florida

Nambiar, S.; Trengove, R. D.; Bong, S. H. and Gummer, J. (2017). “Spatial metabolic profiling of idiopathic pulmonary fibrosis by mass spectral imaging.” Mass Spectrometry: Applications to the Clinical Lab European Congress (Lightning Talk) in Salzburg, Austria

Nambiar, S.; Trengove, R. D.; Bong, S. H. and Gummer, J. (2017). “Matrix-assisted laser desorption/ionization-mass spectrometry imaging (MALDI-MSI) for direct visualization of wheat grain metabolites.” First Australia-China Conference on Science, Technology and Innovation in Western, Australia

Nambiar, S.; Gummer, J.; Bong, S. H.; Moodley, Y. and Trengove, R. D. (2016). “Spatial metabolic profiling of idiopathic pulmonary fibrosis by DESI- and MALDI-mass spectral imaging.” Rottneest New Investigator Session in Rottneest Island, Western Australia

Posters

Nambiar, S.; Bong, S. H. and Trengove, R. D. (2018) "A rapid single tube extraction and clean-up for the detection of organochlorine pesticides in human milk." North American Chemical Residue Workshop in Naples, Florida

Nambiar, S.; Trengove, R. D.; Bong, S. H. and Gummer, J. (2017). "Spatial metabolic profiling of idiopathic pulmonary fibrosis by mass spectral imaging." Mass Spectrometry: Applications to the Clinical Lab European Congress in Salzburg, Austria

Nambiar, S.; Trengove, R. D.; Bong, S. H. and Gummer, J. (2017). "Matrix-assisted laser desorption/ionization-mass spectrometry imaging (MALDI-MSI) for direct visualization of wheat grain metabolites." American Society for Mass Spectrometry 65th Conference in Indianapolis, Indiana

Other Publications

Khalil, Y.; Siddique, K. H. M.; Ward, P.; Piggin, C.; Bong, S. H.; Nambiar, S.; Trengove, R. D. and Flower, K. (2018). "A bioassay for prosulfocarb, pyroxasulfone and trifluralin detection and quantification in soil and crop residues." Crop and Pasture Science 69(6): 606-616.

Nambiar, S.; Trengove, R. D. and Bong, S. H. "Exploiting the aqueous solubility of QuEChERS and dSPE reagents for simultaneous extraction and cleanup of fungicides in a single tube-a miniaturized approach." *Prepared for submission to Journal of Agriculture and Food Chemistry*

Du, J.; Gey, M.; Nambiar, S.; Hartmann, P. E.; Geddes, D. T. and Trengove, R. D. "An evaluation of matrix-induced chromatographic enhancement effect of 88 pesticides in human milk using gas chromatography tandem mass spectrometry" *Prepared for submission to Journal of Chromatography A*

Nambiar, S.*; Germanov, E.*; Rohner, C.; Bong, S. H.; Trengove, R. D. and Loneragan, N. “Persistent organic pollutants in PHP mobulids.” *Prepared for Frontiers in Marine Science: Marine Pollution*

Other presentations

Nambiar, S. and Smith, C. (2018). “Metabolomics in lung diseases.” *Prepared and recorded for The Naked Scientists Podcasts*

Nambiar, S. (2017). “Spatial metabolic profiling of idiopathic pulmonary fibrosis by mass spectral imaging.” YouTube: <https://www.youtube.com/watch?v=6vxqWKiRsUs>

Acknowledgements

Foremost, my deepest appreciation to a very special person. Thank you for taking a chance on me six years ago. Dr Bong Sze How, you are a great supervisor, an incredible mentor and above all, a top bloke! Thanks, macha!

My sincere gratitude goes to my principal supervisor, Associate Professor Robert Trengove for his tremendous help and support throughout my PhD, not to mention his advice and unsurpassed knowledge of mass spectrometry. To my clinical supervisor, Dr Yuben Moodley, where do I even begin? His unwavering passion for this topic kept me constantly engaged with my research and I would like to present this thesis as an early Diwali gift to you. To my co-supervisor, Dr Joel Gummer, thank you for your enthusiasm and for showing me how to “freeze” during my PhD.

This project would not have been accomplished without some of these amazing people. To Adam King and Lisa Reid from Waters, thank you for answering my endless questions and guiding me through all things TOF. To Gerard Spoelstra from Murdoch Histology, thank you for your knowledge of cyro-sectioning and tissue-staining. To Drs Dino Tan, Jade Jaffar and Sacha Macansh, thanks for organising the samples and helping with the associated paperwork (which can be very excruciating). To Dr Hayley Abbiss and Spectral Works, thank you for introducing and allowing me to use the MatrixAnalyzer plug-in that allowed me to carry out some of the QC corrections.

Thank you, Murdoch University and Separation Science and Metabolomics Laboratory (SSML), for the very generous scholarships and stipends received during my PhD. My colleagues and friends from SSML, VLS and all the cafes around uni, thank you for your endless support through countless coffees. You know who you are!

Most importantly, to my family, Acha, Amma, Vimal, Sindoorra and Daisy for their unconditional, infinite love and for never giving up on me. Thank you for being there for me at all times (more than a son or a brother could ask for) and I dedicate this thesis to you. Love you guys!

Above all, I am indebted to my lovely wife, Shreya, whose value to me only grows with age and time. Thank you for coming into my life and teaching me how to love: the true essence of a beautiful soul. You have only known me as a PhD student, so get ready to experience the real me-that's right, you're in for a treat! From babe to schatzi and everything in the middle, this thesis is something for you to cuddle!

Twam dñyāna–mayo vidñyāna–may'osi

A Long, Lung Time Ago...

Metabolomics in chronic lung diseases: a practical review for clinicians

Adapted from **Nambiar, S.**; Bong, S. H.; Gummer, J. P. A.; Trengove, R. D. and Moodley, Y. (2018) “Metabolomics in chronic lung diseases” *Accepted in Respirology*

1.1 Abstract

Chronic lung diseases represent a significant global burden. Their increasing incidence and complexity render a comprehensive, multidisciplinary, and personalized approach to each patient, critically important. Most recently, unique biochemical pathways and disease markers have been identified through large-scale metabolomics studies. Metabolomics is the study of metabolic pathways and the measurement of unique biomolecules in a living system. Analysing samples from different compartments such as broncho-alveolar lavage fluid (BALF) and plasma has proven useful for the characterization of a number of pathological conditions and offers promise as a clinical tool. For example, several studies using mass spectrometry (MS) have shown alterations in the sphingolipid metabolism of chronic obstructive pulmonary disorder (COPD)-sufferers. In this article, we present a practical review of the application of metabolomics to the study of chronic lung diseases; COPD, idiopathic pulmonary fibrosis (IPF) and asthma. The insights, which the analytical strategies employed in metabolomics, have provided to the dissection of the biochemistry of chronic lung diseases and future clinical biomarkers are explored.

Keywords: metabolomics, lung, COPD, asthma, IPF

1.2 Introduction

Chronic lung diseases are complex, progressive disorders with increasing incidence and mortality (Papaioannou *et al.*, 2017). Chronic obstructive pulmonary disease (COPD), asthma and pulmonary fibrosis are examples of chronic lung conditions that can significantly impact the quality of life (Papaioannou *et al.*, 2017; Zhao *et al.*, 2018). The management of such conditions can be greatly enhanced using personalized approaches to direct treatment. There is growing evidence to support the role of metabolic dysfunction in the pathogenesis of chronic lung diseases (Kao *et al.*, 2012; Karampitsakos and Gourgoulisanis, 2016; Kang *et al.*, 2016) and clinicians are now incorporating metabolomics as part of a holistic approach in disease diagnosis and prognosis.

The earliest diagnoses of these diseases is achieved by integrating information derived from multiple sources including clinical assessment, radiology and pulmonary function tests (Flaherty *et al.*, 2007; Jo *et al.*, 2016). Histological assessment generally requires surgical biopsy, but this is impractical for all patients (Semendyayeva *et al.*, 2017). Minimally-invasive diagnostic methods that eliminate bronchoscopic and surgical biopsy in patients are ideal; metabolomics therefore holds considerable promise for the discovery of biomarkers that can aid diagnosis and treatment with greater sensitivity, specificity and precision.

In this review, we provide an overview of how metabolomics has been used to further the understanding of chronic lung diseases, as well as present some of the metabolic pathways that have been investigated in COPD, asthma and idiopathic pulmonary fibrosis (IPF). This manuscript builds on the existing work of Papaioannou *et al.* (2017)

and Zhao *et al.* (2018) who reviewed global metabolic changes in patients with chronic lung disease. In addition to a critical assessment of published outcomes, our review seeks to examine the experimental approaches and instrumental parameters used in these studies, as well as provide some insight into the emerging trends of metabolomics-driven biomarker discovery. We anticipate that readers gain a practical understanding of current and emerging metabolomics approaches applicable to lung disease metabolomics and use the information presented to deliver robust metabolomics experimental designs that result in new insight and ultimately enhanced clinical decision-making.

1.3 Metabolic pathways implicated in chronic lung diseases

1.3.1 Cellular energetics

Cellular energetics are important for the maintenance of lung cell function under various patho-physiological conditions. Metabolic homeostasis is vital in regulating cell proliferation and differentiation, and studies have shown that metabolic dysregulation contributes to various inflammatory responses and apoptosis (King, 2015; Kumar *et al.*, 2017). The catabolism of major nutrient substrates such as sugars, amino acids and fatty acids (FAs) introduces acetyl-CoA into the tricarboxylic acid (TCA) cycle to produce metabolites for the synthesis of nucleotides, proteins and lipids, and most importantly to generate energy. These cellular processes have been implicated in disease pathogenesis; however, the roles of these metabolic dysregulations and the underlying disease mechanisms are not fully understood (Zhao *et al.*, 2018). Figure 1 illustrates the metabolic intermediates involved in cellular energetics and the pathways involved in chronic lung diseases.

1.3.1.1 Glycolysis and TCA cycle

Glycolytic dysregulation is well-defined in lung diseases such as lung cancer (Maher, 2015). Glycolysis is an oxygen-independent metabolic pathway that converts glucose into pyruvate through a 10-step biochemical reaction to produce adenosine triphosphate (ATP). The three main enzymatic reactions responsible for the control of glycolytic flux are catalysed by hexokinase, phosphofructokinase and pyruvate kinase (Hasawi *et al.*, 2014; Sreedhar and Zhao, 2018). Under aerobic conditions, pyruvate is commonly transported into mitochondria and converted to acetyl-CoA. Acetyl-CoA, which is derived via beta-oxidation, enters the TCA cycle to produce nicotinamide adenine dinucleotide (NADH) and flavin adenine dinucleotide (FADH₂), the electron carriers that donate electrons to the electron transport chain. This subsequently leads to ATP generation (Koppenol *et al.*, 2011; Sreedhar and Zhao, 2018). Regulation of the TCA cycle is heavily dependent on the availability of enzyme-substrates. Malate is one of the TCA cycle intermediates exported from the mitochondria to the cytosol, where malic enzyme can then regenerate NADH and pyruvate from malate for cycling back into the mitochondria (Hanse *et al.*, 2017). Like malate, citrate can also cross from the mitochondrial membrane to the cytosol, where it is cleaved by ATP citrate lyase to produce cytosolic acetyl-CoA (Ren *et al.*, 2017) for FA synthesis. Glycolytic energy dysregulation in lung cancer cells has been reported to cause uncontrolled proliferation as cells strive to meet demand for non-essential amino acids and FAs. Glutamine consumption, in addition to glucose, is significantly increased in diseased cells, resulting in its metabolism to alanine, lactate, with an increased production of ammonium ion by-products (Li *et al.*, 2015). Glycolytic hyperactivity followed by lactic acid fermentation, as opposed to steady-state glycolysis followed by pyruvate oxidation, is a hallmark of lung cancer metabolism and is known as the Warburg effect (Warburg

et al., 1927; Gatenby and Gillies, 2004). The exact mechanism of this “aerobic glycolysis” remains unclear; it has been suggested that cellular proliferation and extracellular matrix production are the results of this glycolytic change (Maher, 2015).

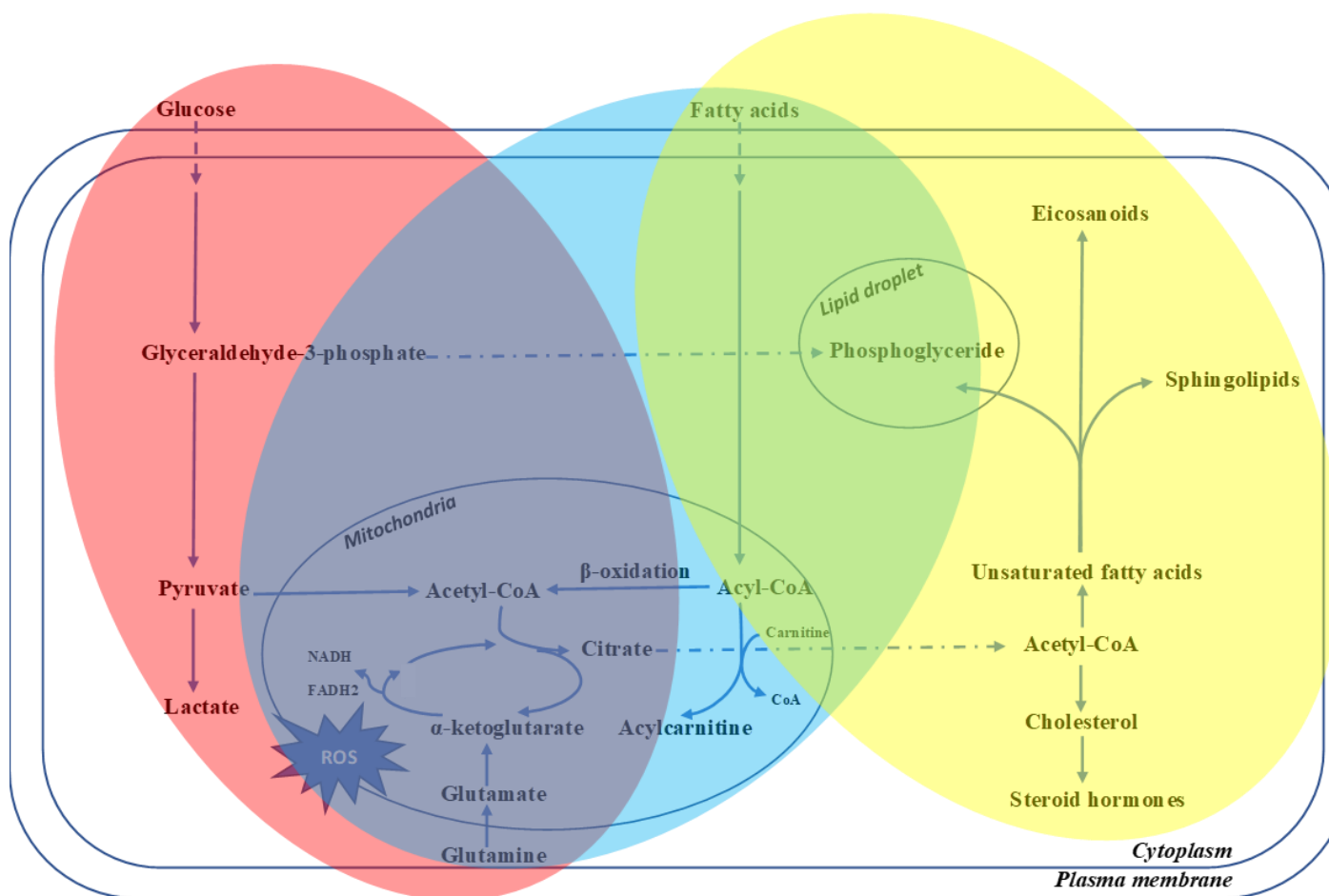


Figure 1.1 An illustration of the metabolic pathways involved in cellular energetics: yellow, blue and red zones correspond to pathways affected in COPD, asthma and IPF, respectively. Sections in green (COPD and IPF) and purple (asthma and IPF) illustrates overlapping pathways in the aforementioned diseases.

1.3.1.2 Mitochondrial-beta oxidation and fatty acid metabolism

The lungs exist in an environment of elevated oxygen. The large surface area and high blood supply make this organ highly susceptible to injuries mediated by oxidative stress. Exogenous exposure to reactive oxygen species (ROS) such as NO₂, SO₂, CO, and dust particles, as well as cigarette smoke, can lead to excessive oxidative stress and trigger inflammatory responses of the lung tissue (Guarnieri and Balme, 2014). Mitochondrial oxidative phosphorylation can also contribute to ROS exposure and may exacerbate pathology. While mitochondria-derived functions (for e.g. ATP production, cellular signalling and differentiation, cell cycle regulation and cell growth) are efficient processes, high-energy electrons are released from the respiratory chain and can form ROS (Bartlett and Eaton, 2004). This was believed to result in mitochondrial oxidative stress and promote degenerative pathology (Vazquez *et al.*, 2015).

Regulation of beta-oxidation and the relationship between FA metabolism and carbohydrate metabolism was defined in the early 80s (McGarry and Foster, 1980). Fatty acid oxidation to acetyl-CoA is well studied and it has been suggested that the enzymes of beta-oxidation are organized into a multi-enzyme complex (Bartlett and Eaton, 2004). Most saturated FAs are catabolized by mitochondrial beta-oxidation, providing acetyl-CoA as a substrate for the TCA cycle. Through FA oxidation, ATPs are produced; however, this is often accompanied by ROS.

1.3.1.3 Lipid metabolism

Lipid metabolism plays a key role in the lung, resulting in the synthesis and oxidation of FAs, lipid esterification, hydrolysis of lipoproteins, synthesis of phosphatidylcholine,

and synthesis and secretion of prostaglandins and other eicosanoids from arachidonic acid precursors (Yan *et al.*, 2017; Merino Salvador *et al.*, 2017). The abnormal lipid/metabolic phenotype of COPD, asthma and IPF have been reported by the work of Teichgraber *et al.* (2008), Yang and Uhlig (2011) and Ley *et al.* (2014) who highlighted a key role for lipid metabolism in lung diseases.

The oxidation of FAs during lipid metabolism also plays an important role in regulating glycolysis. Subsequent steps in FA synthesis is the production of palmitate, a primary FA that can undergo various elongation or unsaturation cycles to yield other FA molecules. FAs need to be activated with CoA by fatty acyl-CoA synthetases which is critical for phospholipid and triglyceride synthesis (Yan *et al.*, 2017). These lipids are fundamental component of cellular membranes, play critical roles in cellular functions including energy storage, signal transduction, formation of membrane bilayer and cellular barriers. Hence, dysregulated FA oxidation can disrupt lipid metabolism that contributes to various pathological features.

The dysregulation of lipid metabolism has been well-described in Alzheimer's disease, diabetes, obesity, atherosclerosis and in several lung diseases such as cystic fibrosis, asthma and COPD (Yan *et al.*, 2017). In the proliferating cell, there is an increase in the uptake of exogenous FA due to an increase in adipogenesis (Bartlett and Eaton, 2004; Merino Salvador *et al.*, 2017).

1.4 Metabolomics- an emerging 'omic modality for clinical research

Metabolomics is generally applied through a targeted, selective measurement strategy, or as part of an untargeted, global profiling approach (Wilson, 2017; Bowler *et al.*,

2017; Bingol, 2018). Targeted metabolomics is a quantitative approach that allows for the measurement of metabolite concentrations while untargeted metabolomics undertakes simultaneous assessment of metabolites without any prior sample knowledge for hypothesis generation (Bingol, 2018). Untargeted metabolomics is a comprehensive strategy for identifying changes in different patho-physiological states (Wang *et al.*, 2010); however, a major disadvantage is that the majority of features are unidentifiable. Feature identification can be improved by using sophisticated data-independent acquisition techniques, which will additionally collect important structural detail in the metabolite measurements for interpretation at a later date without the need for re-measurement of samples (Gethings *et al.*, 2017) since accurate mass measurement alone is insufficient for compound identification (Wang *et al.*, 2010; Bingol, 2018). Additional orthogonal information, such as chromatographic retention time, tandem MS fragmentation (MS/MS), isotopic patterns and collisional cross-section, are also necessary for structural annotation and compound identification (Wang *et al.*, 2010; Bingol, 2018). Advents in analytical technologies and bioinformatics are setting the stage for large-scale, harmonized metabolic profiling suitable for studies at the population level (Wilson, 2017). Metabolic phenotyping considers the total metabolite profile as a unique pattern, or fingerprint, for a specific pathological state without attempting to identify all the features present in the profile.

Confirmatory diagnoses of lung diseases are heavily dependent on the application of high-resolution computed tomography and surgical biopsies (Flaherty *et al.*, 2004; Elicker *et al.*, 2008; Kaarteenaho, 2013). While surgical biopsy is still regarded as the gold standard, diagnostic misinterpretations has been documented (Kaarteenaho, 2013). Lin *et al.* (2014) suggested the application of metabolomics as a clinical tool to support disease diagnostics. Untargeted metabolomics can be useful for clinical research as it

provides practitioners with a systemic approach to understand global changes in response to an alteration in nutrition, genetics, environment and gut microbiota (Griffiths *et al.*, 2010). It also allows for the interrogation of endogenous biochemicals involved in key metabolic processes and provides novel insights into the molecular mechanisms associated with an alteration or perturbation of the physiological status (Zhang *et al.*, 2010). Despite the heterogeneity associated with pulmonary diseases, metabolomics is particularly useful for endotyping and phenotyping, and promises to stratify individuals based on severity and exacerbation as well as enhance the diagnostic accuracy of diseases such as COPD (Comhair *et al.*, 2015; Adamko *et al.*, 2015).

1.5 Analytical techniques in metabolomics

This review will focus on information rich analytical techniques such as nuclear magnetic resonance (NMR) spectroscopy and mass spectrometry (MS) that are routinely used for metabolomics research (Gowda *et al.*, 2008).

1.5.1 NMR spectroscopy

NMR is widely used due its ability to simultaneously measure multiple metabolites within a short acquisition time and with minimal preparation (Stringer *et al.*, 2016; Markley *et al.*, 2017). As a non-destructive technique, NMR is highly advantageous as the samples can be re-used for multiple assays. This is especially important where sample amount is limited, which is common in clinical settings. The major limitation of NMR for metabolomics is its low sensitivity, which results in micromolar detection levels (Gowda and Raftery, 2015). Depending on the nature of the sample and experimental hypotheses, a number of NMR techniques are applied in metabolomics.

^1H -NMR is the most commonly used NMR technique for metabolic phenotyping and biomarker discovery due to its simplicity, robustness and repeatability (Wilson, 2017), followed by ^{31}P -NMR and ^{13}C -NMR (Wang *et al.*, 2010; Gowda and Raftery, 2015). NMR has been used to study the metabolome of lung diseases, including silicosis (Hu *et al.*, 2008), asthma and COPD (Adamko *et al.*, 2015) and respiratory syncytial viral infection (Adamko *et al.*, 2016). One-dimensional (1D) ^1H NMR suffers from low spectral resolution which limits metabolome coverage and accuracy of metabolite analysis (Bingol, 2018). Current NMR developments are focused on reducing spectral overlap. For example, two-dimensional (2D) NMR experiments have been used to improve resolution and sensitivity. However, the main limitation of 2D NMR is its longer method acquisition.

1.5.2 Mass spectrometry

MS-based metabolomics provide increased sensitivity and selectivity for measuring a range of cellular metabolites in various biological samples (Gowda and Raftery, 2015). MS-based metabolic profiling can also be performed using a shotgun approach based on direct infusion MS (Wilson, 2017) or in combination with a number of front-end chromatographic separation techniques (Stringer *et al.*, 2016).

Liquid chromatography (LC)-MS is the analytical approach most often used for metabolomics due to its ability to resolve different classes of metabolites (Wang *et al.*, 2010; Stringer *et al.*, 2016). Some of the advantages of LC-MS based metabolomics are: 1) good coverage of mass ranges, which permits the detection of metabolites with different chemical properties, 2) no requirement for sample derivatization and 3) high sensitivity at nanomolar levels (Stringer *et al.*, 2016). Aqueous metabolites can also be

simultaneously assayed and recent advances are now enabling greater separation and detection of metabolites such as lipids. The disadvantages of LC-MS include its high variability across different instruments, the lack of standardized metabolite libraries as well as the numerous standard preparative steps and data processing workflows (Stringer *et al.*, 2016).

An important consideration for LC-MS based metabolomics is the type of chromatography column used as this determines the class of metabolites for separation. The polarity and pH of the solvents also influences metabolite separation (Stringer *et al.*, 2016). Reverse-phase columns such as C18 columns provide good retention and separation of non-polar compounds (Wang *et al.*, 2010). Alternatively, hydrophilic interaction chromatography (HILIC) columns are preferred for the detection of polar compounds (Wilson, 2017). Electrospray ionization (ESI) is the preferred ion source for coupling LC with MS for metabolomics studies as it provides coverage of both positive and negative ions (Stringer *et al.*, 2016).

Quadrupole, time-of-flight (TOF) and ion traps are some of the more commonly used mass analyzers coupled to LC separation (Wang *et al.*, 2010). Triple quadrupole (QQQ) analyzers, allow for tandem MS experiments (MS/MS) or further fragmentation of ions during analysis. Similarly, ion trap analyzers trap ions of interest and accumulate them for better sensitivity (Stringer *et al.*, 2016). They can also trap and fragment a specific ion multiple times (MS_n) to allow detection of selective ions (Stringer *et al.*, 2016). In contrast, TOF analyzers determine the m/z by accelerating ions and then measure the time required to traverse a flight tube. TOF analyzers have increased mass accuracy and are highly sensitive (Wang *et al.*, 2010). They can be coupled with a quadrupole (Q-TOF; Wang *et al.*, 2010), which is well suited for metabolite detection. Fourier

transform ion cyclotron resonance (FT-ICR) paired with MS detectors have the highest degree of mass accuracy and have MS/MS and MSⁿ capabilities but are limited by high costs (Wang *et al.*, 2010; Stringer *et al.*, 2016).

The advantages of gas chromatography (GC)-MS include high sensitive and specific for the separation and detection of volatile metabolites (Wang *et al.*, 2010; Wilson, 2017). In addition, spectral patterns and retention times of compounds are highly reproducible (Stringer *et al.*, 2016), and allows for the use of established compound libraries such as the National Institute of Standards and Technology (NIST) Mass Spectral Library. There is also lower instrument-to-instrument variability, which is a limitation of LC-MS. However, GC-MS based metabolomics is usually reserved for thermally stable volatile compounds that are of low polarity (Wang *et al.*, 2010) and those that are amenable to derivatization (Wilson, 2017). GC derivatization can lead to a loss of metabolites while incomplete derivatization can result in spectral artifacts.

1.6 Metabolomics-driven discovery of biomarkers

Towards the discovery of biomarkers and in the pursuit of improved disease characterisation, metabolomics has been employed for the study of lung diseases to study a large number of sample types including urine (Adamko *et al.*, 2016), plasma and serum (Kumar *et al.*, 2017), cerebrospinal fluid (Locasale *et al.*, 2012), exhaled breath condensate (EBC; Fermier *et al.*, 2016), bronchoalveolar lavage fluid (BALF; Cruickshank-Quinn *et al.*, 2017), saliva (Barnes *et al.*, 2014), intact tissue (Hu *et al.*, 2008) as well as cells (Luo and Li, 2017) and their extracts. Urine and blood are the most commonly used biofluids for metabolomics studies as both samples contain thousands of detectable metabolic features and can be collected using minimally

invasive methods. Table 1.1 below provides an analysis of recent metabolomics studies of COPD, asthma and IPF and provide a summary of each study according to the metabolic pathways implicated, samples type assayed, and the analytical techniques utilized.

Table 1.1 Summary of recent metabolomics studies reporting the metabolic pathways associated with COPD, asthma and IPF, samples assessed, and analytical techniques used. Ionisation modes are described as positive (+) and/or negative (-) electrospray (ESI) or electron impact (EI) while MS/MS and 1D-¹H and stands for tandem MS technique and one-dimensional proton NMR experiment, respectively. HILIC is abbreviated for hydrophilic interaction chromatography and RP denotes reversed-phase chromatography.

Disease	Investigators	Sample	Separation (method)	MS (ionisation mode)	Metabolic pathways
COPD	Kilk <i>et al.</i> (2018)	EBC, serum	LC (direct injection)	MS (+ and - ESI)	Sphingolipid metabolism Arginine metabolism
	Naz <i>et al.</i> (2017)	Plasma, BALF	LC (HILIC and RP)	MS (+ and - ESI)	TCA-cycle Glycerophospholipid metabolism Fatty acid metabolism Sphingolipid metabolism
	Adamko <i>et al.</i> (2015)	Urine	NMR (600 MHz)	1D- ¹ H	Nitric oxide pathway Coenzyme A biosynthesis
Asthma	Carraro <i>et al.</i> (2018)	Urine	LC (RP)	MS (+ and - ESI)	Tryptophan metabolism Fatty acid metabolism
	Reinke <i>et al.</i> (2017)	Serum	LC (HILIC and RP)	MS (+ and - ESI)	Sphingolipid metabolism Fatty acid metabolism Eicosanoid metabolism
	McGeachie <i>et al.</i> (2015)	Plasma	LC (RP)	MS (+ ESI)	Linoleic acid metabolism Arachidonic acid metabolism

					Sphingolipid metabolism Fatty acid metabolism Taurine metabolism
IPF	Rindlisbacher <i>et al.</i> (2018)	Serum	LC (RP)	MS ^E (+ and - ESI)	Lysophosphatidic acid metabolism
	Zhao <i>et al.</i> (2017)	Lung tissue	LC GC	MS/MS MS	Sphingolipid metabolism Arginine metabolism Glycolysis Mitochondrial beta-oxidation TCA-cycle
	Kang <i>et al.</i> (2016)	Lung tissue	GC	MS (EI)	Glycolysis Glutathione biosynthesis Ornithine aminotransferase metabolism

In the past decade, improvements in high-throughput analytical technologies has allowed for a broader coverage of the metabolome and consequently, increased its utilization in biomarker discovery (Griffiths *et al.*, 2010; Wilson, 2017). Biomarkers are classified as screening, diagnostic, or prognostic chemical markers based on their ability to predict, diagnose or evaluate the condition of a disease, respectively (Biomarkers Definitions Working Group, 2001; Fleming and Powers, 2012). Metabolomics-driven biomarker discovery is focused on the elucidation of patho-physiological mechanisms, with the ultimate objective of carrying out more accurate diagnosis and personalized treatment from an informed perspective (Griffiths *et al.*, 2010). Table 1.2 below provides a list of published candidate biomarkers of chronic lung diseases grouped according to the metabolic pathways reviewed in this paper.

Table 1.2 Putative and candidate biomarkers of chronic lung diseases correlating to the glycolytic and TCA-cycle, mitochondrial beta-oxidation, fatty acid as well as lipid metabolism pathways.

Metabolic pathways	Putative biomarkers		References
Glycolysis & TCA-cycle	glucose pyruvate hexokinase acetyl-CoA NADH FADH2 malate citrate glutamine alanine lactate	aspartate arginine myoinositol fumarate adenosine succinate threonine α -ketoglutarate pyruvate kinase phosphofructokinase	Hasawi <i>et al.</i> (2014) Ren <i>et al.</i> (2017) Bowler <i>et al.</i> (2017) Sreedhar and Zhao (2018)
Mitochondrial-beta oxidation & fatty acid metabolism	carnitine acylcarnitine choline citrate acyl-CoA acetate acetyl-CoA threonine	linoleic acid palmitate malate serine eicosanoids arachidonic acid lysophosphatidic acid	Mehta <i>et al.</i> (2010) Conlon <i>et al.</i> (2015) Bowler <i>et al.</i> (2017)
Lipid metabolism	phospholipids triglycerides sphingolipids arachidonic acid palmitate betaine choline ceramides		Teichgraber <i>et al.</i> (2008) Yang and Uhlig (2011) Ley <i>et al.</i> (2014) Yan <i>et al.</i> (2017) Bowler <i>et al.</i> (2017)

1.6.1 Metabolomics studies of COPD

COPD is a debilitating condition affecting millions of people worldwide and is the leading cause of chronic morbidity and mortality in patients with lung disease (Obi *et al.*, 2018). Tobacco smoking and atmospheric pollution are the main risk factors for the development of COPD (May and Li, 2015). It is characterized by excess mucus production and small airway destruction, causing reduced lung compliance. These pathological changes are associated with oxidative stress and inflammatory responses that leads to an imbalance in cellular proliferation (Fischer *et al.*, 2011; King, 2015).

A number of recent studies has revealed metabolic dysregulation in COPD patients (Kao *et al.*, 2012; Adamko *et al.*, 2015; Naz *et al.*, 2017; Kilk *et al.*, 2018). For example, alterations in the sphingolipid metabolism was identified in COPD patients (Kilk *et al.*, 2018) and patients in the Karolinska smoking-related disease cohort (Naz *et al.*, 2017), suggesting a dysregulation of lipid metabolism during the onset of COPD. This was further supported by the findings of Adamko *et al.* (2015) who identified an increase in betaine and choline levels in COPD patients. Both betaine and choline play important roles in methyl group metabolism and in the synthesis of membrane phospholipids (Lever and Slow, 2010). These studies also support a hypothesis of FA oxidation and tryptophan metabolism dysregulation leading to a state of high oxidative stress. An effect on FA oxidation was also demonstrated in COPD participants by Naz *et al.* (2017) who measured the ratio of carnitine and acylcarnitine using tandem LC-MS. The study found that the ratios between the medium and long-chain carnitines were significantly lower in the COPD samples compared to the healthy controls.

Altered FA oxidation due to reduced levels of free carnitine in lung tissue have also been implicated in progressive emphysema (Conlon *et al.*, 2015) and COPD (Naz *et al.*, 2017). Smoke exposure has been shown to increase FA oxidation through reduced levels of circulating polyunsaturated fatty acids (PUFA) along with other inflammatory processes (Puri *et al.*, 2008; Carraro *et al.*, 2018). Baldassarre *et al.* (2014) outlined the mechanism of smoking-induced changes of plasma FAs that consequently enhanced peroxidative processes. It has been postulated that an increase in smoke exposure increases FA levels in cellular cytosol, resulting in protection against lipotoxicity. Conversely, impaired carnitine metabolism in COPD can cause accumulation of FA in the cytosol which can also lead to lipotoxicity (Baldassarre *et al.*, 2014; Adeva-Andany *et al.*, 2018). Metabolomics in COPD provides insight into the pathogenesis of the disease with alterations in sphingolipid metabolism and changes in lipids during increased oxidant stress.

1.6.2 Metabolomics studies of Asthma

Asthma is one of the most common chronic lung diseases of children and is caused by a range of inflammatory mechanisms (Reinke *et al.*, 2017). It is typically characterised by shortness of breath or episodic wheeze due to airway obstruction resulting from various stimuli (Aziz-Ur-Rehman *et al.*, 2017). In asthma, the symptoms of systemic inflammation are less prevalent than in COPD (Athanasio, 2012; Hawken *et al.*, 2018).

Recent studies by McGeachie *et al.*, (2015), Reinke *et al.* (2017) and Carraro *et al.* (2018) examined inflammatory pathways consequent to lipid and amino acids dysregulation. McGeachie *et al.* (2015) used LC-MS in positive ion mode to reveal increased levels of taurine and glycine in children aged between one to 18 years with

asthma. This observation was supported by Reinke *et al.* (2017). Taurine and glycine has been shown to regulate cytokine overexpression in allergies (McGeachie *et al.*, 2015) and has protective effects. Arginine, like taurine, is also strongly induced by T-helper cytokines such as interleukin (IL)-4 and IL-13. Interestingly, lipid mediators are important in inflammatory responses and have well-defined roles in T-cell recruitment. The elevated levels of linoleic and oleic acids reported by McGeachie *et al.* (2015) is consistent with the enrichment of linoleic acid metabolism which further underpin their involvement in asthma pathogenesis. The role of oxidative stress in asthma has also been well-characterized and suggested that imbalances between oxidation and reducing systems can contribute to the disease state.

Both endogenous and exogenous ROS including superoxide and reactive nitrogen and hydrogen species increase airway inflammation and are key determinants of asthma severity (Mehta *et al.*, 2010). Choline therapy has been shown to reduce inflammation and suppress oxidative stress in patients with asthma (Mehta *et al.*, 2010). An increased level of choline may potentially cause an adaptive response in the lungs by depleting other lipid metabolites. Ried *et al.* (2013) showed that asthmatic patients have significantly lower levels of phosphatidylcholine (PC) in lung surfactant, which can lead to reduced lung function. Metabolomics increasingly demonstrates how inflammation of asthma is modified by metabolomes thus providing future therapeutic targets.

1.6.3 Metabolomics studies of IPF

Idiopathic pulmonary fibrosis is a chronic, progressive lung disease characterized by alveolar epithelial cell damage, proliferation of fibroblasts, and extracellular matrix accumulation leading to irreversible distortion of the lung architecture (Kang *et al.*,

2016). The aetiological causes of IPF remain unknown to date. While genetic and metabolic determinants associated with the development of fibroses have been reported by Gangwar *et al.* (2017) and Zhao *et al.* (2017), the underlying disease pathophysiology remains unclear.

Metabolic profiling studies conducted by Zhao *et al.* (2017) used both GC and LC-MS to demonstrate the abnormalities in metabolic pathways including glycolysis, mitochondrial β -oxidation, TCA cycle and sphingolipid metabolism in association with IPF. Xie *et al.* (2015) showed that the inhibition of glycolysis via 6-phosphofructo-2-kinase/fructose-2,6-biphosphatase 3 (PFKFB3) protects against the development of lung fibrosis in mice by using similar analytical platforms. Kang *et al.* (2016) and Zhao *et al.* (2017) applied a range of untargeted and targeted methods to study accelerated glycolysis in the IPF lung. The results suggested that glycolysis plays a role in the fibrotic phenotype. This is consistent with the observation that an increased rate of glycolysis can cause increased glycine biosynthesis, resulting in its incorporation into collagen, a process central to lung fibrogenesis (Hamanaka *et al.*, 2018).

Hamanaka *et al.* (2018) reported that transforming growth factor (TGF)- β promoted fibrogenesis which included the expression of serine and glycine synthesis pathway in human lung fibroblasts. As TGF- β 1 increases both glycolysis and oxidative phosphorylation, the roles of glucose, glutamine, and fatty acid oxidation during TGF- β mediated fibrosis warrant further investigation. Rindlisbacher *et al.* (2018) used RP separation followed by an exploratory, high resolution, MS^E method to measure increased levels of lysophosphatidylcholine (LysoPC) and 3-hydroxydecanoyl carnitine in IPF patients. Lysophosphatidylcholine is a precursor of Lysophosphatidic acid (LPA), a FA that induces epithelial cell damage, inflammation and fibrosis in kidney (Sakai *et*

al., 2017) and liver (Kaffe *et al.*, 2017). The downregulation of glycolysis, mitochondrial beta-oxidation and TCA pathways suggested that alternative energy pathways have been upregulated to support lung remodelling (Zhao *et al.*, 2017). The changes in lipids in IPF may in future provide insights into intracellular changes that occur in this progressive condition. This may improve treatments in the future.

1.7 Frontiers in metabolomic analysis of chronic lung diseases

Clinical metabolomics applications are presently dominated by the use of tandem MS platforms. These instruments are mainly used for targeted analysis of specific metabolites or metabolite classes such as amino acids, neurotransmitters, steroids and drugs (Jannetto and Fitzgerald, 2016). While technological advancements continue to broaden the metabolite coverage afforded by high resolution analytical instruments such as QTOF-MS, considerable challenges remain in data interrogation and the validation of metabolite identities (Bowler *et al.*, 2017). Efforts to improve, and augment, the metabolomics data pipeline are currently focused on biostatistical and bioinformatics approaches, new resources for biochemical pathway mapping, enrichment analyses and even the application of machine learning principles. It is, nevertheless, well established that joint efforts are needed to promote data sharing, method synchrony and sample storage integrity, because the novelty of metabolomics methodologies and laboratory-specific practices are highly influential to the comparability of metabolomics datasets across studies.

This section of the review endeavours to present cutting-edge tools available for the metabolomics interrogation of lung diseases. In particular, the application of mass spectrometry imaging (MSI) techniques is of great interest due to its ability to provide

spatial information on metabolite distribution within tissue samples. MSI techniques such as matrix-assisted laser desorption/ionisation (MALDI; Caprioli *et al.*, 1997) and desorption electrospray ionization (DESI; Takáts *et al.*, 2004) show promise and offers investigators a means of chemically mapping samples without the requirement for specific staining or labelling agents (Rabinovich *et al.*, 2012). A major advantage of MSI lies in its ability to measure changes in markers that can be directly correlated to morphological features of interest, abrogating the need for time-consuming techniques such as laser capture micro-dissection (Mirnezami *et al.*, 2014). Carter *et al.* (2016) and Brioude *et al.* (2016) have successfully used MSI to characterize region-specific protein or peptide distribution within tissue sections. More recently, Matsumoto *et al.* (2017) used MSI to examine the localisation and distribution of therapeutic compounds in lung tissue samples; this presents clinicians with the opportunity to investigate therapeutic drug efficacy from an entirely novel perspective.

While MALDI-MSI is effective for the study of molecules at the upper end of the mass spectrum, such as proteins and peptides (Mirnezami *et al.*, 2014), its success profiling metabolites at the lower end of the mass range ($<1000\ m/z$) is still advancing (Miura *et al.*, 2012). The DESI approach developed by Takáts *et al.* (2004) may be more suitable for metabolomics studies as ionization occurs under ambient conditions and can provide improved resolution of lower m/z value molecular species. The application of MSI to complement histopathology for the visualisation of metabolites is a promising avenue for studies into chronic lung conditions, where such applications are yet to be applied outside of pulmonary diseases such as lung cancer.

Metabolomics provides complementary insight into disease pathogenesis alongside the measurements of transcriptomics and proteomics. Metabolomics can uniquely provide

detail of perturbations in fundamental biochemical pathways or mechanisms, such as TCA cycle and oxidant metabolism, or the identification of novel and as-yet undescribed biochemical processes. The great strength of metabolomics data however is in its interpretation. Whilst many thousands of features representing metabolism can be measured in any given metabolomics analysis, the unambiguous assignment of chemical identity continues to slow interpretative progress. Efforts of data mining and reduction, which allow resources to quickly channel toward the most relevant metabolite entities for ongoing validation, are integral to study translation.

1.8 Conclusion

For clinical studies, moving from exploratory metabolomics to a biochemical understanding, and ultimately improving patient outcomes, can only be achieved by strict experimental design and the fastidious collection of complementary phenotypic data; including but not limited to, extensive patient observations and prognoses, and wherever can be afforded, other functional diagnostic measurements including existing pathology markers and further exploratory ‘omics analyses. The extensive cataloguing of such metadata remains a challenge, however as the technology continues to advance and metabolomics data become increasingly information-rich, clinical outcomes will also improve, but only if the means to interpret the measurements are also considered. Chronic lung diseases such as COPD, asthma and IPF constitute some of the most common pulmonary disorders and are major causes of mortality worldwide. These diseases of the lung are highly heterogenous and remain difficult to define in a clinical context. The inherent complexity of these disease phenotypes pose difficulties for accurate diagnosis and prognosis, and as such expanding on the currently adopted diagnostic and prognostic tools by inclusion of data-rich metabolomics measurements

will provide new angles of discovery and insight. Here we have highlighted some of the major metabolic pathways perturbed in chronic lung diseases as well as provide an overview of the techniques commonly used for discovery metabolomics. As one of the most rapidly advancing fields in post-genomics research, metabolomics is a promising discovery tool that can facilitate a greater understanding of chronic lung diseases at the phenotypic level, and ultimately lead to the development of personalized approaches in patient diagnosis and treatment.

1.9 References

- Adamko, D. J., E. Saude, M. Bear, S. Regush and J. L. Robinson (2016). "Urine metabolomic profiling of children with respiratory tract infections in the emergency department: a pilot study." BMC Infectious Diseases 16(1): 439.
- Adamko, D. J., P. Nair, I. Mayers, R. T. Tsuyuki, S. Regush and B. H. Rowe (2015). "Metabolomic profiling of asthma and chronic obstructive pulmonary disease: A pilot study differentiating diseases." Journal of Allergy and Clinical Immunology 136(3): 571-580.e573.
- Adeva-Andany, M. M., N. Carneiro-Freire, M. Seco-Filgueira, C. Fernandez-Fernandez and D. Mourino-Bayolo (2018). "Mitochondrial beta-oxidation of saturated fatty acids in humans." Mitochondrion.
- Athanazio, R. (2012). "Airway disease: similarities and differences between asthma, COPD and bronchiectasis." Clinics (Sao Paulo) 67(11): 1335-1343.
- Aziz-Ur-Rehman, A., A. Dasgupta, M. Kjarsgaard, F. E. Hargreave and P. Nair (2017). "Sputum cell counts to manage prednisone-dependent asthma: effects on FEV1 and eosinophilic exacerbations." Allergy, Asthma & Clinical Immunology 13(1): 17.
- Baldassarre, D., M. Amato, B. Frigerio, S. Ghezzi, C. Colombo, S. Castelnovo, A. Ravani, D. Sansaro, E. Tremoli, C. R. Sirtori, P. Risé and C. Galli (2014). "Impact of cigarette smoking on the plasma fatty acid profile and their interaction in determining the burden of subclinical atherosclerosis." Nutrafoods 13(4): 159-167.
- Barnes, V. M., A. D. Kennedy, F. Panagakos, W. Devizio, H. M. Trivedi, T. Jönsson, L. Guo, S. Cervi and F. A. Scannapieco (2014). "Global Metabolomic Analysis of

- Human Saliva and Plasma from Healthy and Diabetic Subjects, with and without Periodontal Disease." PLOS ONE 9(8): e105181.
- Bartlett, K. and S. Eaton (2004). "Mitochondrial β -oxidation." European Journal of Biochemistry 271(3): 462-469.
- Bingol, K. (2018). "Recent Advances in Targeted and Untargeted Metabolomics by NMR and MS/NMR Methods." High-Throughput 7(2): 9.
- Biomarkers Definitions Working Group (2001). "Biomarkers and surrogate endpoints: preferred definitions and conceptual framework." Clinical Pharmacology & Therapeutics 69(3): 89-95.
- Bowler, R. P., C. H. Wendt, M. B. Fessler, M. W. Foster, R. S. Kelly, J. Lasky-Su, A. J. Rogers, K. A. Stringer and B. W. Winston (2017). "New Strategies and Challenges in Lung Proteomics and Metabolomics. An Official American Thoracic Society Workshop Report." Annals of the American Thoracic Society 14(12): 1721-1743.
- Brioude, G., F. Brégeon, D. Trousse, C. Flaudrops, V. Secq, F. De Dominicis, E. Chabrières, X.-B. D'journo, D. Raoult and P.-A. Thomas (2016). "Rapid Diagnosis of Lung Tumors, a Feasibility Study Using MALDI-ToF Mass Spectrometry." PLoS ONE 11(5): e0155449.
- Caprioli, R. M., T. B. Farmer and J. Gile (1997). "Molecular Imaging of Biological Samples: Localization of Peptides and Proteins Using MALDI-TOF MS." Analytical Chemistry 69(23): 4751-4760.
- Carraro, S., S. Bozzetto, G. Giordano, D. El Mazloum, M. Stocchero, P. Pirillo, S. Zanconato and E. Baraldi (2018). "Wheezing preschool children with early-onset asthma reveal a specific metabolomic profile." Pediatric Allergy and Immunology 29(4): 375-382.

- Carter, C. L., J. W. Jones, A. M. Farese, T. J. MacVittie and M. A. Kane (2016). "Inflation-Fixation Method for Lipidomic Mapping of Lung Biopsies by Matrix Assisted Laser Desorption/Ionization–Mass Spectrometry Imaging." Analytical Chemistry 88(9): 4788-4794.
- Church, D. F. and W. A. Pryor (1985). "Free-radical chemistry of cigarette smoke and its toxicological implications." Environmental Health Perspectives 64: 111-126.
- Comhair, S. A. A., J. McDunn, C. Bennett, J. Fetig, S. C. Erzurum and S. C. Kalhan (2015). "Metabolomic Endotype of Asthma." Journal of immunology (Baltimore, Md.: 1950) 195(2): 643-650.
- Conlon, T. M., J. Bartel, K. Ballweg, S. Günter, C. Prehn, J. Krumsiek, S. Meiners, F. J. Theis, J. Adamski, O. Eickelberg and A. O. Yildirim (2015). "Metabolomics screening identifies reduced L-carnitine to be associated with progressive emphysema." Clinical Science.
- Cruickshank-Quinn, C., R. Powell, S. Jacobson, K. Kechris, R. P. Bowler, I. Petrache and N. Reisdorph (2017). "Metabolomic similarities between bronchoalveolar lavage fluid and plasma in humans and mice." Scientific Reports 7(1): 5108.
- Dais, P., R. Plessel, K. Williamson and E. Hatzakis (2017). "Complete ¹H and ¹³C NMR assignment and ³¹P NMR determination of pentacyclic triterpenic acids." Analytical Methods 9(6): 949-957.
- Elicker, B., C. A. d. C. Pereira, R. Webb and K. O. Leslie (2008). "High-resolution computed tomography patterns of diffuse interstitial lung disease with clinical and pathological correlation." Jornal Brasileiro de Pneumologia 34: 715-744.
- Fermier, B., H. Blasco, E. Godat, C. Bocca, J. Moenne-Loccoz, P. Emond, C. R. Andres, M. Laffon and M. Ferrandiere (2016). "Specific Metabolome Profile of Exhaled Breath Condensate in Patients with Shock and Respiratory Failure: A Pilot Study." Metabolites 6(3).

- Fischer, B. M., E. Pavlisko and J. A. Voynow (2011). "Pathogenic triad in COPD: oxidative stress, protease–antiprotease imbalance, and inflammation." International Journal of Chronic Obstructive Pulmonary Disease 6: 413-421.
- Flaherty, K. R., A. C. Andrei, T. E. King, Jr., G. Raghu, T. V. Colby, A. Wells, N. Bassily, K. Brown, R. du Bois, A. Flint, S. E. Gay, B. H. Gross, E. A. Kazerooni, R. Knapp, E. Louvar, D. Lynch, A. G. Nicholson, J. Quick, V. J. Thannickal, W. D. Travis, J. Vyskocil, F. A. Wadenstorer, J. Wilt, G. B. Toews, S. Murray and F. J. Martinez (2007). "Idiopathic interstitial pneumonia: do community and academic physicians agree on diagnosis?" American Journal of Respiratory and Critical Care Medicine 175(10): 1054-1060.
- Flaherty, K. R., T. E. King, Jr., G. Raghu, J. P. Lynch, 3rd, T. V. Colby, W. D. Travis, B. H. Gross, E. A. Kazerooni, G. B. Toews, Q. Long, S. Murray, V. N. Lama, S. E. Gay and F. J. Martinez (2004). "Idiopathic interstitial pneumonia: what is the effect of a multidisciplinary approach to diagnosis?" American Journal of Respiratory and Critical Care Medicine 170(8): 904-910.
- Fleming, T. R. and J. H. Powers (2012). "Biomarkers and surrogate endpoints in clinical trials." Statistics in Medicine 31(25): 2973-2984.
- Gangwar, I., N. Kumar Sharma, G. Panzade, S. Awasthi, A. Agrawal and R. Shankar (2017). "Detecting the Molecular System Signatures of Idiopathic Pulmonary Fibrosis through Integrated Genomic Analysis." Scientific Reports 7(1): 1554.
- Gatenby, R. A. and R. J. Gillies (2004). "Why do cancers have high aerobic glycolysis?" Nature Reviews Cancer 4(11): 891-899.
- Gethings, L. A., K. Richardson, J. Wildgoose, S. Lennon, S. Jarvis, C. L. Bevan, J. P. C. Vissers and J. I. Langridge (2017). "Lipid profiling of complex biological mixtures by liquid chromatography/mass spectrometry using a novel scanning

- quadrupole data-independent acquisition strategy." Rapid Communications in Mass Spectrometry 31(19): 1599-1606.
- Gowda, G. A. and D. Raftery (2015). "Can NMR solve some significant challenges in metabolomics?" Journal of Magnetic Resonance 260: 144-160.
- Gowda, G. A., S. Zhang, H. Gu, V. Asiago, N. Shanaiah and D. Raftery (2008). "Metabolomics-based methods for early disease diagnostics." Expert Review of Molecular Diagnostics 8(5): 617-633.
- Griffiths, W. J., T. Koal, Y. Wang, M. Kohl, D. P. Enot and H. P. Deigner (2010). "Targeted metabolomics for biomarker discovery." Angewandte Chemie International Edition (England) 49(32): 5426-5445.
- Guarnieri, M. and J. R. Balmes (2014). "Outdoor air pollution and asthma." Lancet 383(9928): 1581-1592.
- Hamanaka, R. B., R. Nigdelioglu, A. Y. Meliton, Y. Tian, L. J. Witt, E. O'Leary, K. A. Sun, P. S. Woods, D. Wu, B. Ansbro, S. Ard, J. M. Rohde, N. O. Dulin, R. D. Guzy and G. M. Mutlu (2018). "Inhibition of Phosphoglycerate Dehydrogenase Attenuates Bleomycin-induced Pulmonary Fibrosis." American Journal of Respiratory Cell and Molecular Biology 58(5): 585-593.
- Hanse, E. A., C. Ruan, M. Kachman, D. Wang, X. H. Lowman and A. Kelekar (2017). "Cytosolic malate dehydrogenase activity helps support glycolysis in actively proliferating cells and cancer." Oncogene 36(27): 3915-3924.
- Hasawi, N. A., M. F. Alkandari and Y. A. Luqmani (2014). "Phosphofructokinase: A mediator of glycolytic flux in cancer progression." 92(3): 312-321.
- Hawken, N., I. Gilbert, F. J. Martinez, K. M. Fox, M. M. Ross, A. Duenas, A. Kawata, O. Cooper and T. Tervonen What Symptomatic Patients with Asthma and Chronic Obstructive Pulmonary Disease (COPD) Find Important in Their

- Maintenance Inhaler Therapy: A Focus Group Study. C37. OPTIMIZING ASTHMA CARE ACROSS DIVERSE PATIENTS: A4863-A4863.
- Hu, J. Z., D. N. Rommereim, K. R. Minard, A. Woodstock, B. J. Harrer, R. A. Wind, R. P. Phipps and P. J. Sime (2008). "Metabolomics in lung inflammation: a high-resolution (1)h NMR study of mice exposed to silica dust." Toxicology Mechanisms and Methods 18(5): 385-398.
- Jannetto, P. J. and R. L. Fitzgerald (2016). "Effective Use of Mass Spectrometry in the Clinical Laboratory." Clinical Chemistry 62(1): 92.
- Jo, H. E., T. J. Corte, Y. Moodley, K. Levin, G. Westall, P. Hopkins, D. Chambers and I. Glaspole (2016). "Evaluating the interstitial lung disease multidisciplinary meeting: a survey of expert centres." BMC Pulmonary Medicine 16: 22.
- Kaartenaho, R. (2013). "The current position of surgical lung biopsy in the diagnosis of idiopathic pulmonary fibrosis." Respiratory Research 14(1): 43.
- Kaffe, E., A. Katsifa, N. Xylourgidis, I. Ninou, M. Zannikou, V. Harokopos, P. Foka, A. Dimitriadis, K. Evangelou, A. N. Moulas, U. Georgopoulou, V. G. Gorgoulis, G. N. Dalekos and V. Aidinis (2017). "Hepatocyte autotaxin expression promotes liver fibrosis and cancer." Hepatology 65(4): 1369-1383.
- Kang, Y. P., S. B. Lee, J.-m. Lee, H. M. Kim, J. Y. Hong, W. J. Lee, C. W. Choi, H. K. Shin, D.-J. Kim, E. S. Koh, C.-S. Park, S. W. Kwon and S.-W. Park (2016). "Metabolic Profiling Regarding Pathogenesis of Idiopathic Pulmonary Fibrosis." Journal of Proteome Research 15(5): 1717-1724.
- Kao, C. C., J. W.-C. Hsu, V. Bandi, N. A. Hanania, F. Kheradmand and F. Jahoor (2012). "Glucose and pyruvate metabolism in severe chronic obstructive pulmonary disease." Journal of Applied Physiology 112(1): 42-47.
- Karampitsakos, T. and K. I. Gourgoulianis (2016). "Asthma-COPD Overlap Syndrome (ACOS): Single disease entity or not? Could exhaled nitric oxide be a useful

- biomarker for the differentiation of ACOS, asthma and COPD?" Medical Hypotheses 91: 20-23.
- Kilk, K., A. Aug, A. Ottas, U. Soomets, S. Altraja and A. Altraja (2018). "Phenotyping of Chronic Obstructive Pulmonary Disease Based on the Integration of Metabolomes and Clinical Characteristics." International Journal of Molecular Sciences 19(3): 666.
- King, P. T. (2015). "Inflammation in chronic obstructive pulmonary disease and its role in cardiovascular disease and lung cancer." Clinical and Translational Medicine 4: 26.
- Koppenol, W. H., P. L. Bounds and C. V. Dang (2011). "Otto Warburg's contributions to current concepts of cancer metabolism." Nature Reviews Cancer 11(5): 325-337.
- Kumar, N., M. Shahjaman, M. N. H. Mollah, S. M. S. Islam and M. A. Hoque (2017). "Serum and Plasma Metabolomic Biomarkers for Lung Cancer." Bioinformatics 13(6): 202-208.
- Lever, M. and S. Slow (2010). "The clinical significance of betaine, an osmolyte with a key role in methyl group metabolism." Clinical Biochemistry 43(9): 732-744.
- Ley, B., K. K. Brown and H. R. Collard (2014). "Molecular biomarkers in idiopathic pulmonary fibrosis." American Journal of Physiology-Lung Cellular and Molecular Physiology 307(9): L681-L691.
- Li, X. B., J. D. Gu and Q. H. Zhou (2015). "Review of aerobic glycolysis and its key enzymes - new targets for lung cancer therapy." Thoracic Cancer 6(1): 17-24.
- Lin, P., H. L. Lee, H. I. Cheng, C. Y. Chen, M. H. Tsai and H. J. Liu (2014). "Metabolomic profiling of mice urine and serum associated with trans-trans 2, 4-decadienal induced lung lesions by liquid chromatography-mass spectrometry." Analytical Bioanalytical Chemistry 406(17): 4287-4297.

- Locasale, J. W., T. Melman, S. Song, X. Yang, K. D. Swanson, L. C. Cantley, E. T. Wong and J. M. Asara (2012). "Metabolomics of human cerebrospinal fluid identifies signatures of malignant glioma." Molecular & Cellular Proteomics 11(6): M111 014688.
- Luo, X. and L. Li (2017). "Metabolomics of Small Numbers of Cells: Metabolomic Profiling of 100, 1000, and 10000 Human Breast Cancer Cells." Analytical Chemistry 89(21): 11664-11671.
- Maher, T. M. (2015). "Aerobic Glycolysis and the Warburg Effect. An Unexplored Realm in the Search for Fibrosis Therapies?" American Journal of Respiratory and Critical Care Medicine 192(12): 1407-1409.
- Markley, J. L., R. Brüschweiler, A. S. Edison, H. R. Eghbalnia, R. Powers, D. Raftery and D. S. Wishart (2017). "The future of NMR-based metabolomics." Current Opinion in Biotechnology 43: 34-40.
- Matsumoto, T., H. Kushida, S. Matsushita, Y. Oyama, T. Suda, J. Watanabe, Y. Kase and M. Setou (2017). "Distribution Analysis via Mass Spectrometry Imaging of Ephedrine in the Lungs of Rats Orally Administered the Japanese Kampo Medicine Maoto." Scientific Reports 7: 44098.
- May, S. M. and J. T. C. Li (2015). "Burden of chronic obstructive pulmonary disease: Healthcare costs and beyond." Allergy and Asthma Proceedings 36(1): 4-10.
- McGarry, J. D. and D. W. Foster (1980). "Regulation of hepatic fatty acid oxidation and ketone body production." Annual Review of Biochemistry 49: 395-420.
- McGeachie, M. J., A. Dahlin, W. Qiu, D. C. Croteau-Chonka, J. Savage, A. C. Wu, E. S. Wan, J. E. Sordillo, A. Al-Garawi, F. D. Martinez, R. C. Strunk, R. F. Lemanske, A. H. Liu, B. A. Raby, S. Weiss, C. B. Clish and J. A. Lasky-Su (2015). "The metabolomics of asthma control: a promising link between genetics and disease." Immunity, Inflammation and Disease 3(3): 224-238.

- Mehta, A. K., B. P. Singh, N. Arora and S. N. Gaur (2010). "Choline attenuates immune inflammation and suppresses oxidative stress in patients with asthma." Immunobiology 215(7): 527-534.
- Merino Salvador, M., M. Gómez de Cedrón, J. Moreno Rubio, S. Falagán Martínez, R. Sánchez Martínez, E. Casado, A. Ramírez de Molina and M. Sereno (2017). "Lipid metabolism and lung cancer." Critical Reviews in Oncology/Hematology 112: 31-40.
- Mirnezami, R., K. Spagou, P. A. Vorkas, M. R. Lewis, J. Kinross, E. Want, H. Shion, R. D. Goldin, A. Darzi, Z. Takats, E. Holmes, O. Cloarec and J. K. Nicholson (2014). "Chemical mapping of the colorectal cancer microenvironment via MALDI imaging mass spectrometry (MALDI-MSI) reveals novel cancer-associated field effects." Molecular Oncology 8(1): 39-49.
- Miura, D., Y. Fujimura and H. Wariishi (2012). "In situ metabolomic mass spectrometry imaging: Recent advances and difficulties." Journal of Proteomics 75(16): 5052-5060.
- Naz, S., J. Kolmert, M. Yang, S. N. Reinke, M. A. Kamleh, S. Snowden, T. Heyder, B. Levanen, D. J. Erle, C. M. Skold, A. M. Wheelock and C. E. Wheelock (2017). "Metabolomics analysis identifies sex-associated metabotypes of oxidative stress and the autotaxin-lysoPA axis in COPD." European Respiratory Journal 49(6).
- Obi, J., A. Mehari and R. Gillum (2018). "Mortality Related to Chronic Obstructive Pulmonary Disease and Co-morbidities in the United States, A Multiple Causes of Death Analysis." COPD: Journal of Chronic Obstructive Pulmonary Disease 15(2): 200-205.

- Papaiouannou, O., T. Karampitsakos, I. Barbayianni, S. Chrysikos, N. Xylourgidis, V. Tzilas, D. Bouros, V. Aidinis and A. Tzouvelekis (2017). "Metabolic Disorders in Chronic Lung Diseases." Frontiers in Medicine 4: 246.
- Puri, B. K., I. H. Treasaden, M. Cocchi, S. Tsaluchidu, L. Tonello and B. M. Ross (2008). "A comparison of oxidative stress in smokers and non-smokers: an in vivo human quantitative study of n-3 lipid peroxidation." BMC Psychiatry 8(Suppl 1): S4-S4.
- Rabinovich, E. I., M. G. Kapetanaki, I. Steinfeld, K. F. Gibson, K. V. Pandit, G. Yu, Z. Yakhini and N. Kaminski (2012). "Global Methylation Patterns in Idiopathic Pulmonary Fibrosis." PLoS ONE 7(4): e33770.
- Reinke, S. N., H. Gallart-Ayala, C. Gómez, A. Checa, A. Fauland, S. Naz, M. A. Kamleh, R. Djukanović, T. S. C. Hinks and C. E. Wheelock (2017). "Metabolomics analysis identifies different metabotypes of asthma severity." European Respiratory Journal 49(3).
- Ren, J. G., P. Seth, H. Ye, K. Guo, J. I. Hanai, Z. Husain and V. P. Sukhatme (2017). "Citrate Suppresses Tumor Growth in Multiple Models through Inhibition of Glycolysis, the Tricarboxylic Acid Cycle and the IGF-1R Pathway." Scientific Reports 7(1): 4537.
- Ried, J. S., H. Baurecht, F. Stuckler, J. Krumsiek, C. Gieger, J. Heinrich, M. Kabesch, C. Prehn, A. Peters, E. Rodriguez, H. Schulz, K. Strauch, K. Suhre, R. Wang-Sattler, H. E. Wichmann, F. J. Theis, T. Illig, J. Adamski and S. Weidinger (2013). "Integrative genetic and metabolite profiling analysis suggests altered phosphatidylcholine metabolism in asthma." Allergy 68(5): 629-636.
- Rindlisbacher, B., C. Schmid, T. Geiser, C. Bovet and M. Funke-Chambour (2018). "Serum metabolic profiling identified a distinct metabolic signature in patients

- with idiopathic pulmonary fibrosis – a potential biomarker role for LysoPC." Respiratory Research 19(1): 7.
- Sakai, N., J. Chun, J. S. Duffield, D. Lagares, T. Wada, A. D. Luster and A. M. Tager (2017). "Lysophosphatidic acid signaling through its receptor initiates profibrotic epithelial cell fibroblast communication mediated by epithelial cell derived connective tissue growth factor." Kidney International 91(3): 628-641.
- Semendyayeva, O., N. Monogarova, V. Gavrisyk, E. Merenkova and S. Leshenko (2012). "Surgical lung biopsy - Gold standard for diagnosis of idiopathic interstitial pneumonia?" European Respiratory Journal 40(Suppl 56).
- Sreedhar, A. and Y. Zhao (2018). "Dysregulated metabolic enzymes and metabolic reprogramming in cancer cells." Biomed Rep 8(1): 3-10.
- Stringer, K. A., R. T. McKay, A. Karnovsky, B. Quemerais and P. Lacy (2016). "Metabolomics and Its Application to Acute Lung Diseases." Frontiers in Immunology 7: 44.
- Takáts, Z., J. M. Wiseman, B. Gologan and R. G. Cooks (2004). "Mass Spectrometry Sampling Under Ambient Conditions with Desorption Electrospray Ionization." Science 306(5695): 471-473.
- Teichgraber, V., M. Ulrich, N. Endlich, J. Riethmuller, B. Wilker, C. C. De Oliveira-Munding, A. M. van Heeckeren, M. L. Barr, G. von Kurthy, K. W. Schmid, M. Weller, B. Tummler, F. Lang, H. Grassme, G. Doring and E. Gulbins (2008). "Ceramide accumulation mediates inflammation, cell death and infection susceptibility in cystic fibrosis." Nature Medicine 14(4): 382-391.
- Vazquez, E. J., J. M. Berthiaume, V. Kamath, O. Achike, E. Buchanan, M. M. Montano, M. P. Chandler, M. Miyagi and M. G. Rosca (2015). "Mitochondrial complex I defect and increased fatty acid oxidation enhance protein lysine acetylation in the diabetic heart." Cardiovascular Research 107(4): 453-465.

- Wang, J. H., J. Byun and S. Pennathur (2010). "Analytical Approaches to Metabolomics and Applications to Systems Biology." Seminars in nephrology 30(5): 500-511.
- Warburg, O., F. Wind and E. Negelein (1927). "THE METABOLISM OF TUMORS IN THE BODY." The Journal of General Physiology 8(6): 519-530.
- Wilson, I. (2017). "Methods and techniques for metabolic phenotyping." Bioanalysis 9(1): 1-3.
- Xie, N., Z. Tan, S. Banerjee, H. Cui, J. Ge, R. M. Liu, K. Bernard, V. J. Thannickal and G. Liu (2015). "Glycolytic Reprogramming in Myofibroblast Differentiation and Lung Fibrosis." American Journal of Respiratory Critical Care Medicine 192(12): 1462-1474.
- Yan, F., Z. Wen, R. Wang, W. Luo, Y. Du, W. Wang and X. Chen (2017). "Identification of the lipid biomarkers from plasma in idiopathic pulmonary fibrosis by Lipidomics." BMC Pulmonary Medicine 17(1): 174.
- Yang, Y. and S. Uhlig (2011). "The role of sphingolipids in respiratory disease." Therapeutic Advances in Respiratory Disease 5(5): 325-344.
- Zhang, A., H. Sun, Z. Wang, W. Sun, P. Wang and X. Wang (2010). "Metabolomics: towards understanding traditional Chinese medicine." Planta Medica 76(17): 2026-2035.
- Zhao, H., P. A. Dennery and H. Yao (2018). "Metabolic reprogramming in the pathogenesis of chronic lung diseases, including BPD, COPD, and pulmonary fibrosis." American Journal of Physiology-Lung Cellular and Molecular Physiology 314(4): L544-L554.
- Zhao, Y. D., L. Yin, S. Archer, C. Lu, G. Zhao, Y. Yao, L. Wu, M. Hsin, T. K. Waddell, S. Keshavjee, J. Granton and M. de Perrot (2017). "Metabolic heterogeneity of idiopathic pulmonary fibrosis: a metabolomic study." BMJ Open Respiratory Research 4(1).

Untargeted metabolomics of human plasma reveal unique lipid markers in COPD and IPF patients

Adapted from **Nambiar, S.**; Bong, S. H.; Rawlinson, C.; Gummer, J. P. A.; Moodley, Y.; and Trengove, R. D. (2018) “Untargeted metabolomics of human plasma reveal unique lipid markers in COPD and IPF patients” *Ready for submission to Respiratory Medicine*

2.1 Abstract

New paradigms have been proposed to describe similarities in the pathogenesis of chronic obstructive pulmonary disease (COPD) and idiopathic pulmonary fibrosis (IPF) despite their clinical, radiological and pathological differences. Here, we applied an untargeted metabolomics approach to profile plasma samples from patients with COPD and IPF compared to samples from healthy subjects. The study successfully identified a number of metabolites, particularly lipid constituents which may be indicative of shared responses of these diseases to environmental stress. A total of 65 individual plasma samples were analysed, 21 of which were from patients diagnosed with COPD, 24 from IPF and 20 from healthy control participants (HC). Untargeted metabolomics profiling was performed using an ultra-high performance liquid chromatography-quadrupole time-of-flight mass spectrometer (UHPLC-QTOF-MS) equipped with a C18 column in positive ion acquisition mode. Non-polar metabolites such as fatty acids and membrane lipids were well-resolved using the reversed-phase method and a total of 4,805 features (chromatographic peaks with specific retention time and mass-to-charge ratio) were identified following data normalisation, quality control corrections, and applications of dimensionality reduction techniques such as principal component (PCA) and orthogonal

projections to latent structures discriminant analyses (OPLS-DA). Multivariate statistics performed using both Progenesis QI and EZInfo software packages showed distinct separation between COPD and IPF compared to the healthy controls and the most significant features were identified using multiple database matching. Differences in metabolite compositions such as lipid mediators, bilirubin and dihydrotestosterone were observed between diseased and control groups, as well as within COPD and IPF diseased groups.

Keywords: metabolomics, lung, plasma, COPD, IPF

2.2 Introduction

Chronic lung diseases are complex diseases that affect a significant portion of the population with increasing incidence and mortality (Papaioannou *et al.*, 2018). COPD, a smoking-induced lung disease, accounts for the majority of chronic lung disease mortalities, while more than 15,000 deaths per year are attributed to idiopathic pulmonary fibrosis (Kusko *et al.*, 2016). COPD is defined as a disease state characterized by exposure to a noxious agent such as cigarette smoke-induced with airflow limitation resulting from infiltration of inflammatory cells (Lin and Jiang, 2015; Naz *et al.*, 2017). Patients diagnosed with COPD sustain destruction of lung elastin and other extracellular matrix proteins, increased alveolar cells apoptosis, and cellular repair that leads to airspace enlargement characteristic of emphysema (Kusko *et al.*, 2016). IPF, on the other hand, is characterized by a pattern of ‘usual interstitial pneumonia’ (Chilosi *et al.*, 2012), including active fibroblast proliferation associated with minimal inflammation, extracellular matrix deposition, and abnormal alveolar remodelling (Kusko *et al.*, 2016; Papaioannou *et al.*, 2018). There is growing evidence to support the

role of metabolic dysregulation in the pathogenesis of COPD and IPF. Metabolomics can provide the means to study such changes and can potentially identify biomarkers to improve disease diagnosis and treatment.

The fundamental aim of metabolomics is to identify the changes in metabolite composition associated with physiological or pathological change. Both lung conditions are highly heterogeneous, and the lack of diagnostic and predictive biomarkers has hindered new therapeutic interventions and the implementation of precision treatment. Studies by Reinke *et al.* (2017) and Maniscalco *et al.* (2018) has demonstrated changes in metabolite profiles of asthma, COPD and IPF participants. These studies highlighted the growing appeal of using metabolomics to profile challenging lung diseases as well as discriminate individuals based on levels of disease severity and lung exacerbations (Bowler *et al.*, 2017). Recent metabolomics studies of COPD have focused on targeted mass spectrometry (MS) based approaches which provided absolute quantitation of predetermined proteins of interest (Leung *et al.*, 2016; Niu *et al.*, 2017; Fujii *et al.*, 2017). Kang *et al.* (2016) and Cruickshank-Quinn *et al.* (2017), on the other hand, used untargeted MS-based metabolomics to profile changes in the lung tissue and plasma of IPF and COPD patients and showed changes in a number of biochemical pathways. Untargeted MS-based metabolomics generally result in greater metabolite coverage compared to targeted approaches.

This study was based on the application of untargeted metabolomics to profile plasma samples derived from COPD and IPF patients. Data generation was followed by the application of multivariate statistics for both supervised and unsupervised approaches to identify putative biomarkers of interest. The identity of these compounds were then

elucidated by database matching using LIPID MAPS, Biomolecules, ChEBI, HMDB and Drug Bank.

2.3 Materials and Methods

2.3.1 Chemicals and Reagents

UPLC-grade methanol (MeOH), acetonitrile (ACN), water (H₂O) and chloroform were sourced from Fisher Scientific (Thermo Fisher, Australia). The internal standard d₆ t-cinnamic acid and formic acid were obtained from Sigma-Aldrich (New South Wales, Australia).

2.3.2 Biological samples

A total of 65 plasma samples were used in this study. 21 samples were obtained from patients diagnosed with COPD, 24 samples were obtained from IPF and 20 samples were obtained from healthy controls (HC). The associated demographic information (de-identified) was provided in Supplementary Table 2.1. The samples were stored in -80°C until further analysis. Sample handling and experimental protocols were approved by the Royal Perth Hospital Human Research Ethics Committee (Reference number: REG 15-204).

2.3.3 Sample preparation

Plasma samples were prepared using a modified Bligh and Dyer extraction method. Once thawed on ice, samples were centrifuged (1 min, 4 °C, 16,100 x g) to pellet any

precipitate upon initial freezing. 100 μL of plasma was aliquoted into a new microcentrifuge tube to which 300 μL of MeOH (containing the internal standard d6 t-cinnamic acid at 83.3 ng/mL) and 100 μL of chloroform were added. Samples were then vortexed for 10 s and incubated for 10 mins at 4 $^{\circ}\text{C}$ and 1,600 x rpm in a benchtop Thermomixer (Eppendorf). An additional 200 μL of H_2O was added and vortexed for another 10 s. The samples were then incubated for an additional 10 mins at 4 $^{\circ}\text{C}$ and 1,600 x rpm. After incubation, the precipitate was pelleted by centrifugation for 10 mins at 4 $^{\circ}\text{C}$ and 16,100 x g. The aqueous phase (250 μL ; polar fraction) and organic layer (70 μL ; non-polar fraction) were transferred to fresh microcentrifuge tubes by pipette. The organic layer was dried using a rotary vacuum concentrator for 10 mins and the dried sample stored at -80 $^{\circ}\text{C}$ until analysis. From the aqueous phase, the majority of MeOH were removed by rotary vacuum concentrator for 90 mins followed by the addition of 100 μL of H_2O for the dilution of any remaining MeOH. Samples were frozen by submersion in liquid nitrogen and lyophilized to dryness before storage at -80 $^{\circ}\text{C}$. Pooled samples were also generated for quality control (QC) normalization by aliquoting 20 μL from each sample into a single tube and extractions were carried out as per the above method. Blank extractions were also performed; however, plasma was substituted with 100 μL of H_2O .

2.3.4 Mass spectrometry acquisition

Sample analysis was performed by ultra-high performance liquid chromatography quadrupole-time-of-flight mass spectrometry (UHPLC-QTOF-MS) using a Shimadzu Nexera LC30AD LC system coupled to a SCIEX Triple-TOF 5600 MS. The LC unit was equipped with a 1.7 μm Kinetex C18 (100 x 2.1 mm) column from Phenomenex, and chromatography achieved using mobile phase A at 0.2 % formic acid and ACN

(0.2 % formic acid, B) at a solvent flow rate of 300 $\mu\text{L}/\text{min}$. An isocratic composition of 1 % B was used for the first min, with a subsequent solvent gradient increasing to 99.5 % B over 36 mins and a 1 min hold, before returning to 1 % B at 39 mins and holding to 40 mins. The CTO-20A column oven (Shimadzu) was held at 35 $^{\circ}\text{C}$. The ion source was operated at a temperature of 550 $^{\circ}\text{C}$, using a positive ion spray voltage of 5500 V; and nebulisers, heater and curtain gas pressures of 45, 50 and 30 psi, respectively. Data were acquired with a mass range of m/z 50 – 1,000 using an independent data mode of acquisition (IDA) including a sweeping collision energy of 35 ± 15 . Analyst v1.5 (SCIEX) was used for instrumental control and data acquisition. Due to the limited amount of sample available, this study was focused on positive ion mode acquisition as a first pass.

2.3.5 Data processing and statistical analysis

The raw MS data were imported and processed with Progenesis QI (version 2.2, Nonlinear Dynamics, Newcastle, UK). After chromatographic alignment, ion patterns were deconvoluted between 1 and 36 mins of the acquisitions. Adduct ion signatures for $[\text{M}+\text{H}]^+$, $[\text{M}+\text{Na}]^+$, $[\text{M}+\text{K}]^+$ and $[\text{M}+\text{NH}_4]^+$ were deconvoluted from the acquired raw MS data in positive mode followed by normalisation of the detected features to all compounds. Background correction was performed by excluding ion patterns with a two-fold higher abundance in blank versus QC samples and a coefficient of variation of the peak area $> 30\%$ in the QC samples, as recommended by Dunn *et al.* (2012), Wehrens *et al.* (2016) and Broadhurst *et al.* (2018). The normalized abundances of the remaining features were subjected to multivariate analysis with EZinfo (Umetrics, Umeå, Sweden) for identification of features of interest. The data was Pareto-scaled and principal component analysis (PCA) was performed to visualize trends and detect

outliers among observations in the scores plot. PCA was followed by orthogonal partial least square discriminant analysis (OPLS-DA) including model cross-validation to compare discriminant features between healthy controls (HC) and COPD, HC and IPF as well as between COPD and IPF samples. Results were further interrogated using a variable importance in projection (VIP)-plot to find discriminative metabolite candidates having a score of ≥ 1 . Subsequently, each metabolite candidate was reviewed for its ion alignment and chromatographic peak shape. The features of interests were extracted from S-plots constructed following OPLS-DA analysis based on their contribution to the variation and correlation between the two groups. Selected features were interrogated against databases including LIPID MAPS, Biomolecules, Chemical Entities of Biological Interest (ChEBI), Drug Bank and the Human Metabolome Database (HMDB) at a mass accuracy of 10 ppm for metabolite structure and formula.

2.4 Results and Discussion

A total of 19,955 features were curated to 4,805 following data pre-processing and filtration. PCA was applied to obtain an overview of the variations between COPD, IPF, healthy and QC samples. Two different PCAs were applied to assess the changes in grouping by applying background correction or noise reduction. Figure 2.1 showed two PCA scores plot of which one was generated prior to background correction and the other was generated post-correction. An increased separation of experimental groups was observed upon correction and the pooled QC samples were found to be tightly clustered towards the centre of the scores plot. While complete discrimination was not achieved, a degree of separation of the IPF samples from the other HC and COPD (except sample 6) samples was observed. The COPD sample 6 appeared to be sitting within the IPF cluster while the three HC outliers were still identified prior to and

following QC corrections. These were likely to have been caused by multiple sampling sites, inconsistencies in sample collection or mislabelled samples.



Figure 2.1 Principal component analysis scores plots using the first two principal components showing all samples analysed. PCA plot (A) was generated before background correction and PCA plot (B) was generated after the corrections were applied. Black, blue, green and red squares represent pooled QC samples, IPF samples, healthy controls and COPD samples, respectively.

To further separate the disease groups, a supervised approach using OPLS-DA modelling was applied. OPLS-DA was performed to evaluate the differences between the following groups: HC and COPD, HC and IPF, and between COPD and IPF. The OPLS-DA models presented in Figure 2.2 resulted in acceptable model characteristics and showed distinct sample grouping. The remaining samples (HC *versus* IPF, COPD *versus* IPF) were found to be well-separated along the predictive component axis (t[1]). The OPLS-DA prediction model was able to classify the samples into the respective COPD and IPF diseased groups. The scores plot for COPD *versus* IPF showed a similar trend to the OPLS-DA model for HC *versus* IPF and was presented in Figure 2.3 with two outliers. COPD sample 6 was the same outlier identified in the PCA and was positioned near the IPF cluster while the IPF sample 2 outlier fell outside the disease cluster. To improve the modelling, both the outliers were removed and the OPLS-DA scores plot was fitted again. Figure 2.3B showed an improved, well clustered OPLS-DA model which clearly separated the two diseases.

S-plots were then derived from each of the OPLS-DA models and were used to identify features of interest unique to each group based on covariance and correlation between the ion features and causative factors (Ni *et al.*, 2008; Worley and Powers, 2013). The ions in the S-plot furthest away from the origin were regarded as the most significant endogenous features within the study-specific group. The 10 most statistically significant features from each group within the S-plots were then selected and subjected to database matching. With this approach, only metabolite features with strong model contribution and high reliability were selected. A total of 60 features of interest were annotated using LIPID MAPS, Biomolecules, ChEBI, HMDB and Drug Bank databases with a specified mass error of 10 ppm. By comparing the accurate mass values, chemical formula and isotopic similarities, seven features were putatively identified,

and the results were listed in Table 2.1. The fold-change of the putative identities of interest between COPD and HC, IPF and HC, and COPD and IPF were also calculated and presented in Table 2.1. All other related statistics and database information were summarised in Supplementary Table 2.2.

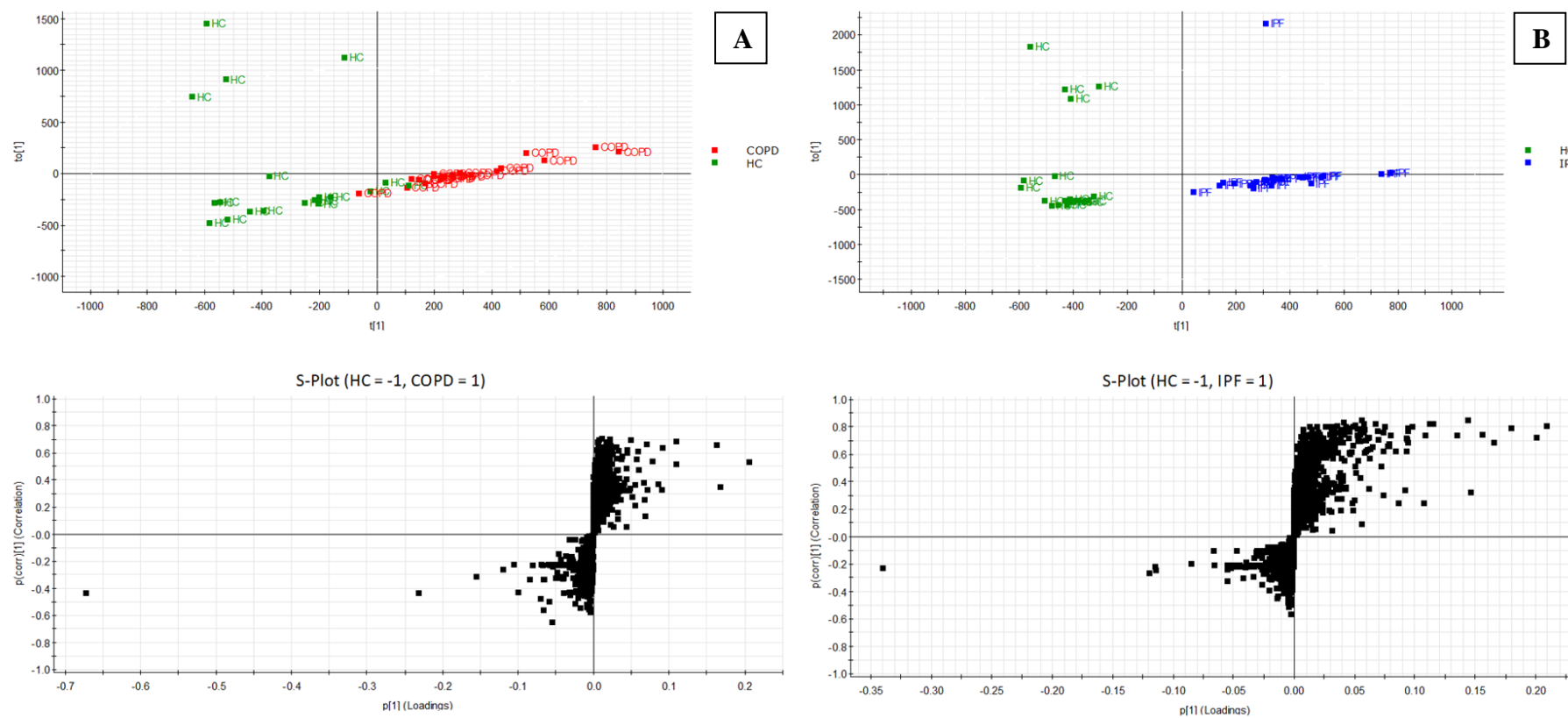


Figure 2.2 Orthogonal Projection to Latent Structure-Discriminant Analysis (OPLS-DA) models between HC and COPD samples (A), and HC and IPF samples (B). The S-plots generated from the respective OPLS-DA scores plots were presented directly below. Blue, green and red squares represent IPF samples, healthy controls and COPD samples, respectively.

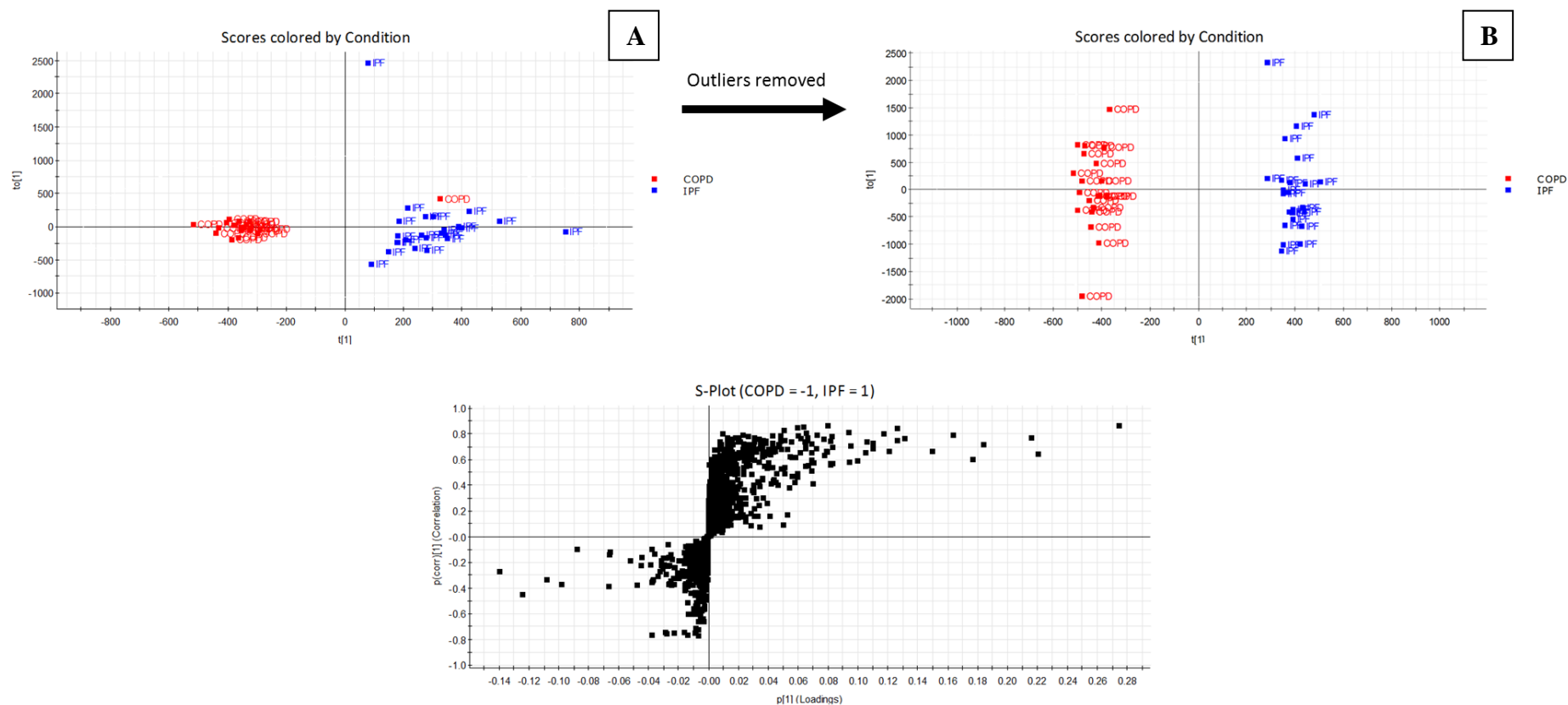


Figure 2.3 Orthogonal Projection to Latent Structure-Discriminant Analysis (OPLS-DA) models between COPD and IPF samples. The two observed outliers (COPD sample 6 and IPF sample 2) were removed and the OPLS-DA scores plot was fitted resulting in the model on the right. The S-plot generated from newly fitted OPLS-DA model was presented directly below. Red and blue squares represent COPD and IPF samples, respectively.

Table 2.1 The m/z values, putative identification and fold changes of features of interest derived using multivariate statistics and database matching. Additional filtering criteria including $CV < 30\%$, mass accuracy < 10 ppm and $VIP \geq 1$ were also applied.

Database	Feature m/z	Putative Identification	Fold Changes		
			COPD→HC	IPF→HC	IPF→COPD
LipidMAPS	281.2491	Linoleic acid	1.73	2.13	1.23
	255.2331	Palmitoleic acid	2.88	2.69	0.93
	283.2647	Oleic acid	2.15	2.48	1.15
	468.3122	Arachidonoyl tyrosine	1.30	0.85	0.65
	447.3488	Dihydrotestosterone	0.06	0.08	1.30
Biomolecules	281.2491	Linoleic acid	1.73	2.13	1.23
	255.2331	Palmitoleic acid	2.79	2.86	1.03
	283.2647	Oleic acid	2.06	2.53	1.23
	585.2721	Bilirubin	1.33	0.70	0.53
ChEBI	281.2491	Linoleic acid	1.73	2.13	1.23
	255.2331	Palmitoleic acid	2.79	2.86	1.03
	283.2647	Oleic acid	2.06	2.53	1.23
	447.3488	Dihydrotestosterone	0.06	0.08	1.36
	585.2721	Bilirubin	1.33	0.70	0.53
HMDB	281.2491	Linoleic acid	1.73	2.13	1.23
	255.2331	Palmitoleic acid	2.79	2.86	1.03
	283.2647	Oleic acid	2.06	2.53	1.23
	447.3488	Dihydrotestosterone	0.06	0.08	1.36
	223.0970	LysoPC	0.41	1.02	2.46
DrugBank	281.2491	Linoleic acid	1.73	2.13	1.23
	255.2331	Palmitoleic acid	2.79	2.86	1.03
	283.2647	Oleic acid	2.06	2.53	1.23

A total of 46 discriminative features were identified after the application of multivariate statistical analyses. Of these, four metabolic features with m/z 468.3122, m/z 496.3437, m/z 313.1556 and m/z 293.0996 were not identified due to unsuccessful library matching. Features m/z 281.2491, m/z 255.2331, m/z 283.2647 were putatively identified as linoleic acid, palmitoleic acid and oleic acid, respectively. Linoleic and oleic acids were shown to be consistently two-folds higher in COPD and IPF samples compared to the HC while palmitoleic acid was more than two-fold up-regulated in both disease cohorts. Two features were shown to be down-regulated; m/z 447.3488 was identified as dihydrotestosterone which was lower in abundance in COPD and IPF compared to HC while m/z 223.0970 was identified as a LysoPC and was approximately two-fold down-regulated in COPD compared to IPF and HC. Bilirubin and arachidonoyl tyrosine were assigned to feature m/z 585.2721 and m/z 468.3122 and showed approximately two-fold decreased in abundance for the IPF cohort compared to COPD and HC. Interestingly, all features with significant differences in abundance were either lipid mediators or constituents except for bilirubin. Of note, work published by Bulmer *et al.* (2013), Vogel *et al.* (2017) and Suh *et al.* (2018) described the potential association between bilirubin homeostasis and lipid pathophysiology in diseases such as Gilbert's syndrome, atherosclerosis and cardiovascular diseases. Bilirubin is an inert anti-oxidant which enhances the peroxisome proliferator-activated receptor alpha (PPAR α) signalling pathway involved in fatty acid beta-oxidation and is a major regulator of the energy metabolism (Stec *et al.*, 2016).

COPD and IPF are both chronic inflammatory disorders of the respiratory system which are characterized by excessive matrix degradation and tissue fibrosis. Clinical phenotypes of COPD and IPF are largely distinguished by airflow limitation, destruction of alveolar cells and pulmonary emphysema in COPD and parenchymal

scarring, alveolar wall thickening and restrictive lung function impairment in IPF. In this study, we have shown that both COPD and IPF were characterized by an increased presence of lipid constituents such as essential fatty acids sampled from circulating plasma.

Results from this study identified an upregulation of the levels of linoleic acid, palmitoleic acid and oleic acid in COPD and IPF compared to HC. De Castro *et al.* (2006), Gangopadhyay *et al.* (2012) and Titz *et al.* (2016) reported that lipid mediators, in particular linoleic acid and oleic acid, were up-regulated in blood samples from COPD patients. The work of Balgoma *et al.* (2016) also supported the findings of this current study by showing an increase in linoleic acid-derived lipid mediators in COPD bronchoalveolar lavage fluid (BALF) samples. Plasma linoleic, palmitoleic and oleic acids were also found to be elevated in patients suffering from interstitial lung disease (Steffen *et al.*, 2018) and cystic fibrosis (Durieu *et al.*, 2007). This increase in fatty acids suggested a tighter and more structured organisation of phospholipids within the plasma membrane resulting in lesser fluidity. Membrane fluidity in erythrocytes have been shown to decrease in COPD patients (Gangopadhyay *et al.*, 2012), causing the lipid rafts to become more tightly packed and less mobile in the plane of membranes leading to their dysfunction.

Linoleic acid can enzymatically produce epoxides via CYP activity which are further converted to leukotoxin and isoleukotoxin diols (Balgoma *et al.*, 2016). These diols have been shown to exert cytotoxicity as they decrease net ion flux in alveolar epithelial monolayers and increase intercellular junction permeability (Shen and Hammock, 2012). These are known to contribute to chronic bronchitis (Balgoma *et al.*, 2016). Chronic bronchitis is a prevalent clinical manifestation among COPD patients, especially within

the “smokers” cohort of the disease. The role of oleic acid as an inhibitor of the Na/K-ATPase activity have been demonstrated in rabbit lung model (Vadasz *et al.*, 2005), increasing endothelial permeability. Oleic acid has also been shown to induce acute respiratory distress syndrome (ARDS) in experimental models and lung injury were associated with elevated levels of lipid mediators (Akella *et al.*, 2014). Gonçalves-de-Albuquerque *et al.* (2012) suggested the participation of the Na/K-ATPase as the main target of oleic acid in the mechanism of ERK activation pathway in lung inflammation.

Although there are limited reports of palmitoleic acid in previous COPD or IPF studies, this FA may be an important biomarker of the disease as it is one of the most abundant FAs in serum, liver and adipose tissues (Frigolet, and Gutiérrez-Aguilar., 2017). This study found an approximate three-fold increase in plasma palmitoleic acid in patients suffering from COPD and IPF compared to HC. Palmitoleic acid have also been associated with some cancer types. Prostate and breast cancer risk and incidence were increased with augmented palmitoleic acid concentration in blood (Chavarro *et al.*, 2013; Pouchieu *et al.*, 2014). The correlation of palmitoleic acid in serum and plasma to variation within the SCD1 gene were shown to be associated with cancer mortality (Byberg *et al.*, (2014); Manni *et al.*, 2017). Mechanistically, SCD1 promotes cell survival through palmitoleic acid production and is hypothesised to be the underlying cause of cell proliferation and survival in cancer progression (Frigolet and Gutiérrez-Aguilar., 2017). Using a bleomycin-induced fibrosis in a mice lung model, Sunaga *et al.* (2013) reported an increase in palmitoleic acid when elongation of the long chain fatty acids (Elovl6) rate-limiting enzyme is deficient. Elovl6 deficiency leads to the apoptotic effect of alveolar type 2 cells and caspase 3 activation in the lung, which result in the initiation and progression of fibrosis (Sunaga *et al.*, 2013).

Interestingly, this study also showed that dihydrotestosterone was severely down-regulated in patients with COPD and IPF by approximately 90%. Dihydrotestosterone and its 5 α -reductase precursor, testosterone, are the predominant androgens in mammals. Testosterone levels have been shown to be reduced in patients with asthma (Canguven and Albayrak, 2011; Montano *et al.*, 2014), cystic fibrosis (Leifke *et al.*, 2003; Blackman and Tangpricha, 2016), hypoxic pulmonary fibrosis (Semple *et al.*, 1984) and COPD (Svartberg *et al.*, 2007; Laghi *et al.*, 2009; Mousavi *et al.*, 2012; Corbo *et al.*, 2014). The relaxant effect of testosterone may be important for understanding the pathophysiology of these lung diseases as it has been shown to affect the responsiveness of tracheal smooth muscles as well as the integrity of epithelium (Kouloumenta *et al.*, 2009).

Factors that decrease testosterone levels in patients with COPD includes smoking, systemic inflammation and ageing (Laghi *et al.*, 2009; Daabis *et al.*, 2016). Testosterone deficiency along with the aforementioned risk factors can exacerbate COPD symptoms through a direct impact on respiratory muscles, diminishing overall strength and breathing capacity. An *in vivo* study conducted by Montano *et al.* (2014) showed that low circulatory testosterone and its metabolite, dihydrotestosterone was positively associated with reduced lung function in guinea pigs with allergic asthma. Furthermore, these androgens have been shown to induce relaxation of airway smooth muscle and mediated via decreased Ca²⁺ influx through the L-type Ca²⁺ channels in tracheal myocytes. Testosterone supplementation have also improved skeletal muscle strength and exercise capacity in COPD patients by acting as bronchoactive compounds to prevent airway spasm (Laghi *et al.*, 2009; Baillargeon *et al.*, 2018).

Like testosterone, LysoPC may also be associated with Ca^{2+} sensitisation in tracheal myocytes. LysoPCs are involved in eosinophils infiltration and bronchoconstriction (Nishiyama *et al.*, 2014), and studies by Kume *et al.* (2001), Nobata *et al.* (2005) and Bansal *et al.* (2016) linked LysoPC to the allergic cascade in airway diseases like asthma. These studies showed LysoPC-induced expression of various adhesion molecules on the vascular endothelium and increases permeability, which led to inflammation in the lungs. However, the LysoPC levels reported were higher in the asthmatic cohort as opposed to the down-regulation observed in our study. Yoder *et al.* (2014) also supported the increased level of LysoPC by demonstrating the elevation in BALF samples of asthmatic patients. A lung cancer biomarker study by Dong *et al.* (2011) reported a decrease of LysoPCs in plasma samples. LysoPCs can be converted to phosphatidylcholines by LysoPC acyltransferase in the lung surfactant, where lung surface tension is maintained to preserve essential respiratory functions. Although there were no changes in LysoPC levels between IPF and HC, the two-fold increase between IPF and COPD was indicative of LysoPC's emerging role in IPF pathogenesis. Rindlisbacher *et al.* (2018) consistently found elevated amounts of LysoPC in serum samples from IPF patients compared to healthy individuals. LysoPC is also a precursor of lysophosphatidic acid (LPA), a bioactive glycerophospholipid. LPA has been shown to induce fibrosis in the lungs and other organs including kidney and liver via epithelial cell death, vascular leakage and fibroblastic proliferation (Tager *et al.*, 2008; Kaffe *et al.*, 2016; Alsafadi *et al.*, 2017; Sakai *et al.*, 2017).

There appeared to be no difference between the levels of bilirubin and arachidonoyl tyrosine in COPD and HC samples. However, the levels of both compounds were found to be down-regulated in the IPF cohort compared to both HC and COPD. In the haem degradation pathway, haem oxygenase converts haem to biliverdin which is then

converted to bilirubin using biliverdin reductase before being excreted (Ye *et al.*, 2008; Zhao *et al.*, 2017). Haem oxygenase and bilirubin are considered to be oxidative stress responsive molecules involved in the pathogenesis of lung diseases such as hypersensitivity pneumonitis, sarcoidosis, lung cancer, COPD and IPF (Ye *et al.*, 2008; Horsfall *et al.*, 2011; Curjuric *et al.*, 2014; Brown *et al.*, 2017; Zhao *et al.*, 2017). Their role in the pathogenesis of IPF may be explained in two ways: the downregulation may either serve as an adaptive mechanism to protect the tissue against harmful effects of haem degradation products (Ye *et al.*, 2008), or it may indicate a loss of protection against oxidative stress (Curjuric *et al.*, 2014). The beneficial effects of serum bilirubin on respiratory outcomes have been reported in several lung studies. High serum bilirubin was associated with lower cancer mortality, including that of lung cancer (Brown *et al.*, 2017). Horsfall *et al.* (2011) demonstrated that higher levels of bilirubin were associated with a lower risk of respiratory diseases such as lung cancer and COPD and caused mortality among patients with normal-range bilirubin levels in primary care practices in the United Kingdom. Zhao *et al.* (2017) showed that an up-regulation of haem degradation pathway that supported the hypothesis of an oxidant-antioxidant imbalance in the pathogenesis of IPF.

We have also identified an endogenous lipid, arachidonoyl tyrosine, responsible for N-arachidonoyl dopamine (NADA) biosynthesis. NADA plays an important role in pain and inflammation and its synthesis primarily occurs through an enzyme-mediated conjugation of arachidonic acid with dopamine (Grabiec and Dehghani, 2017). A study by Wilhelmsen *et al.* (2014) demonstrated that a reduction in NADA led to inflammatory responses in human lung microvascular endothelial cells. The study also reported the ability of inflammatory agonists such as bacterial lipopeptides and tumour necrotic factor-alpha (TNF- α) dampened the activation of the primary endothelial cells.

Although NADA was not detected in our study, the down-regulation of its precursor arachidonoyl tyrosine may potentially contribute to the inflammatory response in IPF.

In this study, we identified a number of unique lipid mediators including linoleic, palmitoleic and oleic acids that suggest dysregulated metabolic pathways associated with lung inflammation and progression of fibrosis (Sunaga *et al.*, 2013; Daabis *et al.*, 2016). The analysis also detected arachidonoyl tyrosine, bilirubin, dihydrotestosterone and lysoPC, metabolites that play key roles in regulating the lung energy metabolism (Brown *et al.*, 2017; Zhao *et al.*, 2017). While the OPLS-DA approach provided robust classification models, a separate validation study is required to confirm these findings. Future correlation studies incorporating patient demographics and metadata (Supplementary Table 2.1) will also strengthen the multivariate statistical models as well as aid in disease stratification. Targeted analysis and data-independent acquisition strategies reported by Gethings *et al.* (2017) and Moseley *et al.* (2018) can also be used to provide qualitative and quantitative measurements to establish reference levels of disease.

2.5 Conclusion

COPD and IPF are complex lung disorders that are poorly defined to their heterogeneous phenotypes and poses considerable challenges in the development of accurate diagnostics. Here, we showed that untargeted profiling of plasma by UHPLC-QTOF-MS followed by the application of multivariate statistics provided an efficient and robust metabolomics pipeline for the investigation of plasma from different pulmonary conditions. The multivariate statistical models generated were able to discriminate diseased patients from healthy controls. In addition, this study also showed potential dysregulation of the cellular energy metabolism in COPD and IPF based on the identification of metabolites that are associated with increased inflammation and oxidative stress in the lung.

2.6 References

- Akella, A., P. Sharma, R. Pandey and S. B. Deshpande (2014). "Characterization of oleic acid-induced acute respiratory distress syndrome model in rat." Indian Journal of Experimental Biology 52(7): 712-719.
- Alsafadi, H. N., C. A. Staab-Weijnitz, M. Lehmann, M. Lindner, B. Peschel, M. Königshoff and D. E. Wagner (2017). "An ex vivo model to induce early fibrosis-like changes in human precision-cut lung slices." American Journal of Physiology-Lung Cellular and Molecular Physiology 312(6): L896-L902.
- Baillargeon, J., R. J. Urban, W. Zhang, M. F. Zaiden, Z. Javed, M. Sheffield-Moore, Y.-F. Kuo and G. Sharma (2018). "Testosterone replacement therapy and hospitalization rates in men with COPD." Chronic Respiratory Disease: 1479972318793004.
- Balgoma, D., M. Yang, M. Sjödin, S. Snowden, R. Karimi, B. Levänen, H. Merikallio, R. Kaarteenaho, L. Palmberg, K. Larsson, D. J. Erle, S.-E. Dahlén, B. Dahlén, C. M. Sköld, Å. M. Wheelock and C. E. Wheelock (2016). "Linoleic acid-derived lipid mediators increase in a female-dominated subphenotype of COPD." European Respiratory Journal 47(6): 1645.
- Bansal, P., S. N. Gaur and N. Arora (2016). "Lysophosphatidylcholine plays critical role in allergic airway disease manifestation." Scientific reports 6: 27430-27430.
- Blackman, S. M. and V. Tangpricha (2016). "Endocrine Disorders in Cystic Fibrosis." Pediatric clinics of North America 63(4): 699-708.
- Bowler, R. P., C. H. Wendt, M. B. Fessler, M. W. Foster, R. S. Kelly, J. Lasky-Su, A. J. Rogers, K. A. Stringer and B. W. Winston (2017). "New Strategies and Challenges in Lung Proteomics and Metabolomics. An Official American

- Thoracic Society Workshop Report." Annals of American Thoracic Society 14(12): 1721-1743.
- Broadhurst, D., R. Goodacre, S. N. Reinke, J. Kuligowski, I. D. Wilson, M. R. Lewis and W. B. Dunn (2018). "Guidelines and considerations for the use of system suitability and quality control samples in mass spectrometry assays applied in untargeted clinical metabolomic studies." Metabolomics 14(6): 72.
- Brown, K. E., D. D. Sin, H. Voelker, J. E. Connett, D. E. Niewoehner, K. M. Kunisaki and C. C. R. Network (2017). "Serum bilirubin and the risk of chronic obstructive pulmonary disease exacerbations." Respiratory research 18(1): 179-179.
- Bulmer, A. C., H. J. Verkade and K. H. Wagner (2013). "Bilirubin and beyond: a review of lipid status in Gilbert's syndrome and its relevance to cardiovascular disease protection." Progress in Lipid Research 52(2): 193-205.
- Byberg, L., L. Kilander, E. Warensjo Lemming, K. Michaelsson and B. Vessby (2014). "Cancer death is related to high palmitoleic acid in serum and to polymorphisms in the SCD-1 gene in healthy Swedish men." American Journal of Clinical Nutrition 99(3): 551-558.
- Canguven, O. and S. Albayrak (2011). "Do low testosterone levels contribute to the pathogenesis of asthma?" Medical Hypotheses 76(4): 585-588.
- Chavarro, J. E., S. A. Kenfield, M. J. Stampfer, M. Loda, H. Campos, H. D. Sesso and J. Ma (2013). "Blood levels of saturated and monounsaturated fatty acids as markers of de novo lipogenesis and risk of prostate cancer." American journal of epidemiology 178(8): 1246-1255.
- Chilosi, M., V. Poletti and A. Rossi (2012). "The pathogenesis of COPD and IPF: distinct horns of the same devil?" Respiratory research 13(1): 3-3.

- Corbo, G. M., A. Di Marco Berardino, A. Mancini, R. Inchingolo, A. Smargiassi, S. Raimondo and S. Valente (2014). "Serum level of testosterone, dihydrotestosterone and IGF-1 during an acute exacerbation of COPD and their relationships with inflammatory and prognostic indices: a pilot study." Minerva Medicine 105(4): 289-294.
- Cruickshank-Quinn, C., R. Powell, S. Jacobson, K. Kechris, R. P. Bowler, I. Petrache and N. Reisdorph (2017). "Metabolomic similarities between bronchoalveolar lavage fluid and plasma in humans and mice." Scientific Reports 7(1): 5108.
- Curjuric, I., M. Imboden, M. Adam, R. W. Bettschart, M. W. Gerbase, N. Künzli, T. Rochat, L. Rohrer, T. B. Rothe, J. Schwartz, D. Stolz, J.-M. Tschopp, A. von Eckardstein, F. Kronenberg and N. M. Probst-Hensch (2014). "Serum bilirubin is associated with lung function in a Swiss general population sample." European Respiratory Journal 43(5): 1278.
- Daabis, R. G., R. N. Abdel Rehem, M. M. Hassan and G. I. Khalil (2016). "Hypogonadism in patients with chronic obstructive pulmonary disease: relationship with airflow limitation, muscle weakness and systemic inflammation." Alexandria Journal of Medicine 52(1): 27-33.
- De Castro, J., A. Hernández-Hernández, M. C. Rodríguez, J. L. Sardina, M. Llanillo and J. Sánchez-Yagüe (2007). "Comparison of changes in erythrocyte and platelet phospholipid and fatty acid composition and protein oxidation in chronic obstructive pulmonary disease and asthma." Platelets 18(1): 43-51.
- Dong J, C. X.-m., ZOU Li-juan, CHEN Cheng, XUE Xing-ya, ZHANG Xiu-li* and L. Xin-miao* (2011). "Lysophosphatidylcholine Biomarkers of Lung Cancer Detected by Ultra-performance Liquid Chromatography Coupled with Quadrupole Time-of-flight Mass Spectrometry." CHEMICAL RESEARCH IN CHINESE UNIVERSITIES 27(5): 750-755.

- Dunn, W. B., I. D. Wilson, A. W. Nicholls and D. Broadhurst (2012). "The importance of experimental design and QC samples in large-scale and MS-driven untargeted metabolomic studies of humans." Bioanalysis 4(18): 2249-2264.
- Durieu, I., F. Abbas-Chorfa, J. Draï, J. Iwaz, J. P. Steghens, M. Puget, R. Ecochard and G. Bellon (2007). "Plasma fatty acids and lipid hydroperoxides increase after antibiotic therapy in cystic fibrosis." European Respiratory Journal 29(5): 958.
- Frigolet, M. E. and R. Gutierrez-Aguilar (2017). "The Role of the Novel Lipokine Palmitoleic Acid in Health and Disease." Advances in Nutrition 8(1): 173S-181S.
- Fujii, K., H. Nakamura and T. Nishimura (2017). "Recent mass spectrometry-based proteomics for biomarker discovery in lung cancer, COPD, and asthma." Expert Reviews of Proteomics 14(4): 373-386.
- Gangopadhyay, S., V. K. Vijayan and S. K. Bansal (2012). "Lipids of Erythrocyte Membranes of COPD Patients: A Quantitative and Qualitative Study." COPD: Journal of Chronic Obstructive Pulmonary Disease 9(4): 322-331.
- Gethings, L. A., K. Richardson, J. Wildgoose, S. Lennon, S. Jarvis, C. L. Bevan, J. P. C. Vissers and J. I. Langridge (2017). "Lipid profiling of complex biological mixtures by liquid chromatography/mass spectrometry using a novel scanning quadrupole data-independent acquisition strategy." Rapid Communications in Mass Spectrometry 31(19): 1599-1606.
- Gonçalves-de-Albuquerque, C. F., A. R. Silva, P. Burth, I. M. M. de Moraes, F. M. d. J. Oliveira, M. Younes-Ibrahim, M. d. C. B. dos Santos, H. D'Ávila, P. T. Bozza, H. C. d. C. Faria Neto and M. V. d. C. Faria (2012). "Oleic acid induces lung injury in mice through activation of the ERK pathway." Mediators of inflammation 2012: 956509-956509.

- Grabiec, U. and F. Dehghani (2017). "N-Arachidonoyl Dopamine: A Novel Endocannabinoid and Endovanilloid with Widespread Physiological and Pharmacological Activities." Cannabis and cannabinoid research 2(1): 183-196.
- Horsfall, L. J., G. Rait, K. Walters and et al. (2011). "Serum bilirubin and risk of respiratory disease and death." JAMA 305(7): 691-697.
- Kaffe, E., A. Katsifa, N. Xylourgidis, I. Ninou, M. Zannikou, V. Harokopos, P. Foka, A. Dimitriadis, K. Evangelou, A. N. Moulas, U. Georgopoulou, V. G. Gorgoulis, G. N. Dalekos and V. Aidinis (2017). "Hepatocyte autotaxin expression promotes liver fibrosis and cancer." Hepatology 65(4): 1369-1383.
- Kang, Y. P., S. B. Lee, J.-m. Lee, H. M. Kim, J. Y. Hong, W. J. Lee, C. W. Choi, H. K. Shin, D.-J. Kim, E. S. Koh, C.-S. Park, S. W. Kwon and S.-W. Park (2016). "Metabolic Profiling Regarding Pathogenesis of Idiopathic Pulmonary Fibrosis." Journal of Proteome Research 15(5): 1717-1724.
- Kouloumenta, V., A. Hatziefthimiou, E. Paraskeva, K. Gourgoulisanis and P. A. Molyvdas (2006). "Non-genomic effect of testosterone on airway smooth muscle." British Journal of Pharmacology 149(8): 1083-1091.
- Kume, H., S. Ito, Y. Ito and K. Yamaki (2001). "Role of lysophosphatidylcholine in the desensitization of beta-adrenergic receptors by Ca(2+) sensitization in tracheal smooth muscle." American Journal of Respiratory Cell and Molecular Biology 25(3): 291-298.
- Kusko, R. L., J. F. Brothers, 2nd, J. Tedrow, K. Pandit, L. Huleihel, C. Perdomo, G. Liu, B. Juan-Guardela, D. Kass, S. Zhang, M. Lenburg, F. Martinez, J. Quackenbush, F. Scieurba, A. Limper, M. Geraci, I. Yang, D. A. Schwartz, J. Beane, A. Spira and N. Kaminski (2016). "Integrated Genomics Reveals Convergent Transcriptomic Networks Underlying Chronic Obstructive Pulmonary Disease

- and Idiopathic Pulmonary Fibrosis." American journal of respiratory and critical care medicine 194(8): 948-960.
- Laghi, F., N. Adiguzel and M. J. Tobin (2009). "Endocrinological derangements in COPD." European Respiratory Journal 34(4): 975.
- Leifke, E., M. Friemert, M. Heilmann, N. Puvogel, C. Smaczny, A. von zur Muhlen and G. Brabant (2003). "Sex steroids and body composition in men with cystic fibrosis." European Journal of Endocrinology 148(5): 551-557.
- Leung, J. M., V. Chen, Z. Hollander, D. Dai, S. J. Tebbutt, S. D. Aaron, K. L. Vandemheen, S. I. Rennard, J. M. FitzGerald, P. G. Woodruff, S. C. Lazarus, J. E. Connett, H. O. Coxson, B. Miller, C. Borchers, B. M. McManus, R. T. Ng and D. D. Sin (2016). "COPD Exacerbation Biomarkers Validated Using Multiple Reaction Monitoring Mass Spectrometry." PloS one 11(8): e0161129-e0161129.
- Lin, H. and S. Jiang (2015). "Combined pulmonary fibrosis and emphysema (CPFE): an entity different from emphysema or pulmonary fibrosis alone." Journal of thoracic disease 7(4): 767-779.
- Maniscalco, M., D. Paris, D. J. Melck, A. Molino, M. Carone, P. Ruggeri, G. Caramori and A. Motta (2018). "Differential diagnosis between newly diagnosed asthma and COPD using exhaled breath condensate metabolomics: a pilot study." European Respiratory Journal 51(3).
- Manni, A., J. P. Richie, S. E. Schetter, A. Calcagnotto, N. Trushin, C. Aliaga and K. El-Bayoumy (2017). "Stearoyl-CoA desaturase-1, a novel target of omega-3 fatty acids for reducing breast cancer risk in obese postmenopausal women." European Journal of Clinical Nutrition 71(6): 762-765.

- Montano, L. M., J. Espinoza, E. Flores-Soto, J. Chavez and M. Perusquia (2014). "Androgens are bronchoactive drugs that act by relaxing airway smooth muscle and preventing bronchospasm." Journal of Endocrinology 222(1): 1-13.
- Moseley, M. A., C. J. Hughes, P. R. Juvvadi, E. J. Soderblom, S. Lennon, S. R. Perkins, J. W. Thompson, W. J. Steinbach, S. J. Geromanos, J. Wildgoose, J. I. Langridge, K. Richardson and J. P. C. Vissers (2018). "Scanning Quadrupole Data-Independent Acquisition, Part A: Qualitative and Quantitative Characterization." Journal of Proteome Research 17(2): 770-779.
- Mousavi, S. A.-J., M.-R. Kouchari, S. H. Samdani-Fard, Z. N. Gilvae and M. Arabi (2012). "Relationship between Serum Levels of Testosterone and the Severity of Chronic Obstructive Pulmonary Disease." Tanaffos 11(3): 32-35.
- Naz, S., J. Kolmert, M. Yang, S. N. Reinke, Muhammad A. Kamleh, S. Snowden, T. Heyder, B. Levänen, D. J. Erle, C. M. Sköld, Å. M. Wheelock and C. E. Wheelock (2017). "Metabolomics analysis identifies sex-associated metabolotypes of oxidative stress and the autotaxin–lysoPA axis in COPD." European Respiratory Journal 49(6).
- Ni, Y., M. Su, J. Lin, X. Wang, Y. Qiu, A. Zhao, T. Chen and W. Jia (2008). "Metabolic profiling reveals disorder of amino acid metabolism in four brain regions from a rat model of chronic unpredictable mild stress." FEBS Letters 582(17): 2627-2636.
- Nishiyama, O., H. Kume, M. Kondo, Y. Ito, M. Ito and K. Yamaki (2004). "Role of lysophosphatidylcholine in eosinophil infiltration and resistance in airways." Clinical and Experimental Pharmacology and Physiology 31(3): 179-184.
- Niu, R., Y. Liu, Y. Zhang, Y. Zhang, H. Wang, Y. Wang, W. Wang and X. Li (2017). "iTRAQ-Based Proteomics Reveals Novel Biomarkers for Idiopathic Pulmonary Fibrosis." PLOS ONE 12(1): e0170741.

- Nobata, K., K. Kurashima, M. Fujimura, M. Abo, Y. Ishiura, K. Kasahara and S. Nakao (2005). "Inhaled lysophosphatidylcholine provokes bronchoconstriction in guinea pigs in vivo." European Journal of Pharmacology 520(1-3): 150-155.
- Papaioannou, O., T. Karampitsakos, I. Barbayianni, S. Chrysikos, N. Xylourgidis, V. Tzilas, D. Bouros, V. Aidinis and A. Tzouvelekis (2018). "Metabolic Disorders in Chronic Lung Diseases." Frontiers in medicine 4: 246-246.
- Pouchieu, C., V. Chajès, F. Laporte, E. Kesse-Guyot, P. Galan, S. Hercberg, P. Latino-Martel and M. Touvier (2014). "Prospective associations between plasma saturated, monounsaturated and polyunsaturated fatty acids and overall and breast cancer risk - modulation by antioxidants: a nested case-control study." PloS one 9(2): e90442-e90442.
- Reinke, S. N., H. Gallart-Ayala, C. Gómez, A. Checa, A. Fauland, S. Naz, M. A. Kamleh, R. Djukanović, T. S. C. Hinks and C. E. Wheelock (2017). "Metabolomics analysis identifies different metabotypes of asthma severity." European Respiratory Journal 49(3).
- Rindlisbacher, B., C. Schmid, T. Geiser, C. Bovet and M. Funke-Chambour (2018). "Serum metabolic profiling identified a distinct metabolic signature in patients with idiopathic pulmonary fibrosis - a potential biomarker role for LysoPC." Respiratory research 19(1): 7-7.
- Sakai, N., J. Chun, J. S. Duffield, D. Lagares, T. Wada, A. D. Luster and A. M. Tager (2017). "Lysophosphatidic acid signaling through its receptor initiates profibrotic epithelial cell fibroblast communication mediated by epithelial cell derived connective tissue growth factor." Kidney International 91(3): 628-641.
- Semple, P. D., G. H. Beastall, T. M. Brown, K. W. Stirling, R. J. Mills and W. S. Watson (1984). "Sex hormone suppression and sexual impotence in hypoxic pulmonary fibrosis." Thorax 39(1): 46-51.

- Shen, H. C. and B. D. Hammock (2012). "Discovery of Inhibitors of Soluble Epoxide Hydrolase: A Target with Multiple Potential Therapeutic Indications." Journal of Medicinal Chemistry 55(5): 1789-1808.
- Stec, D. E., K. John, C. J. Trabbic, A. Luniwal, M. W. Hankins, J. Baum and T. D. Hinds, Jr. (2016). "Bilirubin Binding to PPAR α Inhibits Lipid Accumulation." PLOS ONE 11(4): e0153427.
- Steffen, B., A. Podolanczuk, S. Kawut, G. Raghu, E. Hoffman, M. Tsai, R. G. Barr and D. "Lederer Association Between Plasma Polyunsaturated Fatty Acids and Subclinical Interstitial Lung Disease: The MESA Study." A23. ILD: DIAGNOSIS: A1101-A1101.
- Suh, S., Y. R. Cho, M. K. Park, D. K. Kim, N. H. Cho and M.-K. Lee (2018). "Relationship between serum bilirubin levels and cardiovascular disease." PLOS ONE 13(2): e0193041.
- Sunaga, H., H. Matsui, M. Ueno, T. Maeno, T. Iso, M. R. A. A. Syamsunarno, S. Anjo, T. Matsuzaka, H. Shimano, T. Yokoyama and M. Kurabayashi (2013). "Deranged fatty acid composition causes pulmonary fibrosis in Elovl6-deficient mice." Nature Communications 4: 2563.
- Svartberg, J., H. Schirmer, A. Medbø, H. Melbye and U. Aasebø (2007). "Reduced pulmonary function is associated with lower levels of endogenous total and free testosterone. The Tromsø Study." European Journal of Epidemiology 22(2): 107.
- Tager, A. M., P. LaCamera, B. S. Shea, G. S. Campanella, M. Selman, Z. Zhao, V. Polosukhin, J. Wain, B. A. Karimi-Shah, N. D. Kim, W. K. Hart, A. Pardo, T. S. Blackwell, Y. Xu, J. Chun and A. D. Luster (2007). "The lysophosphatidic acid receptor LPA1 links pulmonary fibrosis to lung injury by mediating fibroblast recruitment and vascular leak." Nature Medicine 14: 45.

- Titz, B., K. Luettich, P. Leroy, S. Boue, G. Vuillaume, T. Vihervaara, K. Ekroos, F. Martin, M. C. Peitsch and J. Hoeng (2016). "Alterations in Serum Polyunsaturated Fatty Acids and Eicosanoids in Patients with Mild to Moderate Chronic Obstructive Pulmonary Disease (COPD)." International journal of molecular sciences 17(9): 1583.
- Vadasz, I., R. E. Morty, M. G. Kohstall, A. Olschewski, F. Grimminger, W. Seeger and H. A. Ghofrani (2005). "Oleic acid inhibits alveolar fluid reabsorption: a role in acute respiratory distress syndrome?" American Journal of Respiratory and Critical Care Medicine 171(5): 469-479.
- Vogel, M. E., G. Idelman, S. Konaniah Eddy and D. Zucker Stephen "Bilirubin Prevents Atherosclerotic Lesion Formation in Low - Density Lipoprotein Receptor - Deficient Mice by Inhibiting Endothelial VCAM - 1 and ICAM - 1 Signaling." Journal of the American Heart Association 6(4): e004820.
- Wehrens, R., J. A. Hageman, F. van Eeuwijk, R. Kooke, P. J. Flood, E. Wijnker, J. J. B. Keurentjes, A. Lommen, H. D. L. M. van Eekelen, R. D. Hall, R. Mumm and R. C. H. de Vos (2016). "Improved batch correction in untargeted MS-based metabolomics." Metabolomics: Official journal of the Metabolomic Society 12: 88-88.
- Wilhelmsen, K., S. Khakpour, A. Tran, K. Sheehan, M. Schumacher, F. Xu and J. Hellman (2014). "The endocannabinoid/endovanilloid N-arachidonoyl dopamine (NADA) and synthetic cannabinoid WIN55,212-2 abate the inflammatory activation of human endothelial cells." The Journal of biological chemistry 289(19): 13079-13100.
- Worley, B. and R. Powers (2013). "Multivariate Analysis in Metabolomics." Current Metabolomics 1(1): 92-107.

- Ye, Q., Y. Dalavanga, N. Poulakis, S. U. Sixt, J. Guzman and U. Costabel (2008). "Decreased expression of haem oxygenase-1 by alveolar macrophages in idiopathic pulmonary fibrosis." European Respiratory Journal 31(5): 1030.
- Yoder, M., Y. Zhuge, Y. Yuan, O. Holian, S. Kuo, R. van Breemen, L. L. Thomas and H. Lum (2014). "Bioactive lysophosphatidylcholine 16:0 and 18:0 are elevated in lungs of asthmatic subjects." Allergy, asthma & immunology research 6(1): 61-65.
- Zhao, Y. D., L. Yin, S. Archer, C. Lu, G. Zhao, Y. Yao, L. Wu, M. Hsin, T. K. Waddell, S. Keshavjee, J. Granton and M. de Perrot (2017). "Metabolic heterogeneity of idiopathic pulmonary fibrosis: a metabolomic study." BMJ Open Respiratory Research 4(1).

Supplementary Table 2.1 Patient demographics and clinical characteristics including sex, age, history of smoking as well as c-reactive protein (CRP), soluble tumour necrosis factor receptor-1 (sTNFR1), forced expiratory volume in 1 sec (FEV1) and forced vital capacity (FVC) levels.

	Sex	Age	Smoking	CRP (mg/L)	sTNFR1 (pg/mL)	FEV1 (L)	FEV1 (%)	FVC	FVC %	FEV1/FVC ratio
Healthy subjects										
1	Male	63	non-smoker	0.06	588	n/a	n/a	n/a	n/a	n/a
2	Female	57	non-smoker	0.06	513	n/a	n/a	n/a	n/a	n/a
3	Male	63	non-smoker	0.89	767	n/a	n/a	n/a	n/a	n/a
4	Male	60	non-smoker	4.46	480	n/a	n/a	n/a	n/a	n/a
5	Female	54	non-smoker	6.14	413	n/a	n/a	n/a	n/a	n/a
6	Male	90	non-smoker	0.65	642	n/a	n/a	n/a	n/a	n/a
7	Female	77	non-smoker	0.80	652	n/a	n/a	n/a	n/a	n/a
8	Male	56	non-smoker	5.96	557	n/a	n/a	n/a	n/a	n/a
9	Male	61	non-smoker	0.84	715	n/a	n/a	n/a	n/a	n/a
10	Female	77	non-smoker	0.40	502	n/a	n/a	n/a	n/a	n/a
11	Male	78	ex-smoker	0.39	477	n/a	n/a	n/a	n/a	n/a
12	Male	84	ex-smoker	0.58	410	n/a	n/a	n/a	n/a	n/a
13	Male	75	never smoked	1.01	621	n/a	n/a	n/a	n/a	n/a
14	Male	78	ex-smoker	0.69	374	n/a	n/a	n/a	n/a	n/a
15	Female	74	never smoked	1.00	517	n/a	n/a	n/a	n/a	n/a
16	Male	76	ex-smoker	2.34	737	n/a	n/a	n/a	n/a	n/a
17	Female	76	ex-smoker	0.41	529	n/a	n/a	n/a	n/a	n/a
18	Male	83	never smoked	7.12	622	n/a	n/a	n/a	n/a	n/a
19	Female	80	never smoked	0.85	524	n/a	n/a	n/a	n/a	n/a
20	Female	77	ex-smoker	2.02	443	n/a	n/a	n/a	n/a	n/a

COPD patients

1	Male	64	ex-smoker	10.73	297	2.07	55%	3.80	75%	0.54
2	Male	83	ex-smoker	6.95	901	0.57	25%	n/a	n/a	n/a
3	Male	69	ex-smoker	11.23	503	1.01	34%	3.26	81%	0.31
4	Male	84	ex-smoker	45.21	990	1.19	63%	2.49	89%	0.48
5	Female	77	ex-smoker	5.80	468	0.77	38%	2.68	99%	0.29
6	Female	60	ex-smoker	5.24	630	0.99	41%	2.97	95%	0.33
7	Male	70	ex-smoker	2.52	351	0.60	21%	2.79	71%	0.22
8	Female	77	ex-smoker	2.84	563	0.63	42%	1.28	63%	0.49
9	Male	75	ex-smoker	2.84	365	1.13	47%	2.66	79%	0.42
10	Male	76	ex-smoker	8.67	518	0.83	30%	2.28	60%	0.36
11	Male	82	ex-smoker	6.26	599	0.99	34%	2.27	56%	0.44
12	Male	82	ex-smoker	3.02	650	1.29	54%	2.90	84%	0.44
13	Male	79	ex-smoker	26.15	1432	0.73	31%	n/a	n/a	n/a
14	Male	69	ex-smoker	26.61	449	0.86	25%	n/a	n/a	n/a
15	Male	65	ex-smoker	2.81	558	1.45	42%	4.12	89%	0.35
16	Male	69	ex-smoker	38.10	854	1.43	45%	2.88	66%	0.50
17	Female	89	ex-smoker	177.83	1321	0.67	41%	1.88	85%	0.36
18	Female	79	ex-smoker	2.64	760	0.81	49%	1.55	69%	0.52
19	Female	66	ex-smoker	11.69	504	0.64	26%	1.92	59%	0.33
20	Male	81	ex-smoker	12.64	662	1.75	74%	3.56	106%	0.49

IPF patients

1	Male	64	ex-smoker	n/a	n/a	n/a	n/a	2.79	68	n/a
2	Male	73	ex-smoker	n/a	n/a	n/a	n/a	1.38	59	n/a
3	Male	75	ex-smoker	n/a	n/a	n/a	n/a	2.84	67	n/a

4	Male	69	ex-smoker	n/a	n/a	n/a	n/a	2.31	64	n/a
5	Male	79	only teen	n/a	n/a	n/a	n/a	2.65	103	n/a
6	Male	71	ex-smoker	n/a	n/a	n/a	n/a	3.7	85.1	n/a
7	Female	71	ex-smoker	n/a	n/a	n/a	n/a	2.53	95.5	n/a
8	Male	67	3 pack/years	n/a	n/a	n/a	n/a	3.43	79	n/a
9	Male	74	ex-smoker	n/a	n/a	n/a	n/a	2.18	60	n/a
10	Male	63	ex-smoker	n/a	n/a	n/a	n/a	1.56	48	n/a
11	Male	73	ex-smoker	n/a	n/a	n/a	n/a	4.09	83	n/a
12	Male	60	never smoked	n/a	n/a	n/a	n/a	3.63	69	n/a
13	Male	63	ex-smoker	n/a	n/a	n/a	n/a	2.7	69	n/a
14	Male	66	ex-smoker	n/a	n/a	n/a	n/a	1.72	38	n/a
15	n/a	n/a	n/a	n/a	n/a	n/a	n/a	n/a	n/a	n/a
16	n/a	n/a	n/a	n/a	n/a	n/a	n/a	n/a	n/a	n/a
17	n/a	n/a	n/a	n/a	n/a	n/a	n/a	n/a	n/a	n/a
18	n/a	n/a	n/a	n/a	n/a	n/a	n/a	n/a	n/a	n/a
19	n/a	n/a	n/a	n/a	n/a	n/a	n/a	n/a	n/a	n/a
20	n/a	n/a	n/a	n/a	n/a	n/a	n/a	n/a	n/a	n/a
21	n/a	n/a	n/a	n/a	n/a	n/a	n/a	n/a	n/a	n/a
22	n/a	n/a	n/a	n/a	n/a	n/a	n/a	n/a	n/a	n/a
23	n/a	n/a	n/a	n/a	n/a	n/a	n/a	n/a	n/a	n/a
24	n/a	n/a	n/a	n/a	n/a	n/a	n/a	n/a	n/a	n/a

Supplementary Table 2.2 The m/z values, chemical formulas, mass error, percentage isotopic similarities, ANOVA p -values as well as the mean abundances, relative standard deviations and fold changes of metabolite features annotated using LIPID MAPS, Biomolecules, ChEBI, HMDB and Drug Bank databases.

Database	Feature m/z	Adduct	Chemical Formula	Mass error ppm	Isotope similarity %	ANOVA p -value	HC		COPD			IPF			
							Mean	%RSD	Mean	%RSD	FoldChange (HC)	Mean	%RSD	FoldChange (HC)	FoldChange (COPD)
LipidMAPS	281.2491	M+H	C18H32O2	5.54	97.27	1.49E-02	4536.05	56.00	8064.56	53.36	1.78	9360.56	71.77	2.06	1.16
	255.2331	M+H	C16H30O2	5.06	98.13	3.71E-03	1609.23	78.95	4631.58	80.14	2.88	4321.82	109.58	2.69	0.93
	496.3438	M+H	C24H50NO7P	8.08	97.56	1.62E-01	39778.32	51.50	44409.52	36.73	1.12	43429.30	43.27	1.09	0.98
	520.3439	M+H	C26H50NO7P	7.88	95.52	5.87E-02	80004.33	51.42	93608.97	48.55	1.17	101194.74	32.95	1.26	1.08
	283.2647	M+H	C18H34O2	5.36	98.25	7.68E-03	7578.42	69.48	16301.89	63.55	2.15	18783.78	86.80	2.48	1.15
	522.3599	M+H	C26H52NO7P	8.61	97.12	4.75E-02	67351.83	49.75	87303.54	40.89	1.30	82801.42	41.51	1.23	0.95
	468.3122	M+H	C29H41NO4	2.87	94.11	3.14E-01	15422.84	56.00	20010.25	77.11	1.30	13094.73	48.42	0.85	0.65
	331.0558	M+Na	C18H12O5	-6.21	87.60	1.71E-06	4708.33	230.43	100.70	96.11	0.02	1171.62	458.27	0.25	11.63
	293.0996	M+H	C15H16O6	-8.12	96.49	4.32E-09	209813.07	229.66	2847.12	440.84	0.01	52210.26	487.94	0.25	18.34
	447.3488	M+H	C28H46O4	4.26	90.74	8.20E-03	2921.88	249.00	172.58	56.53	0.06	225.02	80.78	0.08	1.30
	585.2721	M+H	C32H40O10	4.61	94.42	1.40E-01	11453.01	104.67	14930.72	66.02	1.30	7569.45	73.91	0.66	0.51
496.3437	M+Na	C29H47NO4	8.28	98.60	1.80E-02	249023.62	50.68	270223.09	37.53	1.09	263898.71	33.44	1.06	0.98	
Biomolecules	281.2491	M+H	C18H32O2	5.54	97.27	1.49E-02	4536.05	56.00	7837.51	54.66	1.73	9647.57	70.19	2.13	1.23
	255.2331	M+H	C16H30O2	5.06	98.13	3.71E-03	1609.23	78.95	4490.77	83.51	2.79	4606.20	109.22	2.86	1.03
	283.2647	M+H	C18H34O2	5.36	98.25	7.68E-03	7578.42	69.48	15582.64	64.67	2.06	19196.91	86.39	2.53	1.23
	468.3122	M+H	C29H41NO4	2.87	94.11	3.14E-01	15422.84	56.00	20004.03	79.14	1.30	14213.15	44.43	0.92	0.71
	429.2415	M+H	C25H28N6O	4.12	96.62	4.32E-07	17499.11	282.30	18062.47	225.41	1.03	26.04	86.34	0.00	0.00

	313.1556	M+H	C18H20N2O3	3.14	96.44	n/a	144.47	38.64	869.71	329.98	6.02	20131.64	50.55	139.34	23.15
	315.0818	M+H	C16H14N2O3S	6.44	89.81	8.65E-08	26567.24	213.41	2046.02	259.84	0.08	9644.79	413.46	0.36	4.71
	331.0558	M+H	C10H16N2O8	6.70	93.02	1.71E-06	4708.33	230.43	99.76	99.44	0.02	1390.65	422.95	0.30	13.94
	293.0996	M+K	C11H18N4O3	-5.73	93.13	4.32E-09	209813.07	229.66	2982.96	431.17	0.01	62615.82	445.68	0.30	20.99
	447.3488	M+K	C28H46O4	4.26	90.74	8.20E-03	2921.88	249.00	169.17	58.41	0.06	229.82	82.81	0.08	1.36
	585.2721	M+H	C33H36N4O6	2.32	95.97	1.40E-01	11453.01	104.67	15262.54	65.47	1.33	8041.90	74.82	0.70	0.53
	223.0970	M+H	C12H14O4	2.31	98.15	1.80E-02	4507.94	80.66	1863.27	106.55	0.41	4590.72	93.35	1.02	2.46
	239.0920	M+H	C12H14O5	2.58	97.78	4.63E-02	3225.57	66.91	1005.22	125.71	0.31	2495.10	75.73	0.77	2.48
	496.3437	M+H	C29H47NO4	8.28	98.60	3.18E-02	249023.62	50.68	269158.70	38.61	1.08	277718.21	31.27	1.12	1.03
ChEBI	281.2491	M+Na	C18H32O2	5.54	97.27	1.49E-02	4536.05	56.00	7837.51	54.66	1.73	9647.57	70.19	2.13	1.23
	255.2331	M+H	C16H30O2	5.06	98.13	3.71E-03	1609.23	78.95	4490.77	83.51	2.79	4606.20	109.22	2.86	1.03
	496.3438	M+H	C24H50NO7P	8.08	97.56	1.62E-01	39778.32	51.50	44017.40	37.79	1.11	46390.68	39.97	1.17	1.05
	283.2647	M+H	C18H34O2	5.36	98.25	7.68E-03	7578.42	69.48	15582.64	64.67	2.06	19196.91	86.39	2.53	1.23
	522.3599	M+H	C26H52NO7P	8.61	97.12	4.75E-02	67351.83	49.75	87148.02	42.02	1.29	87175.00	39.70	1.29	1.00
	468.3122	M+H	C29H41NO4	2.87	94.11	3.14E-01	15422.84	56.00	20004.03	79.14	1.30	14213.15	44.43	0.92	0.71
	429.2415	M+H	C25H28N6O	4.12	96.62	4.32E-07	17499.11	282.30	18062.47	225.41	1.03	26.04	86.34	0.00	0.00
	308.0520	M+H	C9H13Cl2N6O2	-9.78	54.88	8.99E-08	5.67	253.33	6612.98	163.54	1166.63	862.41	307.46	152.14	0.13
	313.1556	M+H	C18H20N2O3	3.14	96.44	n/a	144.47	38.64	869.71	329.98	6.02	20131.64	50.55	139.34	23.15
	315.0818	M+H	C16H14N2O3S	6.44	89.81	8.65E-08	26567.24	213.41	2046.02	259.84	0.08	9644.79	413.46	0.36	4.71
	371.1036	M+H	C19H18N2O4S	-6.42	77.03	1.97E-02	26571.60	70.41	45650.74	52.16	1.72	39475.60	69.44	1.49	0.86
	331.0558	M+H	C10H16N2O8	6.70	93.02	1.71E-06	4708.33	230.43	99.76	99.44	0.02	1390.65	422.95	0.30	13.94
	293.0996	M+H	C11H18N4O3	-5.73	93.13	9.00E-03	209813.07	229.66	2982.96	431.17	0.01	62615.82	445.68	0.30	20.99
	447.3488	M+K	C28H46O4	4.26	90.74	4.32E-09	2921.88	249.00	169.17	58.41	0.06	229.82	82.81	0.08	1.36

	346.0119	M+K	C9H13Cl2N6O2	3.50	56.12	8.20E-03	23944.57	204.03	1718.13	300.36	0.07	4754.14	425.09	0.20	2.77
	585.2721	M+H	C33H36N4O6	2.32	95.97	1.40E-01	11453.01	104.67	15262.54	65.47	1.33	8041.90	74.82	0.70	0.53
	223.0970	M+K	C12H14O4	2.31	98.15	2.08E-08	4507.94	80.66	1863.27	106.55	0.41	4590.72	93.35	1.02	2.46
	239.0920	M+H	C12H14O5	2.58	97.78	1.14E-04	3225.57	66.91	1005.22	125.71	0.31	2495.10	75.73	0.77	2.48
	496.3437	M+H	C29H47NO4	8.28	98.60	1.80E-02	249023.62	50.68	269158.70	38.61	1.08	277718.21	31.27	1.12	1.03
HMDB	281.2491	M+H	C18H32O2	5.54	97.27	1.49E-02	4536.05	56.00	7837.51	54.66	1.73	9647.57	70.19	2.13	1.23
	255.2331	M+Na	C16H30O2	5.06	98.13	3.71E-03	1609.23	78.95	4490.77	83.51	2.79	4606.20	109.22	2.86	1.03
	496.3438	M+H	C24H50NO7P	8.08	97.56	1.62E-01	39778.32	51.50	44017.40	37.79	1.11	46390.68	39.97	1.17	1.05
	520.3439	M+H	C26H50NO7P	7.88	95.52	5.87E-02	80004.33	51.42	94824.45	48.80	1.19	106630.98	31.66	1.33	1.12
	283.2647	M+H	C18H34O2	5.36	98.25	7.68E-03	7578.42	69.48	15582.64	64.67	2.06	19196.91	86.39	2.53	1.23
	522.3599	M+H	C26H52NO7P	8.61	97.12	4.75E-02	67351.83	49.75	87148.02	42.02	1.29	87175.00	39.70	1.29	1.00
	468.3122	M+H	C29H41NO4	2.87	94.11	3.14E-01	15422.84	56.00	20004.03	79.14	1.30	14213.15	44.43	0.92	0.71
	429.2415	M+H	C25H28N6O	4.12	96.62	4.32E-07	17499.11	282.30	18062.47	225.41	1.03	26.04	86.34	0.00	0.00
	313.1556	M+H	C18H20N2O3	3.14	96.44	n/a	144.47	38.64	869.71	329.98	6.02	20131.64	50.55	139.34	23.15
	315.0818	M+H	C16H14N2O3S	6.44	89.81	8.65E-08	26567.24	213.41	2046.02	259.84	0.08	9644.79	413.46	0.36	4.71
	604.2959	M+H	C29H41N5O9	-2.95	78.11	1.71E-06	4.53	84.40	629.06	438.73	138.75	5037.93	86.00	1111.20	8.01
	331.0558	M+H	C10H16N2O8	6.70	93.02	4.32E-09	4708.33	230.43	99.76	99.44	0.02	1390.65	422.95	0.30	13.94
	293.0996	M+H	C28H46O4	4.26	90.74	8.20E-03	209813.07	229.66	2982.96	431.17	0.01	62615.82	445.68	0.30	20.99
	447.3488	M+H	C33H36N4O6	2.32	95.97	1.40E-01	2921.88	249.00	169.17	58.41	0.06	229.82	82.81	0.08	1.36
	585.2721	M+K	C12H14O4	2.31	98.15	4.63E-02	11453.01	104.67	15262.54	65.47	1.33	8041.90	74.82	0.70	0.53
	223.0970	M+H	C24H48NO7P	6.18	95.04	1.09E-01	4507.94	80.66	1863.27	106.55	0.41	4590.72	93.35	1.02	2.46
	239.0920	M+H	C12H14O5	2.58	97.78	4.63E-02	3225.57	66.91	1005.22	125.71	0.31	2495.10	75.73	0.77	2.48
	496.3437	M+H	C29H47NO4	8.28	98.60	3.18E-02	249023.62	50.68	269158.70	38.61	1.08	277718.21	31.27	1.12	1.03

DrugBank	281.2491	M+H	C18H32O2	5.54	97.27	1.49E-02	4536.05	56.00	7837.51	54.66	1.73	9647.57	70.19	2.13	1.23
	255.2331	M+H	C16H30O2	5.06	98.13	3.71E-03	1609.23	78.95	4490.77	83.51	2.79	4606.20	109.22	2.86	1.03
	283.2647	M+Na	C18H34O2	5.36	98.25	7.68E-03	7578.42	69.48	15582.64	64.67	2.06	19196.91	86.39	2.53	1.23
	468.3122	M+H	C29H41NO4	2.87	94.11	3.14E-01	15422.84	56.00	20004.03	79.14	1.30	14213.15	44.43	0.92	0.71
	429.2415	M+H	C25H28N6O	4.12	96.62	4.32E-07	17499.11	282.30	18062.47	225.41	1.03	26.04	86.34	0.00	0.00
	315.0818	M+H	C16H14N2O3S	6.44	89.81	8.65E-08	26567.24	213.41	2046.02	259.84	0.08	9644.79	413.46	0.36	4.71
	371.1036	M+H	C20H16N2O4	9.77	73.89	1.97E-02	26571.60	70.41	45650.74	52.16	1.72	39475.60	69.44	1.49	0.86
	293.0996	M+H	C10H16N2O8	5.65	92.55	4.32E-09	209813.07	229.66	2982.96	431.17	0.01	62615.82	445.68	0.30	20.99
	239.0920	M+H	C6H12N3O4P	7.45	92.53	3.18E-02	3225.57	66.91	1005.22	125.71	0.31	2495.10	75.73	0.77	2.48

SONAR enhances the specificity of unbiased lipid plasma profiling of idiopathic pulmonary fibrosis using UPLC-QTOF-MS

Adapted from Nambiar, S.; Bong, S. H.; King, A.; Moodley, Y.; and Trengove, R. D. (2018) "SONAR enhances the specificity of unbiased lipid plasma profiling of idiopathic pulmonary fibrosis using UPLC-QTOF-MS" *Ready for submission to Analytica Chimica Acta*

3.1 Abstract

Idiopathic pulmonary fibrosis (IPF) is a chronic interstitial disease characterized by fibrosis and progressive loss of lung function. The pathophysiological pathways involved in IPF are not well understood. IPF is believed to be caused by repetitive alveolar epithelial cell injury and dysregulated repair mechanisms leading to uncontrolled proliferation of lung fibroblasts and excessive deposition of extracellular matrix in the interstitial space. In this study, we used ultra-performance liquid chromatography-quadrupole time-of-flight mass spectrometry (UPLC-QTOF-MS) to characterize lipid changes in plasma derived from patients with stable and progressive IPF. We further applied a data independent acquisition (DIA) technique to improve the specificity by generating class-specific fragment ions through the use of a scanning quadrupole positioned prior to orthogonal acceleration TOF mass analyser. This DIA approach, known as SONAR, allowed specific precursor (MS1) and associated product ions (MS2) to be aligned on the basis of the quadrupole m/z position during the scan. Supervised partial least-squares discriminant analysis (OPLS-DA) modelling showed discrimination between the stable and progressive subjects. The study revealed up-regulation of triglycerides while phosphatidylcholines were down-regulated in the

progressors *versus* stable group. These lipids were then identified by matching experimental fragment ions with *in silico* product ion spectra from LIPID MAPS with a mass tolerance of 10 ppm. The result of this study suggested a role for lipid metabolism dysregulation and mitochondrial-beta oxidation in progressive IPF samples and highlighted a number of promising candidates for biomarker development.

Keywords: lipids, plasma, IPF, DIA, SONAR

3.2 Introduction

Idiopathic pulmonary fibrosis (IPF) is a chronic, progressive lung disease characterized by alveolar epithelial cell damage, proliferation of activated fibroblasts and extracellular matrix accumulation that leads to irreversible distortion of the lung architecture (Kang *et al.*, 2016). Previous studies suggested that IPF is related to abnormalities in a number of biological processes including glycolysis (Kang *et al.*, 2016), fatty acid oxidation (Hamanaka *et al.*, 2018) and vascular remodelling (Zhao *et al.*, 2017). While genetic and molecular mechanisms associated with the development of fibrosis have been reported by Gangwar *et al.* (2017) and Zhao *et al.* (2017), the underlying disease pathophysiology remains unclear.

Advances in analytical technologies have enabled the analysis of complex biological matrices by liquid chromatography-mass spectrometry (LC-MS). The ability to determine specific biomolecules and their relative abundance has been key to the understanding of biochemical change. Lipidomics, like metabolomics, is a developing field of systems biology research that studies lipids as key intermediates of cellular mechanisms and their roles in diseases such as asthma (Berry *et al.*, 2017) and chronic

obstructive pulmonary disorder (COPD; Telenga *et al.*, 2014). Lipidomic studies of complex biological matrices (plasma and tissue extracts) are routinely performed using targeted tandem mass spectrometry (MS/MS) or data dependent acquisition (DDA) methods for their high sensitivity and selectivity (Dautel *et al.*, 2017; Kyle *et al.*, 2018). The advent of high-resolution MS and data-independent acquisition (DIA) modes can now provide broad coverage for both MS and MS/MS data simultaneously in a single analytical run (Gethings *et al.*, 2017).

A key challenge in the analysis of complex lipid extracts from crude plasma samples is the co-elution of isomeric lipid species that can lead to false identification and quantitative inaccuracies (Cajka and Fiehn, 2014; Kyle *et al.*, 2016). Here, we apply SONAR, a rapidly scanning DIA method in tandem with a UPLC-TOF-MS acquisition to provide additional MS/MS information. SONAR utilizes a narrow quadrupole scan window to provide cleaner spectra (Gethings *et al.*, 2017), increase MS/MS spectral quality and consequently, improve compound database matching (Moseley *et al.*, 2018). The qualitative and quantitative performance of SONAR compared to conventional quadrupole time-of-flight (QTOF)-MS method were assessed using plasma samples from stable and progressive IPF patients. Healthy controls were not included in this study as the principal aim of the study was to investigate plasma lipid differences between diseased groups.

3.3 Materials and Methods

3.3.1 Chemicals and Reagents

SPLASH LipidoMix standard (deuterium-labelled standard, SKU 330707), normalised against human plasma lipid levels, was purchased from Avanti Polar Lipids (Alabaster, USA). UPLC–MS grade water (H₂O), acetonitrile (ACN) and isopropanol (IPA) were purchased from Thermo Fisher Scientific (Victoria, Australia). Formic acid and ammonium formate were sourced from Sigma-Aldrich (New South Wales, Australia) and the leucine enkephalin standard for lock-mass acquisition was supplied by Waters (Wilmslow, United Kingdom).

3.3.2 Biological samples

A total of 60 plasma samples (30 stable and 30 progressors) were obtained from the Australian IPF registry and stored in -80 °C until further analysis. Sample handling and material transfer was approved by the Royal Perth Hospital Human Research Ethics Committee (Reference number: REG 15-204) and the experimental protocol used for this work was approved by the Murdoch University Human Research Ethics Committee (Approval number: 2017/254).

3.3.3 Sample preparation

The SPLASH LipidoMix standard was initially diluted 1:50 with IPA. Plasma samples were thawed on ice and immediately transferred to 96-well plates. 20 µL of samples were pipetted into each well followed by the addition of 30 µL of H₂O. The extraction of lipids was carried out by adding 200 µL of IPA (consisting of the diluted SPLASH

LipidoMix) into each well. The plates were immediately heat-sealed using Eppendorf® heat sealing foil and mixed briefly before incubation for 2 hrs at 4 °C. Sample plates were removed and centrifuged at 4,500 x g for 10 mins at 4 °C. 100 µL of the supernatant were then transferred into two 96-well plates corresponding to positive and negative modes of acquisition. Pooled samples were also generated by aliquoting 20 µL of every sample into a 2-mL centrifuge tube and placed on ice. 20 µL of pooled QC was pipetted into every 12th well as the study reference or quality control (QC) checks. The extractions for study reference or QC samples were performed in the same way as the test samples.

3.3.4 UPLC configuration

UPLC separation was performed using an ACQUITY I-class system (Waters Corporation, Milford, MA, U. S. A) equipped with a Waters CSH C18 column (2.1 x 100 mm, 1.8 µm). Mobile phase A consisted of ACN/H₂O (60:40, v/v) containing 10 mM ammonium formate with 0.1 % formic acid, while mobile phase B was IPA/ACN (90:10, v/v) with 0.1 % formic acid. Chromatographic separation was achieved with a gradient of 40 to 99 % mobile phase B over 18 mins. Solvent flow rate and column temperature was maintained at 0.4 mL/min and 55 °C, respectively. The lock-mass compound, leucine enkephalin (200 pg/µL) was prepared in ACN/H₂O (50:50, v/v), and was delivered at 10 µL/min to the reference sprayer source of the mass spectrometer.

3.3.5 Mass spectrometry acquisition

MS-based lipid analysis was performed using a Xevo G2-XS QTOF mass spectrometer (Waters Corporation, Wilmslow, United Kingdom) in both positive and negative

electrospray ionisation (ESI) modes. The source temperature was set to 120 °C and the capillary voltage set to 2.0 kV and 1.0 kV for positive and negative mode respectively. The time-of-flight (TOF) mass analyser of the mass spectrometer was calibrated using a sodium formate mixture for m/z 50 to 1200. TOF-MS data were collected for the time-of-flight-mass spectrometry (TOF-MS) method as well as SONAR DIA. During SONAR acquisition the quadrupole was rapidly scanned between m/z 350 to 950 and m/z 150 to 750 for positive and negative modes, respectively, using a quadrupole transmission window of 10 Da. For each quadrupole transmission window, the orthogonal-TOF mass spectra were recorded as the quadrupole scans into 200 discrete bins. Two data functions (modes) were acquired in an alternating fashion, differing only in the collision energy applied to the gas cell. In the low-energy function mode, data were collected with a constant gas cell collision energy of 6 eV. In the high-energy function mode, the gas cell collision energy was ramped from 20 to 40 eV. As such, the resulting data contained both lipid precursor ions as well as associated fragment ions. Collision energies were not applied for the TOF-MS method. The spectral scan time in each mode was 0.1 s and both TOF-MS and SONAR acquisitions were performed in sensitivity mode. The reference sprayer was sampled every 60 s and the data were lock-mass corrected post-acquisition using leucine enkephalin at 200 pg/ μ L. This provides a “snapshot” of the reference mass that can be used to perform exact mass measurements with a high degree of accuracy.

3.3.6 Data processing

All MS acquisitions were processed using Progenesis QI (Nonlinear Dynamics, Newcastle upon Tyne, United Kingdom) where samples were chromatographically aligned with respect to the mid-acquisition reference (QC3). Peak picked features were

statistically analysed using EZinfo (MKS Data Analytics Solutions, Umeå, Sweden) and the significant features of interest were imported back into Progenesis QI. Identifications were achieved whereby experimental fragments were matched against the theoretical fragmentation product ion spectra from LIPID MAPS (Lipidomics Gateway, United Kingdom). A mass tolerance of 10 ppm was applied for both precursor and product ions. The fragmentation scores and relative isotopic compositions of matched fragment ions derived from LIPID MAPS were used for structural elucidation and identification purposes. Additional manual annotation was also conducted using the Lipid Reporter toolkit and reported according to the shorthand nomenclature defined by Liebisch *et al.* (2013).

3.3.7 Statistical analysis

QC features with $CV < 30\%$ were applied for overall statistical analyses. Principal component analysis (PCA) and orthogonal projection to latent structures-discriminant analysis (OPLS-DA) were performed using EZinfo (Umetrics, Umeå, Sweden). The data were mean-centered and pareto-scaled prior to PCA and OPLS-DA. The features of interests were extracted from S-plots constructed following OPLS-DA analysis based on their contribution to the variation and correlation between the two groups (stable *versus* progressors). The variable importance in projection (VIP) scores of each feature was also calculated using the OPLS-DA model, and the features with VIP scores ≥ 1 were considered as significant (Bujak *et al.*, 2016). The potential lipid features with p-value of less than 0.05 and VIP score of ≥ 1 were subjected to database searching against LIPID MAPS for fragment matching and lipid identification.

3.4 Results and Discussion

Using the TOF-MS method, approximately 9,000 features in positive mode and 5,000 features in negative mode were resolved in each analytical run. In comparison, SONAR detected 5,000 and 800 features for positive and negative mode respectively. Figures 3.1 and 3.2 illustrate the sensitivity and selectivity of both the TOF-MS and SONAR acquisition methods by overlaying the total ion chromatograms (TIC) of a representative QC sample in positive and negative modes. Signal intensities of the TOF-MS TICs were approximately five-fold (positive mode) and ten-fold (negative mode) greater than the TICs generated from SONAR. The TICs from the positive modes also displayed a typical lipid spectral pattern consistent with the work of Knittelfelder *et al.* (2014) and Cajka and Fiehn (2014).

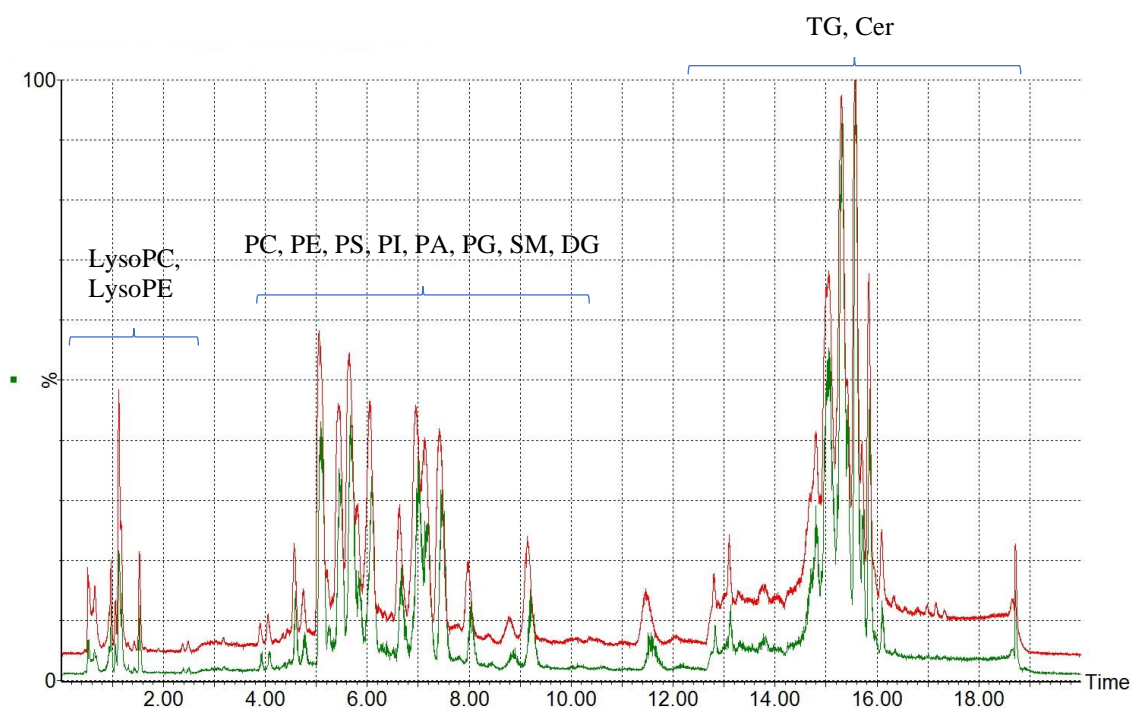


Figure 3.1 Overlaid total ion chromatograms of both TOF-MS (red) and SONAR (green) acquisitions in positive mode. The highlighted regions of the chromatogram illustrate the elution of lysophosphatidylcholine (LysoPC), lysophosphatidylethanolamine (LysoPE), phosphatidylcholine (PC), phosphatidylethanolamine (PE), phosphatidylserine (PS), phosphatidylinositol (PI), phosphatidic acid (PA), phosphatidylglycerol (PG), sphingomyelin (SM), diacylglycerol (DG), triglyceride (TG) and ceramide (Cer).

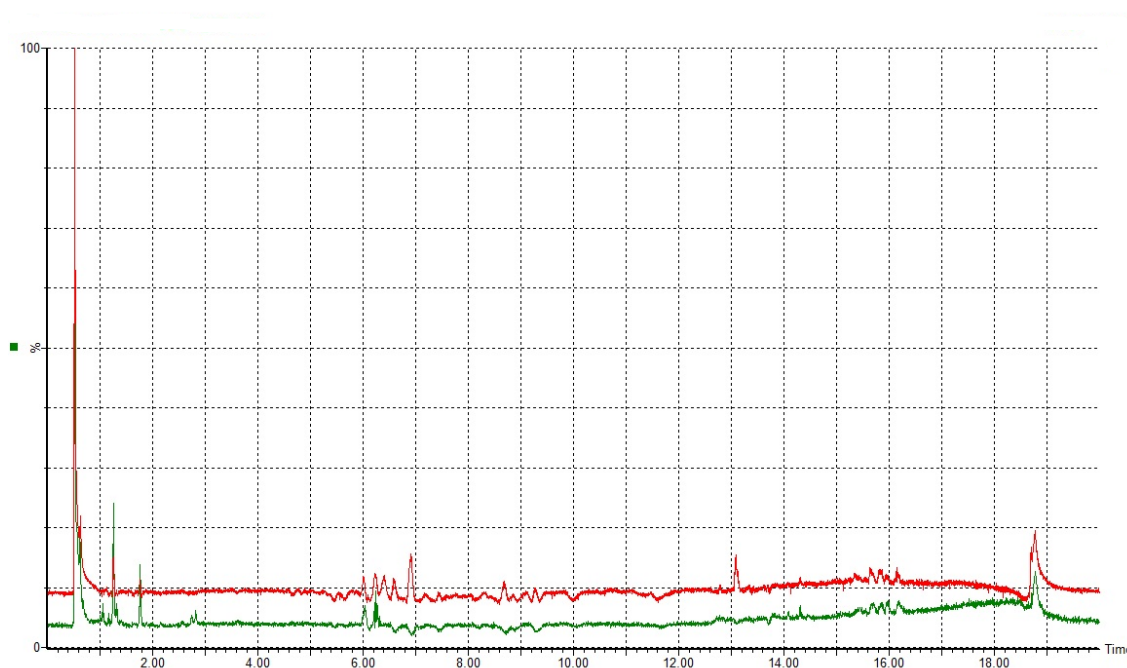


Figure 3.2 Overlaid total ion chromatograms of both TOF-MS (red) and SONAR (green) acquisitions in negative mode showing poor lipids resolution.

Although the sensitivity of the SONAR method was lower than that of TOF-MS, the results showed good selectivity for SPLASH LipidoMix fragment ions. SONAR utilizes the scanning quadrupole technique to filter ions over the mass range of m/z 350 to 950 and as a result, provided spectra with considerably less background (Moseley *et al.*, 2018). The selectivity and specificity of the method was further demonstrated where precursor ions from deuterium labelled-lipid standards were successfully extracted. Figure 3.3 represents the extracted ion chromatogram (XIC) of lipids in positive ion mode, showing that all lipid classes were equally resolved using both SONAR and TOF-MS. However, only four lipids were detected using SONAR in negative mode while nine lipids were detected by TOF-MS acquisitions (Figure 3.4).

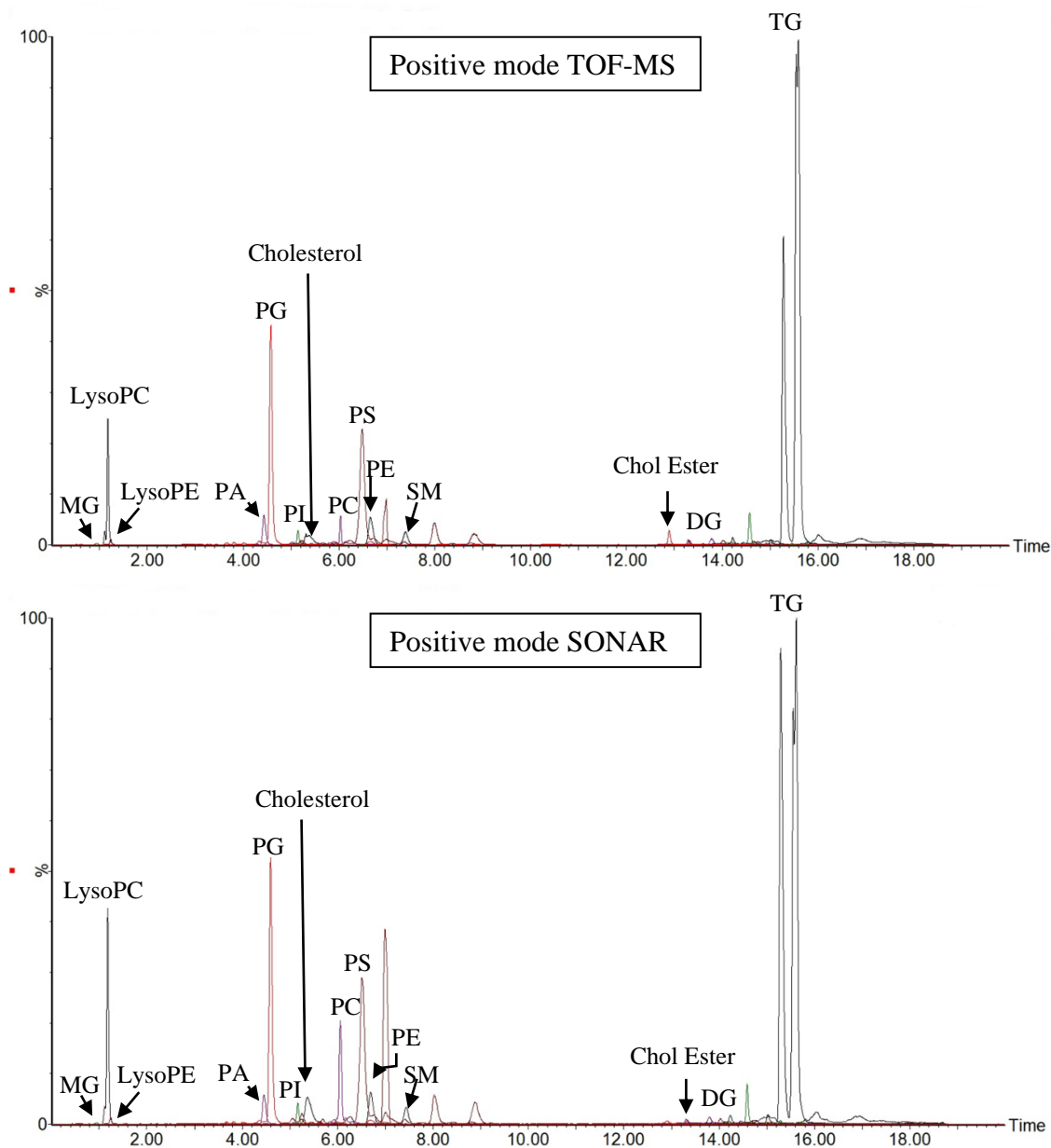


Figure 3.3 The extracted ion chromatograms of spiked deuterium-labelled SPLASH LipidoMix standards in positive ion mode showing peaks corresponding to 15:0-18:1(d7) PC, 15:0-18:1(d7) PE, 15:0-18:1(d7) PS, 15:0-18:1(d7) PG, 15:0-18:1(d7) PI, 15:0-18:1(d7) PA, 18:1(d7) LysoPC, 18:1(d7) LysoPE, 18:1(d7) Chol Ester, 18:1(d7) MG, 15:0-18:1(d7) DG, 15:0-18:1(d7)-15:0 TG, 18:1(d9) SM and cholesterol (d7).

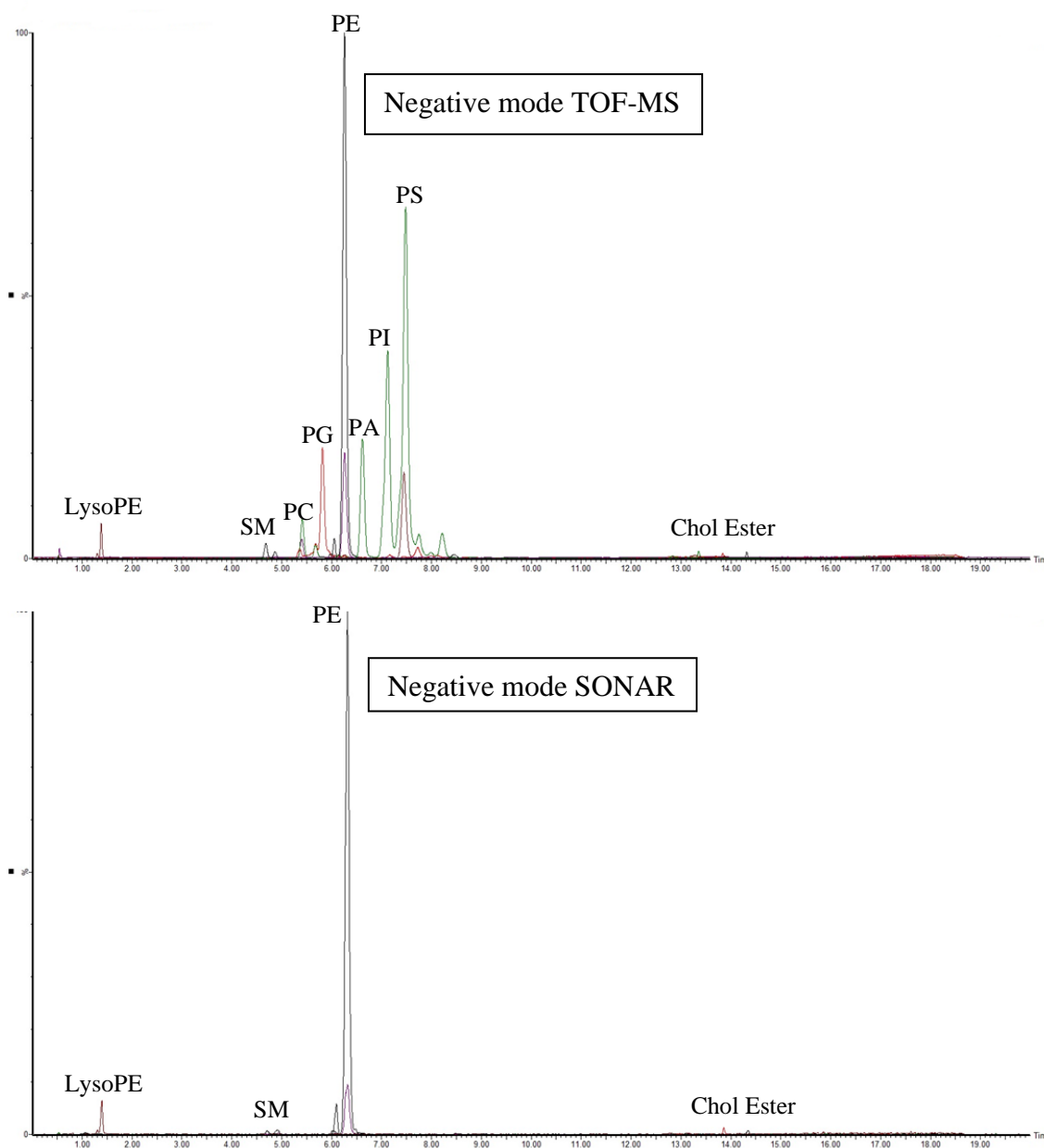
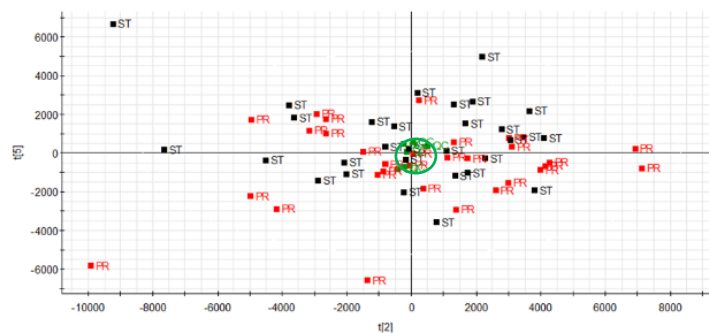
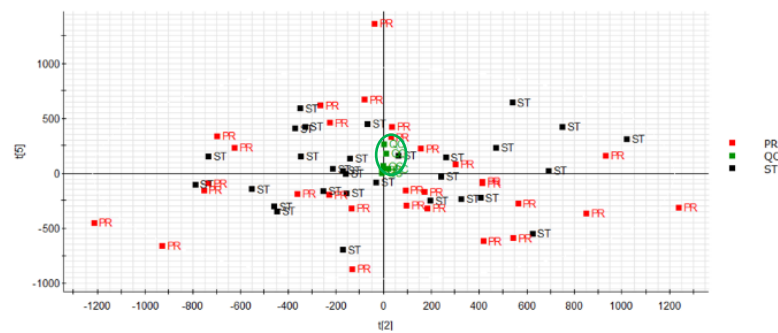


Figure 3.4 The extracted ion chromatograms of spiked deuterium-labelled SPLASH LipidoMix standards in negative ion mode showing peaks corresponding to 15:0-18:1(d7) PC, 15:0-18:1(d7) PE, 15:0-18:1(d7) PS, 15:0-18:1(d7) PG, 15:0-18:1(d7) PI, 15:0-18:1(d7) PA, 18:1(d7) LysoPE, 18:1(d7) Chol Ester and 18:1(d9) SM.

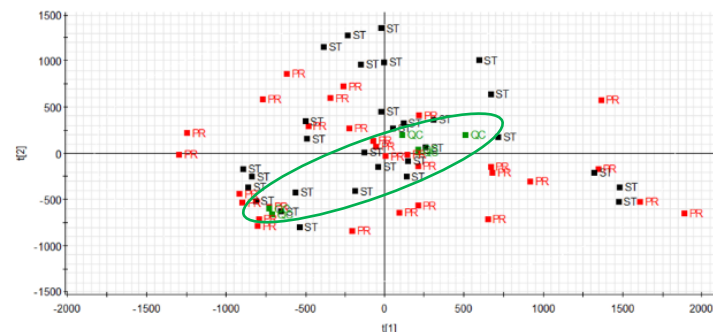
Features of interest from both the stable and progressor groups were then interrogated using Progenesis QI and EZinfo. To assess the contribution of experimental variability, QC samples were used for the filtration of features that experienced a variation coefficient higher than those measured in the QC data set (Calderón-Santiago *et al.*, 2017). The number of features in pooled QC samples with $CV \geq 30\%$ were 3,716 and 1,880 in positive mode TOF-MS and SONAR, and 969 and 402 in negative mode TOF-MS and SONAR, respectively. A filter to remove these features were generated within the software and applied to all groups based on the acceptable bioanalytical variation limit of $\leq 30\%$ relative standard deviation (Naz *et al.*, 2014; Schoeman *et al.*, 2018). PCA of QC samples were then applied to assess experiment quality. Figure 3.5 illustrates the clustering of pooled QC samples in both positive and negative modes for TOF-MS acquisition and in negative mode for SONAR only. It was noted that the final two run-order QCs for the positive mode of SONAR did not cluster. Further evaluation of the raw data showed a rising baseline shift of the entire chromatogram from samples 51 through to 66. A rising baseline is typically observed in LC-MS acquisitions due to the systemic noise of gradient elution (Urban and Štys, 2015); however, it was possible that the total baseline shift observed was caused by detector drift (Yang *et al.*, 2011). An increased chemical noise by the addition of new mobile phase or inconsistency in sample preparation can also contribute to the baseline shift but this was highly unlikely as the same extracted samples and mobile phases were used for both TOF-MS and SONAR acquisitions in both modes.



Positive mode TOF-MS



Negative mode TOF-MS



Positive mode SONAR



Negative mode SONAR

Figure 3.5 PCA score plots generated from all stable (ST, black), progressor (PR, red) and QC (QC, green) samples in all four modes of acquisition. The clustering of the pooled QC samples in each acquisition modes were shown encircled in green.

Using MatrixAnalyzer software (SpectralWorks Ltd, United Kingdom), the global intensities of QCs 5 and 6 acquired using SONAR in positive mode were shown to be considerably increased. A QC correction was then applied for sample intensities from injection number 50 to 60 to normalize the data (Figure 3.6). This normalization approach was based on the assumption that the QCs were technical replicates and that their intensities were independent of batch label and injection number (Wehrens *et al.*, 2016). The QC correction function from MatrixAnalyzer plug-in (Hill and Roessner, 2013; Tolstikov *et al.*, 2014) was then applied to improve data normalisation. In line with Wehrens *et al.* (2016), the corrections for this study were based only on features present within QC pooled samples.

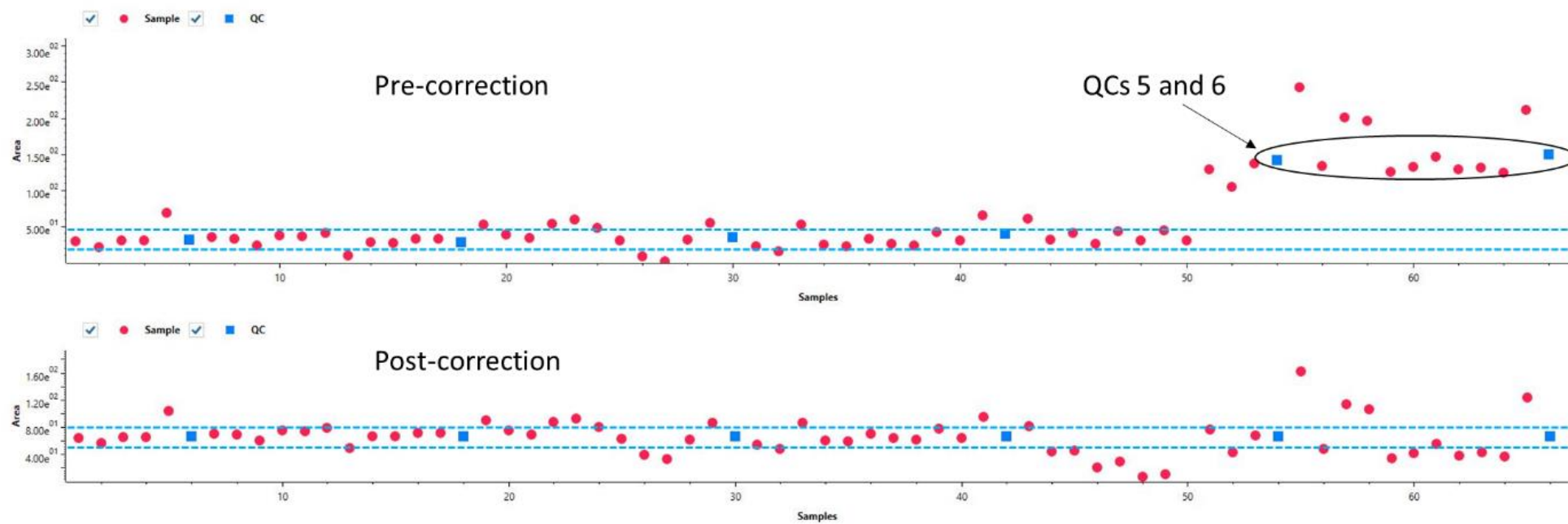


Figure 3.6 Global sample projection of positive SONAR showing an overall intensity of uncorrected data for QCs 5 and 6 (circled), and normalised intensity post-correction using the MatrixAnalyzer tool. Correction lines (dotted blue) were fitted through the QCs and the samples and QCs were represented by the red and blue dots.

For statistical analysis, PCA was initially performed to decompose the stable and progressive patient dataset; however, unsupervised multivariate analysis did not reveal significant differences between both groups. The heterogenous nature of the grouping between these two diseased datasets supported similar assumptions made by Chang and Keinan (2014) where diseases with similar underlying mechanisms were more likely to cluster together in a principal component space. Supervised multivariate data analysis OPLS-DA was then used to generate a biased regression model to disentangle group-predictive and group-unrelated variation in the measured data (Worley and Powers, 2016). The OPLS-DA model clearly distinguished the stable and progressor groups and a scores plot (S-plot) was then generated. An S-Plot is a statistical tool for visualizing both the covariance and correlation between the endogenous features and the modelled group designation (ST *versus* PR). The S-Plot is useful for the identification of biochemically atypical features with statistical significance based on both the contributions to the model and their reliabilities (Dong *et al.*, 2017).

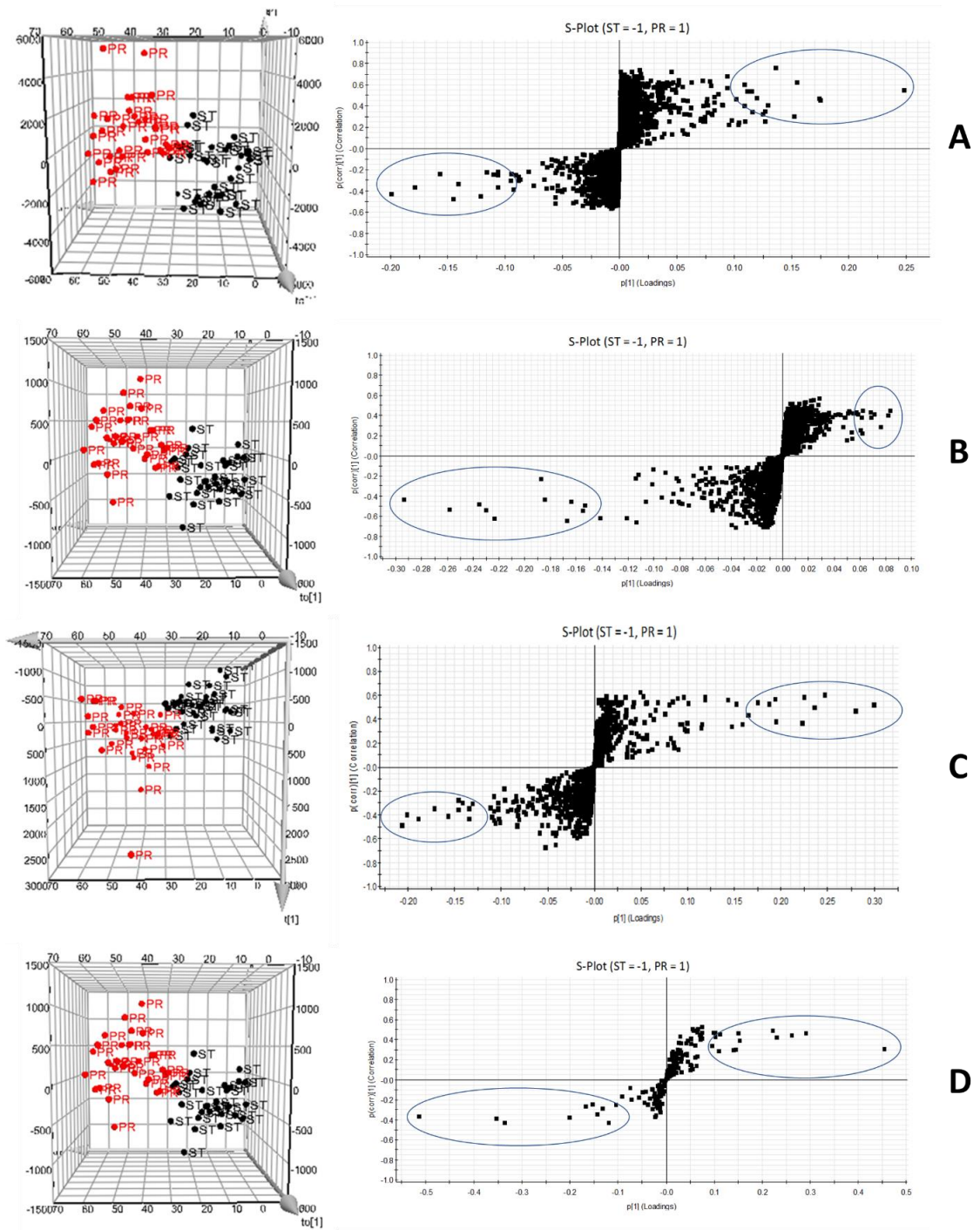


Figure 3.7 OPLS-DA and S-plots comparing stable *versus* progressors plasma samples in positive mode TOF-MS (A), negative mode TOF-MS (B), positive mode SONAR (C) and negative mode SONAR (D). The ten features of interest in each group (circled) were exported into Progenesis QI software for identification.

By consolidating the S-plots from the OPLS-DA model as well as features with VIP scores ≥ 1 , the top 10 features of interest in each group were exported into Progenesis QI software for identification. The differential features between the groups were analysed and database searched against LIPID MAPS. From the 20 features exported using EZinfo, 15 lipids from positive TOF-MS, 11 lipids from negative TOF-MS and 11 lipids from positive SONAR mode were putatively identified. Negative mode SONAR experiment did not yield metabolite identifications with sufficient stringencies.

The spiked deuterium-labelled SPLASH LipidoMix standards were then used to confirm the identity of putative lipids based on their retention times and m/z values. The TOF-MS experiments were successful at resolving the lipid classes chromatographically as shown in Figures 3.3 and 3.4; however, compound identification was still challenging due to the lack of precursor-product assignments. A number of features were not successfully resolved (Table 3.1). In particular, phosphatidylethanolamine (PE) and phosphatidylcholine (PC) were indistinguishable for a number of putative features; this was a commonly encountered problem with phospholipids due to the large number of structural isomers (Godzien *et al.*, 2015). Resolving lipids chromatographically by class may aid in identification; however, with TOF-MS where no quadrupole isolation occurs, co-eluting species can still be challenging (Gethings *et al.*, 2017). The precursor and product ions generated by SONAR contributed to the specificity of the method by providing additional MS/MS information for structural elucidation, and therefore increased the probability of successful lipid library matching (Satomi *et al.*, 2017; Gethings *et al.*, 2017). The advantages of SONAR DIA is evident in positive mode where each triglyceride (TG) was accurately identified by matching the generated fragmentation pattern with the theoretical product ion spectra from LIPID MAPS with $> 90\%$ probability scores. Putative lipid identifications were annotated using the

shorthand nomenclature defined by Liebisch *et al.* (2013) that builds upon the current LIPID MAPS terminology.

In addition to the successful identification of the lipid species, the relative quantitation of lipids identified was also achieved using known amounts of spiked deuterium-labelled standards. The quantitative values were calculated by comparing the chromatographic peak area of each analyte to the peak area of the internal standard of the representative lipid class (Table 3.1). All other related statistics are presented in the Supplementary Table 3.1.

Table 3.1 Table showing the plasma lipids that were identified for stable and progressors of IPF through different acquisition modes and their associated fold changes.

MS mode	Feature <i>m/z</i>	Putative ID	Stable mmol/L	Progressor mmol/L	Fold Changes
Positive TOF-MS	820.7382	TG [48:2]	1.29	1.22	0.95
	524.3730	PE [21:0]	0.01	0.37	0.90
		PC [18:0]	33.46	29.99	
		PC [O-18:0]			
	879.7440	TG [52:3]	0.98	1.05	1.08
	924.8041	TG [56:6]	0.56	0.63	1.11
	794.7233	TG [46:1]	0.46	0.43	0.92
	920.7704	TG [56:8]	0.52	0.66	1.27
	822.7558	TG [48:1]	0.62	0.58	0.95
	951.7406	TG [58:9]	0.07	0.10	1.38
	788.6164	PC [36:1]	60.63	56.68	0.93
		PE [39:1]	0.01	0.69	
	834.5986	PC [40:6]	16.42	13.80	0.84
		PE [43:6]	0.01	0.17	
	784.5851	PC [36:3]	59.40	57.57	0.97
		PE [39:3]	0.01	0.71	
	878.8198	TG [52:1]	1.00	0.98	0.98
	812.6164	PC [38:3]	44.66	39.08	0.88
		PC [36:0]			
		PE [39:0]	0.01	0.49	
PE [41:3]					
PA [43:4]		1.07	0.94		
785.5885	PA [O-40:0]	1.10	1.04	0.94	
881.7600	TG [54:5]	0.92	0.98	1.06	
	TG [52:2]				

Negative TOF-MS	856.6105	PS [41:2]	0.07	0.06	0.83
	768.5570	PC [35:3]	13.41	11.88	0.89
		PE [38:3]	0.01	0.01	
	828.5780	PS [39:2]	0.16	0.14	0.89
	480.3094	PE [18:0]	0.02	0.01	0.85
		LysoPE [18:0]	0.60	0.51	
		PC [15:0]	17.66	14.95	
	832.6102	PS [39:0]	0.08	0.07	0.87
	830.5927	PS [39:1]	0.34	0.31	0.90
	770.5717	PC [35:2]	26.37	23.78	0.90
		PE [38:2]	0.03	0.02	
		PS [O-37:1]	0.13	0.12	
		PS [P-37:0]			
	797.6063	PG [O-40:2]	0.36	0.37	1.01
		PG [P-40:1]			
PA [43:2]		0.08	0.08		
TG [50:9]		30.35	30.70		
802.5605	PS [37:1]	0.50	0.48	0.95	
885.5519	PI [38:4]	0.05	0.05	0.84	
Positive SONAR	923.7138	TG [56:9]	0.04	0.05	1.37
	868.7379	TG [52:6]	0.10	0.10	1.01
	894.7547	TG [54:7]	0.38	0.42	1.09
	920.7718	TG [56:8]	0.99	1.19	1.21
	896.7703	TG [54:6]	0.20	0.21	1.04
	922.7879	TG [56:7]	0.81	0.89	1.09
	603.5333	DG [O-34:1]	n/a	n/a	1.09
	784.5847	PC [36:3]	136.01	132.54	0.97
	806.5665	PC [36:3]	49.84	44.75	0.90
	808.5829	PC [36:2]	118.50	108.08	0.91
	812.6160	PC [38:3]	100.89	80.86	0.80

3.4.1 Lipid markers correlated to IPF

Abnormal lipid metabolism has been shown to result in lung diseases including asthma (Zehethofer *et al.*, 2015; Yuan *et al.*, 2018) and COPD (Higham *et al.*, 2012; Naik *et al.*, 2014). However, its potential role in IPF pathogenesis remains unclear. In this study, a scanning DIA technique facilitated improved lipid identification of a number of spiked lipid standards. In addition, the lipid profiles from 30 patients diagnosed with progressive IPF showed changes in lipid plasma composition when compared to the 30 stable subjects. The fold changes calculated revealed minimal variability (+/- 20%) in levels of the identified lipids between the two groups. This was expected as both groups were derived from diseased individuals. Healthy controls were not included in this study as the aim was to investigate the ability of the DIA technique to discriminate plasma lipid differences between diseased groups only.

Using SONAR, a number of triglycerides (TG), diglyceride (DG) and PCs that were unique lipid markers of IPF progression were identified and this was shown to be consistent with the findings of Hu *et al.* (2015) and Yan *et al.* (2017). The levels of these TGs (56:9, 54:7, 56:8 and 56:7) and DG (O-34:1) appeared to be elevated while PCs (36:3, 36:2 and 38:3) was reduced in the samples of progressors compared to stable patients. A recent study by Yan *et al.* (2017) showed that 6 DGs (16:0/18:1/0:0, O-16:0/18:1, 18:0/18:2/0:0, 16:0/18:2/0:0, 18:1/18:3/0:0 and 18:1/18:2/0:0) and 9 TGs (16:0/18:2/18:2, 16:0/18:1/18:2, 16:0/18:1/20:3, 16:0/18:3/20:0, 16:0/16:1/18:1, 18:4/20:3/22:0, 17:0/18:1/19:1, 18:1/20:3/20:4 and 16:0/20:3/20:5) were found to be increased while 13 PCs (22:6/16:0, 16:0/18:2, 0:0/16:0, 22:4/18:2, 20:2/18:2, 18:1/18:1, 18:0/18:1, 18:0/0:0, 22:6/18:2, 20:3/P-18:1, 20:5/0:0 and 17:0/19:1) were decreased in IPF patients compared to healthy control subjects. Using a bleomycin mouse model of

pulmonary fibrosis, Kulkarni *et al.* (2018) observed a four-fold upregulation of DG but showed unchanged levels of TG. Both DGs and TGs are the most abundant lipids found in circulating plasma (Ishikawa *et al.*, 2016; Tham *et al.*, 2018) and are important bioactive mediators of cell membranes (Yan *et al.*, 2017; Dautel *et al.*, 2017). DG is not only an important source of free fatty acids but is also a precursor for the synthesis of more complex lipids. The conversion of phosphatidic acid into DG is crucial for the synthesis of PC, PE, and phosphatidylserine (PS; Sarri *et al.*, 2011; Ferraz-Nogueira *et al.*, 2014). DG synthesis has been shown to be implicated in several lung diseases including cystic fibrosis (Aureli *et al.*, 2016), asthma and COPD (Hichami *et al.*, 2005) as well as IPF (Hu *et al.*, 2015).

TG was only found to be elevated in smokers with exacerbated COPD suggesting a causal effect of smoking on the inhibition of lipoprotein lipase by nicotine (Titz *et al.*, 2016). Lipoprotein lipase activity is rate limiting for the removal of TG from the circulation of blood. Pro-inflammatory cytokines such as tumour necrosis factor α (TNF- α) are known to be mediators of hyperlipidemia in infection and in severe stress because they both inhibit lipoprotein lipase activity (Popa *et al.*, 2007). We hypothesised that the TG clearance was decreased due to the inhibition of lipoprotein lipase activity thereby stimulating lipogenesis. Although cytokine concentrations were not measured, Figueroa *et al.* (2002) speculated that hypertriglyceridemia (elevated TG) in cystic fibrosis patients may be positively correlated with TNF- α concentrations.

Changes in phospholipids such as PCs in lung diseases have been reported since the late 80s in animal models of rapidly developing pulmonary fibrosis (Baker *et al.*, 1986; Low, 1989). Guerrero *et al.* (2009) revealed significant decrease in plasma PCs in cystic fibrosis patients using matrix-assisted laser desorption (MALDI)-TOF experiment. This

study also suggested that a decrease in PCs levels by 20% may be correlated with the progression of disease. This decrease is further supported by Yan *et al.* (2017) who also found lower levels of plasma PCs in patients with IPF. PCs are lipids that incorporate choline as head group and form the most abundant component in the outer leaflet of the cell membrane (Nicolson and Ash, 2014; Pöyry and Vattulainen, 2016). Phospholipase A2 converts phospholipids into lysophosphatidic acid and arachidonic acid via hydrolysis (Yamamoto *et al.*, 2011), which are then modified into eicosanoids that include proinflammatory mediators such as prostaglandins and leukotrienes (Yui *et al.*, 2015). Bleomycin-induced overproduction of proinflammatory cytokines such as thromboxane and leukotrienes are significantly reduced in mice with phospholipase inhibition, implicating a direct role for phospholipase as well as a putative role for PC in the pathogenesis of pulmonary fibrosis (Zhu *et al.*, 2010; Cheng *et al.*, 2015). The surfactant proteins SP-B and SP-C as well as phospholipid PCs are key components of lung surfactant produced by alveolar epithelial cell type 2 (Han and Mallampalli, 2015). An alteration in the composition of lung surfactants which are predominantly comprised of PCs can cause reduced elasticity and lead to an overall decrease in lung compliance. However, our findings were in contrast to those of Kulkarni *et al.* (2018), who reported a marked increase of approximately two-fold in the relative content of PCs (12:0/20:4, 18:2p/15:1, 16:1p/15:1, 15:1/20:4, 18:0e/20:4, 4:0/19:0, 24:6/24:7, 16:0e/20:4, 16:1/20:4, 16:1p/13:0, 15:0/20:4, 18:0/19:1, 16:0p/18:2, 16:1/18:2, 18:1/18:2, 18:0p/18:2, 22:6/24:7, 16:0e/18:2 and 18:0/18:1) in bleomycin-treated mice. Previous interstitial lung disease studies comparing IPF and sarcoidosis revealed a reduced amount of saturated fatty acids, in particular palmitic acids in the PC fraction of bronchoalveolar lavage. This supported our finding of decreased levels of PCs in IPF progressors (Honda *et al.*, 1988; Schmidt *et al.*, 2002).

Negative TOF-MS data revealed a number of lipid species such as PE (38:3, 18:0 and 38:2), PS (41:2, 39:2, 39:0, 39:1 and 37:1) and phosphatidylinositol (PI; 38:4). The down-regulation of these lipids in the progressors of IPF lent further support to Yan *et al.* (2017) observations of reduced PE (20:0/17:2 and 22:6/19:0), PS (20:0/19:0, 22:0/0:0, 0-20:0/20:0 and P-18:0/19:0) and PI (Cer d20:0/16:0) levels. PE is the second most abundant phospholipid in biological membranes and along with PC forms the hydrocarbon-backbone linkage of most cell membranes. PE is crucial for cell division as PE deficient cells show abnormal mitochondrial morphology and are unable to complete cell division and separate. However, studies by Poyton *et al.* (2016) and Calzada *et al.* (2016) reported that an increase in cellular PE leads to increased lipid oxidation, a common hallmark in neurological diseases. A separate study by Fahrman *et al.* (2016) showed evidence of elevated PE (34:2, 36:2 and 38:4) as important biomarkers to distinguish between malignant and benign lung cancers. Although PS and PI are not as well understood as PC and PE, their elucidation using negative TOF-MS warrants further investigation. These phospholipid classes are associated with inflammation and cellular apoptosis and may be associated with IPF and its severity.

A potential limitation in this study was the small cohort size. Nevertheless, the availability of the two diseased sample groups (stable *versus* progressors) allowed us to study global lipid changes associated with disease progression. The selectivity of the SONAR DIA approach was highlighted in this study using the deuterium-labelled lipid standards that were representative of the different classes of lipids found in human plasma. The isolation of the molecular ions prior to fragmentation allowed fragment ions to be easily assigned to its relevant precursors for specific compound identification (Gethings *et al.*, 2017). Although the sensitivity of SONAR was lower than the TOF-MS acquisition, a reduction in the total number of features resolved generated cleaner

lipid spectra and less interferences (Meyer and Schilling, 2017). Another advantage of SONAR is that the data generated were significantly smaller in size compared to other acquisition data files. This has considerable operational and resource benefits in terms of data processing, handling and storage.

3.5 Conclusion

This project successfully profiled plasma samples obtained from two groups of IPF patients using a DIA approach to enhance the specificity of unbiased lipid profiling derived from UPLC-QTOF-MS. In particular, this study demonstrated the advantages of the SONAR DIA technique for the characterization of lipid signatures such as TGs and PCs in IPF plasma samples. The use of labelled lipid internal standards allowed for the identification and quantitation of markers involved in pathways associated with disease pathogenesis such as lipid metabolism and mitochondrial-beta oxidation pathways.

3.6 References

- Aureli, M., D. Schiumarini, N. Loberto, R. Bassi, A. Tamanini, G. Mancini, M. Tironi, S. Munari, G. Cabrini, M. C. Dehecchi and S. Sonnino (2016). "Unravelling the role of sphingolipids in cystic fibrosis lung disease." Chemistry and Physics of Lipids 200: 94-103.
- Baker, G., C. Duck-Chong, K. Cleland and N. Berend (1986). "The Surfactant System as an Intrinsic Monitor of Acute Interstitial Lung Disease." CHEST 89(3): 126S-127S.
- Berry, K. A., R. C. Murphy, B. Kosmider and R. J. Mason (2017). "Lipidomic characterization and localization of phospholipids in the human lung[S]." Journal of Lipid Research 58(5): 926-933.
- Bujak, R., E. Dagher-Wojtkowiak, R. Kaliszan and M. J. Markuszewski (2016). "PLS-Based and Regularization-Based Methods for the Selection of Relevant Variables in Non-targeted Metabolomics Data." Frontiers in molecular biosciences 3: 35-35.
- Cajka, T. and O. Fiehn (2014). "Comprehensive analysis of lipids in biological systems by liquid chromatography-mass spectrometry." Trends in analytical chemistry: TRAC 61: 192-206.
- Calderón-Santiago, M., M. A. López-Bascón, Á. Peralbo-Molina and F. Priego-Capote (2017). "MetaboQC: A tool for correcting untargeted metabolomics data with mass spectrometry detection using quality controls." Talanta 174: 29-37.
- Calzada, E., O. Onguka and S. M. Claypool (2016). "Phosphatidylethanolamine Metabolism in Health and Disease." International Review of Cell and Molecular Biology 321: 29-88.

-
- Chang, D. and A. Keinan (2014). "Principal component analysis characterizes shared pathogenetics from genome-wide association studies." PLoS computational biology 10(9): e1003820-e1003820.
- Cheng, J., R. T. Dackor, J. A. Bradbury, H. Li, L. M. DeGraff, L. K. Hong, D. King, F. B. Lih, A. Gruzdev, M. L. Edin, G. S. Travlos, G. P. Flake, K. B. Tomer and D. C. Zeldin (2016). "Contribution of alveolar type II cell-derived cyclooxygenase-2 to basal airway function, lung inflammation, and lung fibrosis." The FASEB Journal 30(1): 160-173.
- Dautel, S. E., J. E. Kyle, G. Clair, R. L. Sontag, K. K. Weitz, A. K. Shukla, S. N. Nguyen, Y.-M. Kim, E. M. Zink, T. Luders, C. W. Frevert, S. A. Gharib, J. Laskin, J. P. Carson, T. O. Metz, R. A. Corley and C. Ansong (2017). "Lipidomics reveals dramatic lipid compositional changes in the maturing postnatal lung." Scientific Reports 7: 40555.
- Dong, S., R. Zhang, Y. Liang, J. Shi, J. Li, F. Shang, X. Mao and J. Sun (2017). "Changes of myocardial lipidomics profiling in a rat model of diabetic cardiomyopathy using UPLC/Q-TOF/MS analysis." Diabetology & Metabolic Syndrome 9: 56.
- Fahrman, J. F., D. Grapov, B. C. DeFelice, S. Taylor, K. Kim, K. Kelly, W. R. Wikoff, H. Pass, W. N. Rom, O. Fiehn and S. Miyamoto (2016). "Serum phosphatidylethanolamine levels distinguish benign from malignant solitary pulmonary nodules and represent a potential diagnostic biomarker for lung cancer." Cancer Biomarkers 16(4): 609-617.
- Ferraz-Nogueira, J. P., F. J. Díez-Guerra and J. Llopis (2014). "Visualization of Phosphatidic Acid Fluctuations in the Plasma Membrane of Living Cells." PLOS ONE 9(7): e102526.

-
- Figuroa, V., C. Milla, E. J. Parks, S. J. Schwarzenberg and A. Moran (2002). "Abnormal lipid concentrations in cystic fibrosis." The American Journal of Clinical Nutrition 75(6): 1005-1011.
- Gangwar, I., N. Kumar Sharma, G. Panzade, S. Awasthi, A. Agrawal and R. Shankar (2017). "Detecting the Molecular System Signatures of Idiopathic Pulmonary Fibrosis through Integrated Genomic Analysis." Scientific Reports 7(1): 1554.
- Gethings, L. A., K. Richardson, J. Wildgoose, S. Lennon, S. Jarvis, C. L. Bevan, J. P. C. Vissers and J. I. Langridge (2017). "Lipid profiling of complex biological mixtures by liquid chromatography/mass spectrometry using a novel scanning quadrupole data-independent acquisition strategy." Rapid Communications in Mass Spectrometry 31(19): 1599-1606.
- Godzien, J., M. Ciborowski, M. P. Martínez-Alcázar, P. Samczuk, A. Kretowski and C. Barbas (2015). "Rapid and Reliable Identification of Phospholipids for Untargeted Metabolomics with LC-ESI-QTOF-MS/MS." Journal of Proteome Research 14(8): 3204-3216.
- Guerrera, I. C., G. Astarita, J.-P. Jais, D. Sands, A. Nowakowska, J. Colas, I. Sermet-Gaudelus, M. Schuereberg, D. Piomelli, A. Edelman and M. Ollero (2009). "A Novel Lipidomic Strategy Reveals Plasma Phospholipid Signatures Associated with Respiratory Disease Severity in Cystic Fibrosis Patients." PLoS ONE 4(11): e7735.
- Hamanaka, R. B., R. Nigdelioglu, A. Y. Meliton, Y. Tian, L. J. Witt, E. O'Leary, K. A. Sun, P. S. Woods, D. Wu, B. Ansbro, S. Ard, J. M. Rohde, N. O. Dulin, R. D. Guzy and G. M. Mutlu (2018). "Inhibition of Phosphoglycerate Dehydrogenase Attenuates Bleomycin-induced Pulmonary Fibrosis." American Journal of Respiratory Cell and Molecular Biology 58(5): 585-593.

-
- Han, S. and R. K. Mallampalli (2015). "The Role of Surfactant in Lung Disease and Host Defense against Pulmonary Infections." Annals of the American Thoracic Society 12(5): 765-774.
- Hichami, A., C. Morin, E. Rousseau and N. A. Khan (2005). "Diacylglycerol-Containing Docosahexaenoic Acid in Acyl Chain Modulates Airway Smooth Muscle Tone." American Journal of Respiratory Cell and Molecular Biology 33(4): 378-386.
- Higham, A., S. Lea, K. Simpson and D. Singh (2012). "Lipids in the lung: Respiratory inflammation in COPD." European Respiratory Journal 40(Suppl 56).
- Hill, C. B. and Roessner, U. (2013). Metabolic Profiling of Plants by GC–MS. In the Handbook of Plant Metabolomics (eds W. Weckwerth and G. Kahl). doi:10.1002/9783527669882.ch1
- Honda, Y., K. Tsunematsu, A. Suzuki and T. Akino (1988). "Changes in phospholipids in bronchoalveolar lavage fluid of patients with interstitial lung diseases." Lung 166(1): 293-301.
- Hu, C., Y. Wang, Y. Fan, H. Li, C. Wang, J. Zhang, S. Zhang, X. Han and C. Wen (2015). "Lipidomics revealed idiopathic pulmonary fibrosis-induced hepatic lipid disorders corrected with treatment of baicalin in a murine model." The AAPS journal 17(3): 711-722.
- Ishikawa, M., K. Saito, H. Yamada, N. Nakatsu, K. Maekawa and Y. Saito (2016). "Plasma lipid profiling of different types of hepatic fibrosis induced by carbon tetrachloride and lomustine in rats." Lipids in health and disease 15: 74-74.
- Kang, Y. P., S. B. Lee, J.-m. Lee, H. M. Kim, J. Y. Hong, W. J. Lee, C. W. Choi, H. K. Shin, D.-J. Kim, E. S. Koh, C.-S. Park, S. W. Kwon and S.-W. Park (2016). "Metabolic Profiling Regarding Pathogenesis of Idiopathic Pulmonary Fibrosis." Journal of Proteome Research 15(5): 1717-1724.

-
- Knittelfelder, O. L., B. P. Weberhofer, T. O. Eichmann, S. D. Kohlwein and G. N. Rechberger (2014). "A versatile ultra-high performance LC-MS method for lipid profiling." Journal of chromatography. B, Analytical technologies in the biomedical and life sciences 951-952(100): 119-128.
- Knittelfelder, O. L., B. P. Weberhofer, T. O. Eichmann, S. D. Kohlwein and G. N. Rechberger (2014). "A versatile ultra-high performance LC-MS method for lipid profiling." Journal of chromatography. B, Analytical technologies in the biomedical and life sciences 951-952(100): 119-128.
- Kulkarni, Y. M., S. Dutta, A. K. V. Iyer, C. A. Wright, V. Ramesh, V. Kaushik, O. J. Semmes and N. Azad (2018). "A Lipidomics Approach to Identifying Key Lipid Species Involved in VEGF-Inhibitor Mediated Attenuation of Bleomycin-Induced Pulmonary Fibrosis." Proteomics Clinical Applications 12(3): e1700086.
- Kyle, J. E., G. Clair, G. Bandyopadhyay, R. S. Misra, E. M. Zink, K. J. Bloodsworth, A. K. Shukla, Y. Du, J. Lillis, J. R. Myers, J. Ashton, T. Bushnell, M. Cochran, G. Deutsch, E. S. Baker, J. P. Carson, T. J. Mariani, Y. Xu, J. A. Whitsett, G. Pryhuber and C. Ansong (2018). "Cell type-resolved human lung lipidome reveals cellular cooperation in lung function." Scientific Reports 8(1): 13455.
- Kyle, J. E., X. Zhang, K. K. Weitz, M. E. Monroe, Y. M. Ibrahim, R. J. Moore, J. Cha, X. Sun, E. S. Lovelace, J. Wagoner, S. J. Polyak, T. O. Metz, S. K. Dey, R. D. Smith, K. E. Burnum-Johnson and E. S. Baker (2016). "Uncovering Biologically Significant Lipid Isomers with Liquid Chromatography, Ion Mobility Spectrometry and Mass Spectrometry." The Analyst 141(5): 1649-1659.
- Liebisch, G., J. A. Vizcaíno, H. Köfeler, M. Trötz Müller, W. J. Griffiths, G. Schmitz, F. Spener and M. J. O. Wakelam (2013). "Shorthand notation for lipid structures derived from mass spectrometry." Journal of lipid research 54(6): 1523-1530.

-
- Low, R. B. (1989). "Bronchoalveolar Lavage Lipids in Idiopathic Pulmonary Fibrosis." CHEST 95(1): 3-5.
- Meyer, J. G. and B. Schilling (2017). "Clinical applications of quantitative proteomics using targeted and untargeted data-independent acquisition techniques." Expert review of proteomics 14(5): 419-429.
- Moseley, M. A., C. J. Hughes, P. R. Juvvadi, E. J. Soderblom, S. Lennon, S. R. Perkins, J. W. Thompson, W. J. Steinbach, S. J. Geromanos, J. Wildgoose, J. I. Langridge, K. Richardson and J. P. C. Vissers (2018). "Scanning Quadrupole Data-Independent Acquisition, Part A: Qualitative and Quantitative Characterization." Journal of Proteome Research 17(2): 770-779.
- Naik, D., A. Joshi, T. V. Paul and N. Thomas (2014). "Chronic obstructive pulmonary disease and the metabolic syndrome: Consequences of a dual threat." Indian journal of endocrinology and metabolism 18(5): 608-616.
- Naz, S., M. Vallejo, A. Garcia and C. Barbas (2014). "Method validation strategies involved in non-targeted metabolomics." Journal of Chromatography A 1353: 99-105.
- Nicolson, G. L. and M. E. Ash (2014). "Lipid Replacement Therapy: A natural medicine approach to replacing damaged lipids in cellular membranes and organelles and restoring function." Biochimica et Biophysica Acta (BBA) - Biomembranes 1838(6): 1657-1679.
- Popa, C., M. G. Netea, P. L. C. M. van Riel, J. W. M. van der Meer and A. F. H. Stalenhoef (2007). "The role of TNF- α in chronic inflammatory conditions, intermediary metabolism, and cardiovascular risk." Journal of Lipid Research 48(4): 751-762.

-
- Pöyry, S. and I. Vattulainen (2016). "Role of charged lipids in membrane structures — Insight given by simulations." Biochimica et Biophysica Acta (BBA) - Biomembranes 1858(10): 2322-2333.
- Poyton, M. F., A. M. Sendekci, X. Cong and P. S. Cremer (2016). "Cu(2+) Binds to Phosphatidylethanolamine and Increases Oxidation in Lipid Membranes." Journal of American Chemical Society 138(5): 1584-1590.
- Sarri, E., A. Sicart, F. Lázaro-Diéguez and G. Egea (2011). "Phospholipid Synthesis Participates in the Regulation of Diacylglycerol Required for Membrane Trafficking at the Golgi Complex." Journal of Biological Chemistry 286(32): 28632-28643.
- Satomi, Y., M. Hirayama and H. Kobayashi (2017). "One-step lipid extraction for plasma lipidomics analysis by liquid chromatography mass spectrometry." Journal of Chromatography B 1063: 93-100.
- Schmidt, R., U. Meier, P. Markart, F. Grimminger, H. G. Velcovsky, H. Morr, W. Seeger and A. Günther (2002). "Altered fatty acid composition of lung surfactant phospholipids in interstitial lung disease." American Journal of Physiology-Lung Cellular and Molecular Physiology 283(5): L1079-L1085.
- Schoeman, J. C., A. C. Harms, M. van Weeghel, R. Berger, R. J. Vreeken and T. Hankemeier (2018). "Development and application of a UHPLC-MS/MS metabolomics based comprehensive systemic and tissue-specific screening method for inflammatory, oxidative and nitrosative stress." Analytical and bioanalytical chemistry 410(10): 2551-2568.
- Telenga, E. D., R. F. Hoffmann, t. K. Ruben, S. J. Hoonhorst, B. W. Willemse, A. J. van Oosterhout, I. H. Heijink, M. van den Berge, L. Jorge, P. Sandra, D. S. Postma, K. Sandra and N. H. ten Hacken (2014). "Untargeted lipidomic analysis in

-
- chronic obstructive pulmonary disease. Uncovering sphingolipids." American Journal of Respiratory Critical Care Medicine 190(2): 155-164.
- Tham, Y. K., B. C. Bernardo, K. Huynh, J. Y. Y. Ooi, X. M. Gao, H. Kiriazis, C. Giles, P. J. Meikle and J. R. McMullen (2018). "Lipidomic Profiles of the Heart and Circulation in Response to Exercise versus Cardiac Pathology: A Resource of Potential Biomarkers and Drug Targets." Cell Reports 24(10): 2757-2772.
- Titz, B., K. Luettich, P. Leroy, S. Boue, G. Vuillaume, T. Vihervaara, K. Ekroos, F. Martin, M. C. Peitsch and J. Hoeng (2016). "Alterations in Serum Polyunsaturated Fatty Acids and Eicosanoids in Patients with Mild to Moderate Chronic Obstructive Pulmonary Disease (COPD)." International journal of molecular sciences 17(9): 1583.
- Tolstikov, V., A. Nikolayev, S. Dong, G. Zhao and M.-S. Kuo (2014). "Metabolomics Analysis of Metabolic Effects of Nicotinamide Phosphoribosyltransferase (NAMPT) Inhibition on Human Cancer Cells." PLOS ONE 9(12): e114019.
- Urban, J. and D. Štys (2015). Noise and Baseline Filtration in Mass Spectrometry. Bioinformatics and Biomedical Engineering, Cham, Springer International Publishing.
- Wehrens, R., J. A. Hageman, F. van Eeuwijk, R. Kooke, P. J. Flood, E. Wijnker, J. J. B. Keurentjes, A. Lommen, H. D. L. M. van Eekelen, R. D. Hall, R. Mumm and R. C. H. de Vos (2016). "Improved batch correction in untargeted MS-based metabolomics." Metabolomics 12: 88.
- Weigel, C., M. R. Veldwijk, C. C. Oakes, P. Seibold, A. Slynko, D. B. Liesenfeld, M. Rabionet, S. A. Hanke, F. Wenz, E. Sperk, A. Benner, C. Rösli, R. Sandhoff, Y. Assenov, C. Plass, C. Herskind, J. Chang-Claude, P. Schmezer and O. Popanda (2016). "Epigenetic regulation of diacylglycerol kinase alpha promotes radiation-induced fibrosis." Nature communications 7: 10893-10893.

-
- Worley, B. and R. Powers (2016). "PCA as a practical indicator of OPLS-DA model reliability." Current Metabolomics 4(2): 97-103.
- Yamamoto, K., Y. Isogai, H. Sato, Y. Taketomi and M. Murakami (2011). "Secreted phospholipase A2, lipoprotein hydrolysis, and atherosclerosis: integration with lipidomics." Analytical and bioanalytical chemistry 400(7): 1829-1842.
- Yan, F., Z. Wen, R. Wang, W. Luo, Y. Du, W. Wang and X. Chen (2017). "Identification of the lipid biomarkers from plasma in idiopathic pulmonary fibrosis by Lipidomics." BMC Pulmonary Medicine 17: 174.
- Yang, K., X. Fang, R. W. Gross and X. Han (2011). "A practical approach for determination of mass spectral baselines." Journal of the American Society for Mass Spectrometry 22(11): 2090-2099.
- Yu, Z., H. Chen, J. Ai, Y. Zhu, Y. Li, J. A. Borgia, J.-S. Yang, J. Zhang, B. Jiang, W. Gu and Y. Deng (2017). "Global lipidomics identified plasma lipids as novel biomarkers for early detection of lung cancer." Oncotarget 8(64): 107899-107906.
- Yuan, Y., N. Ran, L. Xiong, G. Wang, X. Guan, Z. Wang, Y. Guo, Z. Pang, K. Fang, J. Lu, C. Zhang, R. Zheng, J. Zheng, J. Ma and F. Wang (2018). "Obesity-Related Asthma: Immune Regulation and Potential Targeted Therapies." Journal of Immunology Research 2018: 13.
- Yui, K., G. Imataka, H. Nakamura, N. Ohara and Y. Naito (2015). "Eicosanoids Derived From Arachidonic Acid and Their Family Prostaglandins and Cyclooxygenase in Psychiatric Disorders." Current neuropharmacology 13(6): 776-785.
- Zehethofer, N., S. Bermbach, S. Hagner, H. Garn, J. Müller, T. Goldmann, B. Lindner, D. Schwudke and P. König (2015). "Lipid Analysis of Airway Epithelial Cells for Studying Respiratory Diseases." Chromatographia 78(5): 403-413.

-
- Zhao, Y. D., L. Yin, S. Archer, C. Lu, G. Zhao, Y. Yao, L. Wu, M. Hsin, T. K. Waddell, S. Keshavjee, J. Granton and M. de Perrot (2017). "Metabolic heterogeneity of idiopathic pulmonary fibrosis: a metabolomic study." BMJ Open Respiratory Research 4(1).
- Zhu, Y., Y. Liu, W. Zhou, R. Xiang, L. Jiang, K. Huang, Y. Xiao, Z. Guo and J. Gao (2010). "A prostacyclin analogue, iloprost, protects from bleomycin-induced pulmonary fibrosis in mice." Respiratory research 11(1): 34-34.

Supplementary Table 3.1 Progenesis output of the features detected including m/z, chemical formula, mass error, putative identification (ID) as well as the calculated mean abundance, percentage relative standard deviation (%RSD), fold-changes and the relative concentrations based on the SPLASH LipidoMix standards.

MS mode	Feature <i>m/z</i>	Chemical Formula	Mass error ppm	Putative ID	Stable (ST)			Progressor (PR)			
					Mean	%RSD	Concentration (mmol/L)	Mean	%RSD	Concentration (mmol/L)	Fold- Change
Positive TOF-MS	820.7382	C51H94O6	-5.70	TG [48:2]	3922230.27	35.27	1.29	3708641.14	43.31	1.22	0.95
	524.3730	C26H54NO7P	3.69	PE [21:0]	1181324.53	28.33	0.01	1058805.34	23.63	0.37	0.90
		C26H54NO7P	3.69	PC [18:0]							
		C26H54NO7P	3.69	PC [O- 18:0]							
	879.7440	C55H100O6	-1.47	TG [52:3]	3162371.36	20.35	0.98	3411677.49	10.60	1.05	1.08
	924.8041	C59H102O6	3.20	TG [56:6]	1938446.34	30.97	0.56	2161005.90	22.05	0.63	1.11
	794.7233	C49H92O6	-4.82	TG [46:1]	1359110.87	43.81	0.46	1252028.51	66.42	0.43	0.92
920.7704	C59H98O6	7.12	TG [56:8]	1787751.49	42.00	0.52	2264408.98	31.17	0.66	1.27	

822.7558	C51H96O6	1.60	TG [48:1]	1876332.83	33.05	0.62	1779940.41	36.50	0.58	0.95
951.7406	C61H100O6	-0.62	TG [58:9]	257870.68	32.51	0.07	354931.15	36.26	0.10	1.38
788.6164	C44H86NO8P	-0.02	PC [36:1]	3221172.70	30.93	60.63	3011316.08	23.61	56.68	0.93
	C44H86NO8P	-0.02	PE [39:1]			0.01			0.69	
834.5986	C48H84NO8P	-2.55	PC [40:6]	923395.13	38.88	16.42	776133.27	35.49	13.80	0.84
	C44H83NO13	5.86	PE [43:6]			0.01			0.17	
784.5851	C44H82NO8P	-0.02	PC [36:3]	3139547.70	26.30	59.40	3043281.89	26.72	57.57	0.97
	C44H82NO8P	-0.02	PE [39:3]			0.01			0.71	
878.8198	C55H104O6	3.16	TG [52:1]	3250208.57	31.44	1.00	3183352.66	26.92	0.98	0.98
812.6164	C46H86NO8P	0.01	PC [38:3]	2445269.59	35.04	44.66	2139828.78	30.90	39.08	0.88
	C44H88NO8P	3.06	PC [36:0]							
	C44H88NO8P	3.06	PE			0.01			0.49	

				[39:0]							
		C46H86NO8P	0.01	PE							
		C46H83O8P	0.01	[41:3] PA [43:4]			1.07			0.94	
785.5885	C43H87O7P	8.54	PA [O- 40:0]	2362037.61	28.48	1.10	2219762.12	24.44	1.04	0.94	
881.7600	C57H100O6	0.81	TG	3077766.22	20.66	0.92	3257735.02	8.23	0.98	1.06	
	C55H102O6	3.63	[54:5] TG [52:2]								
Negative TOF-MS	856.6105	C47H88NO10P	1.31	PS [41:2]	74416.05	25.10	0.07	62036.87	35.15	0.06	0.83
	768.5570	C43H80NO8P	1.45	PC	67730.51	18.77	13.41	60031.62	30.03	11.88	0.89
		C43H80NO8P	1.45	[35:3] PE [38:3]			0.01			0.01	
	828.5780	C45H84NO10P	2.59	PS [39:2]	165448.74	18.33	0.16	147108.90	29.87	0.14	0.89
	480.3094	C23H48NO7P	-0.24	PE	55791.69	17.18	0.02	47244.98	30.48	0.01	0.85
		C23H48NO7P	-0.24	[18:0] LysoPE [18:0]			0.60			0.51	
		C23H48NO7P	-0.24	PC			17.66			14.95	

[15:0]										
832.6102	C45H88NO10P C46H87NO9	3.49 3.43	PS [39:0]	86008.62	22.56	0.08	74745.40	28.41	0.07	0.87
830.5927	C45H86NO10P	1.24	PS [39:1]	359209.72	10.82	0.34	324924.30	29.37	0.31	0.90
770.5717	C43H82NO8P	1.57	PC [35:2]	133594.03	12.05	26.37	120452.91	30.95	23.78	0.90
	C43H82NO8P	1.57	PE [38:2]			0.03			0.02	
	C43H84NO9P	1.53	PS [O- 37:1]			0.13			0.12	
	C43H84NO9P	1.53	PS [P- 37:0]							
	C43H82NO8P	1.57	PE- NMe2 [36:2]							
	C44H81NO7	1.40	DGTS [34:2]							
797.6063	C46H89O9P	-0.34	PG [O- 40:2]	67610.32	10.95	0.36	68389.40	22.07	0.37	1.01
	C46H89O9P	-0.34	PG [P- 40:1]							
	C46H87O8P	-0.35	PA [43:2]			0.08			0.08	
	C53H84O6	-3.24	TG [50:9]			30.35			30.70	

	802.5605	C43H82NO10P	0.20	PS [37:1]	515132.53	10.28	0.50	487701.69	27.47	0.48	0.95
		C43H82NO10P	0.20	PT [36:1]							
	885.5519	C47H83O13P	2.36	PI [38:4]	154232.67	22.78	0.05	129368.60	29.20	0.05	0.84
		C47H83O13P	2.36	Glc-GP [38:4]							
Positive SONAR	923.7138	C57H102O6	2.55	TG [56:9]	3076.29	62.00	0.04	4224.01	81.20	0.05	1.37
	868.7379	C55H96O6	1.21	TG [52:6]	7640.05	86.83	0.10	7706.59	72.50	0.10	1.01
	894.7547	C57H98O6	-4.19	TG [54:7]	30733.15	69.55	0.38	33646.03	63.16	0.42	1.09
	920.7718	C56H94O6	9.16	TG [56:8]	81674.38	51.30	0.99	98617.58	45.81	1.19	1.21
	896.7703	C57H100O6	1.73	TG [54:6]	16442.49	61.27	0.20	17179.25	55.30	0.21	1.04
	922.7879	C55H104O6	2.18	TG [56:7]	67636.37	38.61	0.81	74015.93	51.46	0.89	1.09
	603.5333	C37H72O4	1.83	DG [O- 34:1]	69975.54	46.43	n/a	76449.96	65.02	n/a	1.09
	784.5847	C44H78NO8P	-1.12	PC [36:3]	354079.28	29.03	136.01	345040.15	39.73	132.54	0.97
	806.5665	C46H82NO8P	-1.44	PC [36:3]	129744.46	25.50	49.84	116483.47	39.00	44.75	0.90
	808.5829	C44H84NO8P	-0.64	PC [36:2]	309271.88	24.07	118.50	282083.51	31.34	108.08	0.91

812.6160	C46H86NO8P	-0.19	PC [38:3]	272053.56	33.73	100.89	218044.34	43.11	80.86	0.80
----------	------------	-------	--------------	-----------	-------	--------	-----------	-------	-------	------

MALDI-mass spectrometry imaging by freeze-spot deposition of the matrix

Adapted from Nambiar, S.; Trengove, R. D.; and Gummer, J. P. A (2018) “MALDI-mass spectrometry imaging by freeze-spot deposition of the matrix” *Ready for submission to Analytical Chemistry*

4.1 Abstract

Imaging mass spectrometry is emerging as a powerful tool for the visualisation of metabolite distribution as well as the measurement of metabolites without the loss of spatial dimensionality in a sample. In MALDI-MSI, deposition of the chemical-matrix onto the sample serves to simultaneously extract biomolecules to the sample surface and concurrently render the sample amenable to MALDI. However, the mechanism of matrix application can mobilise the metabolites and together with the matrix-crystal size formation limit the spatial resolution which may otherwise be achieved by MSI. The chosen method of matrix deposition is thus integral to maintaining the spatial dimensionality endogenous to a sample. Here, we described a matrix application technique, herein referred to as the “freeze-spot” method. The method was conceived as a low-cost preparative approach requiring minimal amounts of chemical matrix which maintains the spatial dimensionality of the sample for MALDI-MSI. Matrix deposition is achieved by spot or spray application of the matrix solution, solubilised within an organic solvent with a freezing step using a chilled sample stage to which the sample section is mounted. The matrix solution freezes upon contact with the sample and the solvent is removed by lyophilisation. The technique was found to be particularly useful for MALDI-MSI of small sample sections and is well suited to efficient and cost-

effective method development whilst maintaining the spatial dimensionality that traditional spotting methods lack.

Keywords: MALDI, MSI, matrix, freeze-spot, adduct

4.2 Introduction

Mass spectrometry imaging (MSI) is a powerful tool for the measurement of metabolites which captures the spatial dimensionality of metabolite distribution of a sample. MSI has wide-ranging application in all areas of biological (Rompp *et al.*, 2015), biomedical (Liu and Ouyang, 2013), clinical research (Addie *et al.*, 2015) and diagnostics (Ye *et al.*, 2013; Norris *et al.*, 2017), with a diversity of dedicated sample preparative approaches. MSI is performed by positioning the sample within a purpose-build ion source of a mass spectrometer, whereby the ionisation process which starts from a single focal point of the sample is then rastered across the sample surface and a mass spectrum generated at each pixel coordinate. These mass spectra can be assembled into an ion-map image representing the relative signal intensity and spatial distribution of the measured biomolecular species co-registered to the original sample section. From sample collection through to MS acquisition, MSI experiments require a number of key preparative steps which serve to influence the final interpretative outcome and are therefore worthy of careful consideration. Each has been well described in the literature (McDonnell and Heeren, 2007; Amstalden van Hove *et al.*, 2010) as well as in a recent systematic review by Boughton *et al.* (2016).

Matrix-assisted laser desorption ionisation (MALDI) continues to dominate as the most common ionisation mechanism in MSI (Boughton and Hamilton, 2017). A key step in

preparing a sample for MALDI-MSI is application of the chemical matrix (Vergeiner *et al.*, 2014), and consequently, consideration of the choice of MALDI matrix and methods for its deposition onto a sample are critical. A uniform matrix application is crucial to extract and desorb molecules efficiently from within the section, to the sample surface. Uneven matrix deposition may result in sample coordinates with less than desirable ion signal intensity due to insufficient amount of matrix, or biomolecule delocalization caused by excessive or lengthy contact with the solvated matrix (Gemperline *et al.*, 2014).

Matrix application plays a critical role in the quality of the mass spectral images generated, specifically when aiming to achieve the highest spatial resolution images. The spatial dimensionality and reproducibility are limited by matrix crystal size (Gemperline *et al.*, 2014), solvent composition (Li *et al.*, 2016) and availability of elemental species which lend themselves to ion/adduct formation upon ionisation. Conventional methods for matrix application include the use of airbrush, automatic sprayer, and sublimation (Gemperline *et al.*, 2014). These methods share a common goal of achieving small matrix crystal size formation and minimising contact with the liquid solvent. Application of the matrix solution by airbrush spraying is commonly used in MALDI imaging and is relatively simple and quick, requiring relatively inexpensive apparatus (Gemperline *et al.*, 2014; Li *et al.*, 2016). The major limitation of this technique is that the sprayer and the velocity of the spray are controlled manually which causes the quality of the application to be user dependent and may greatly affect the reproducibility of data. Variations in the spray velocity and duration cause inconsistent application and applying too much solvent to the tissue can cause analyte delocalization, and predominantly of the small molecules (Baluya *et al.*, 2007). Automatic sprayer systems, such as the TM-Sprayer from HTX Technologies, have

been developed to remove the variability seen with manual airbrush application by robotically controlling the temperature, solvent flow rate, velocity of the matrix spraying nozzle during each pass, and number of passes (Gemperline *et al.*, 2014; Li *et al.*, 2016). With appropriate optimisation of methodology an automatic sprayer system can achieve uniform matrix density and crystal size formation, and experimental results more reproducible. This specialised equipment however, is not always readily available to researchers. Recently, the solvent-free sublimation technique has gained popularity for MSI of small molecules (Gemperline *et al.*, 2014; Van Nuffel *et al.*, 2018). Sublimation reduces analyte diffusion because the matrix deposits onto the sample surface free of liquid solvent which may otherwise delocalize molecules within the sample (Van Nuffel *et al.*, 2018). Murphy *et al.* (2011), Weishaupt *et al.* (2015) and Yang *et al.* (2017) previously reported that the formation of fine matrix crystals by the sublimation method translates to improved spatial measurements of the metabolites. However, one considered drawback of this method is if the liquid solvent does not make contact with the sample surface and thus not being available as an analyte extractant. This may result in some compound classes going undetected, though maintaining the superior spatial resolution of those that do.

While these presently applied techniques are routinely used in MALDI-MSI, matrix deposition techniques such as the “dried droplet” method, achieved by simple pipette-spotting, are still used when maintaining the spatial dimensionality. Traditionally in this approach the matrix solution is combined with the sample and spotted onto the target surface for analysis (Gabriel *et al.*, 2014). The sample/matrix droplet is subsequently dried. This approach lends itself to rapid method optimisation by permitting small amounts of matrix solution of any desirable composition to be applied to a sample section for rapid screening. The ease and robustness of the method validates its more

recent application in studies involving peptide identification (Schlosser *et al.*, 2009), lipid profiling (Murphy *et al.*, 2011) and pharmacotherapy (Grove *et al.*, 2011). However, the critical problems associated with this method is the sample preparation and the creation of “hot spots”, regions of relative high sample intensity. This is due in part to the uncontrolled matrix crystallisation. These “hot spots” present a major challenge to the detection and quantitation of analytes due to certain regions containing high intensity data while some regions may not have sufficient signal to generate a spectrum (Gabriel *et al.*, 2014; Fukuyama *et al.*, 2015).

In this study, we introduce a novel matrix application technique coined “freeze-spot”. This technique was conceived as a low-resource-intensive matrix application for spatially small samples for MALDI-MSI. This method is hypothesised to improve the throughput of method optimisations whilst maintaining the spatial localisation of metabolites endogenous to the sample. Matrix application is achieved by pipette-spotting the matrix solution onto the sample which is mounted on a chilled sample stage. When using a relatively high freezing point solvent, the matrix solution freezes upon contact with the sample and the solvent is then removed by lyophilisation. The “freeze-spot” method was found to be quick, cost-effective; requiring minimal amounts of chemical matrix, quantitative; with data not suffering from hot spots, and with the spatial resolution of the acquired MALDI-MS image maintained.

4.3 Experimental section

4.3.1 Chemicals

Ultra-pure LC-MS grade solvents including acetonitrile (ACN), isopropanol (IPA) and water (H₂O) as well as trifluoroacetic acid (TFA) were purchased from Thermo Fisher Scientific (Massachusetts, USA). Sodium acetate (NaOAc), potassium acetate (KOAc) and 2,5-dihydroxybenzoic acid (DHB) were obtained from Sigma-Aldrich (Castle Hill, Australia) and used without further purification.

4.3.2 Sample preparation

The technique is demonstrated using wheat seed. Wheat seed sections were embedded in boiled-egg white matrix as recently described in Bøgeskov Schmidt *et al.* (2018). Briefly, commercial chicken eggs were boiled, and the denatured egg white composed of albumin was collected. Wheat seedlings of the Chara cultivar were harvested directly from the plant and embedded in a 2 cm cube of denatured albumin. The albumin block was then gently frozen by placing it directly above liquid nitrogen, and subsequently mounted to a cryotome chuck using an optimal cutting temperature (OCT) compound. Wheat seeds were cryo-sectioned at -20 °C and at 20 µm thickness, taking care to avoid OCT material contact with the sectioned tissue. The seed sections were transferred onto pre-chilled glass microscope slides by thaw-mounting. All microscopy glass slides were thoroughly rinsed with IPA and chilled in the cryotome prior to sample mounting. All sections were stored at -80 °C.

4.3.3 Matrix application

To prepare for matrix application, the same sections were lyophilised to dryness under vacuum of approximately 50 Torr for 30 mins using a Labconco Freezone 2.5 Plus freeze-dryer depressurized with a JLT-10 JAVAC high vacuum pump.

For freeze-spot matrix application, DHB matrix was prepared at a concentration of 20 mg/mL in 80 % ACN (0.1 % TFA). Where reported, the matrix solution also contained 10 mM of either sodium acetate (NaOAc) or potassium acetate (KOAc), to promote sodium ($[M+Na]^+$) or potassium ($[M+K]^+$) adduct formation, respectively. The mounted sample sections were placed onto a stainless-steel stage, pre-chilled on dry ice and 5 μ L DHB (20 mg/mL) matrix was transferred onto the sample section by pipette. The solvent immediately froze upon contact with the sample. The glass slides were transferred to a polypropylene 50-mL centrifuge tube, which was sealed, submerged briefly in liquid nitrogen and the solvent removed by lyophilisation.

Similarly, DHB matrix prepared at 20 mg/mL in 80 % ACN (0.1 % TFA) was also used for the dried droplet and the automated matrix application techniques. For the dried-droplet approach, 5 μ L of DHB was pipetted onto the lyophilised section and the matrix droplet was left to dry for 15 mins at room temperature. For the automated approach, a TM-Sprayer (HTX Technologies; North Carolina, U.S.A.) fitted with a Shimadzu LC20-AD HPLC pump (Shimadzu Australia, New South Wales, Australia) was utilised. The sample loop was filled with 6 mL of DHB matrix solution and deposited onto the section using a flow rate of 0.25 mL/min; spray nozzle temperature and velocity at 110 °C and 700 mm/min, respectively, with four passes at 2 mm spacing, followed by

alternate passes at 90° offset. Slides from both the dried droplet and automated approaches were then placed in the freeze-dryer for lyophilisation.

4.3.4 Microscopy

The dimensional distribution of the DHB crystals formed under different matrix application techniques were examined by optical microscopy using an Olympus BX51 (Olympus Australia Pty Ltd, Victoria, Australia) with an objective magnification of 40x and sensitivity set at ISO200. Microscopy images were acquired using an “auto” exposure mode with an exposure time of 1/2,000 s at 50 µm scale.

4.3.5 MALDI-MSI acquisition

All MALDI-MSI analyses were performed using a Waters Synapt G2S mass spectrometer equipped with an orthogonal MALDI ion source and Nd:YAG laser (Waters Corporation, Manchester, U.K.). Prior to the analytical acquisition, digital scans of the tissue sections were obtained using an Epson WorkForce Pro WP-4540 scanner (Epson America, Inc.) and imported into the MALDI Imaging Pattern Creator software (Waters Corporation, Manchester, UK). Data were acquired from the selected regions of interest using positive ionisation mode, operating at a 350 J laser energy, with a 1,000 Hz firing rate. All data were acquired over the mass range m/z 50 to 1,200 using an “automatic” scan speed setting. Raw signal intensities of the mass spectra were extracted using MassLynx version 4.0 (Waters Corporation, Manchester, UK). The MSI images were acquired at a spatial resolution set at 600 laser shots per position and ion images were generated with Biomap 3.7.5.5 software.

4.4 Results and Discussion

Mass spectrometry imaging approaches typically require optimization for each parameter, including the screening of appropriate matrix application techniques. The initial work was focused on the uniformity of matrix deposition across a microscopy glass slide. Three commonly used techniques, automatic sprayer and manual spotting, along with the newly developed freeze-spot method, were employed using the prepared DHB matrix at 20 mg/mL.

The freeze spot approach performed comparably to deposition of matrix by automatic spray application, whilst manual spotting lacked uniformity and inconsistency in application (Figure 4.1). Chemical matrices can be applied in a controlled manner using an automated device to spray the matrix onto the sample in a programmable way. Commercially available automatic sprayers although differing in mechanism, use the same basic principle of spraying a fine aerosol of matrix which deposits onto the surface of the sample (Mounfield and Garrett, 2012). Multiple offset spray coats were required to deposit enough of the chemical matrix to sufficiently cover the section of interest (Figure 4.1), which made this more time intensive and a more chemical matrix-consuming approach to the freeze spot. The advantage of this automatic system over the manual approach is to achieve reproducibility in application, particularly of large sample sections, with another benefit that the conditions of coating can be adjusted in a systematic way to optimize the coating procedure for the given sample tissue (Gemperline *et al.*, 2014).

Manual spotting of chemical matrices has the advantage that it is inexpensive and easy to implement. Earlier studies have used this approach to coat specific sample regions of

interest with the matrix, for a focussed MSI acquisition. For the trained user, this technique can be used to generate very high-resolution images of the tissue; however, the major disadvantage of manual spotting is that it is user dependant and it is difficult to standardize across multiple samples (Figure 4.2; Gemperline *et al.*, 2014). Matrix is deposited directly onto the tissue and then allowed to dry. Each of these demonstrated manual spot applications (Figure 4.1) were performed with a single pipetting step, and with just 5 μL of DHB. The spotting techniques were further investigated to understand the resultant matrix crystal formation and uniformity (Figure 4.2).

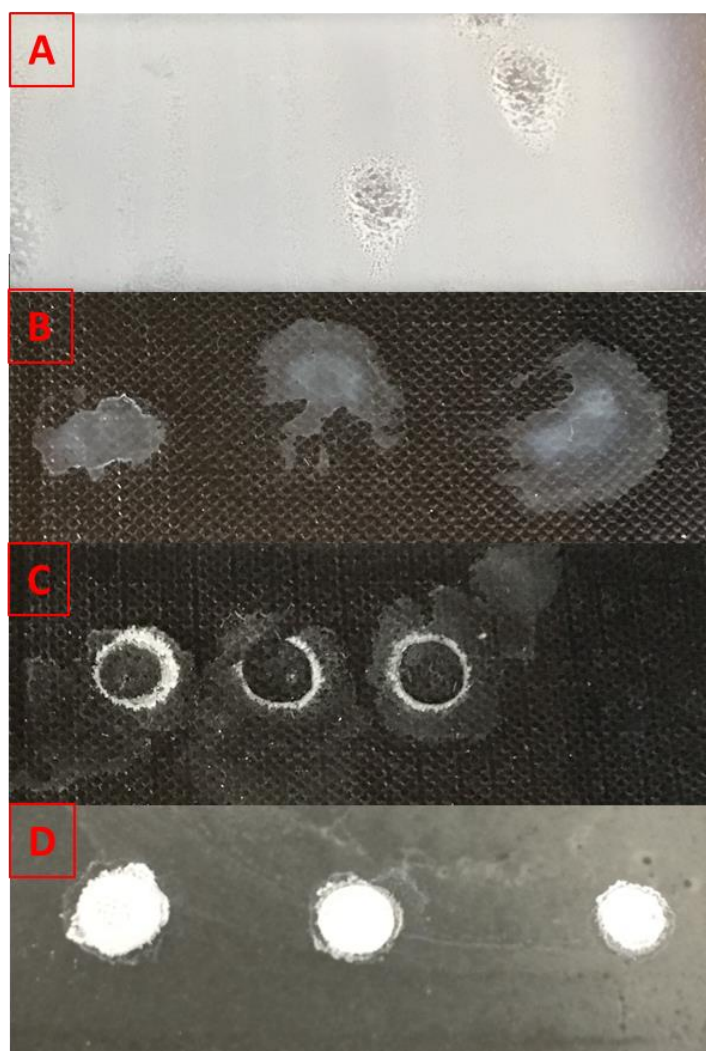


Figure 4.1 The different matrix application approaches using DHB prepared at 20 mg/mL. (A) Automatic sprayer; (B) manual spotting with an ambient dry-out step; (C) manual spotting on dry ice followed by a dry-out step; and (D) freeze-spotting technique.

The capture of phase-contrast images (Yin *et al.*, 2012) by conventional light microscopy allowed the morphology of the matrix crystals to also be examined (Figure 4.2). Crystallisation of the DHB matrix after deposition by automatic sprayer (Figure 4.2; A) was compared to deposition by manual spotting; one was dried at room temperature and the other on dry ice, respectively (Figure 4.2; B, C). The matrix crystals formation using the freeze-spot approach is also presented for comparison (Figure 4.2; D). A comparatively fine “web” of crystals was observed using the freeze-spot approach, which together with the observed depth of matrix presented a far more homogeneous application (Figures 4.1 and 4.2).

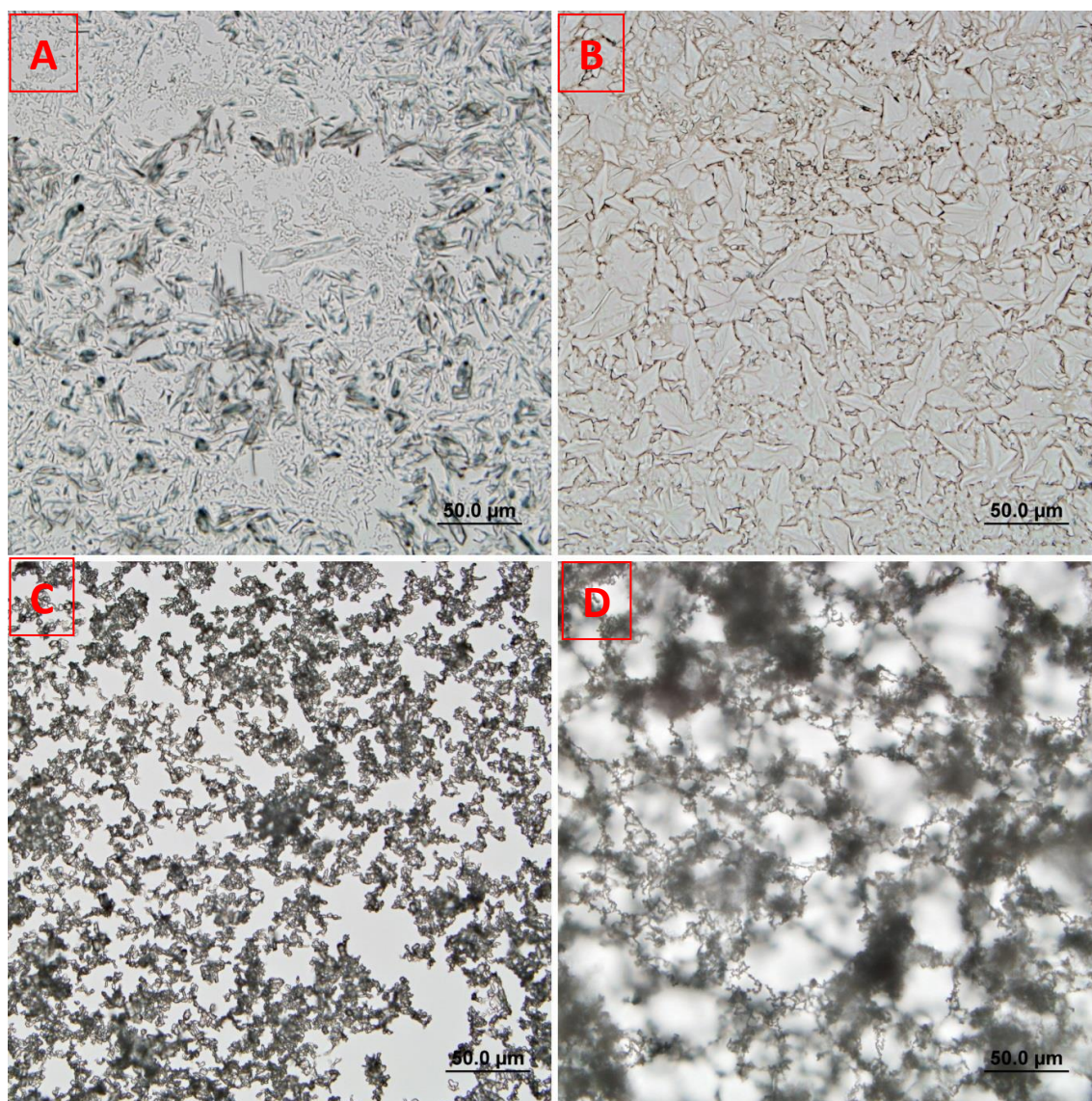


Figure 4.2 Light microscopic images of the matrix crystals obtained by the different application approaches using DHB prepared at 20 mg/mL. (A) Automatic sprayer; (B) manual spotting with an ambient dry-out step; (C) manual spotting on dry ice followed by a dry-out step; and (D) freeze-spotting technique.

Direct application of the chemical matrix onto cryo-sectioned samples can be challenging due to the thaw rate of samples (Xu *et al.*, 2016). Differing sample moisture content may also introduce inconsistencies by changing the solvent composition and conditions of matrix application. Previously, a two-step approach for matrix application has been reported in which the samples are dried by vacuum at room temperature or oven prior to matrix deposition (Li *et al.*, 2016). Metabolite degradation is a concern when using dehydration procedures, particularly with prolonged heat treatments (Goodwin *et al.*, 2010; Shariatgorji *et al.*, 2014). As such, here we dried the sample section by lyophilisation prior to matrix application. This allowed preservation of native metabolite species and improved reproducibility in matrix application. Lyophilisation of the matrix-applied sample section was also employed as the final step in the freeze-spot approach, to maintain sample integrity. The removal of the solvent by lyophilisation also promotes the formation of a very fine crystal structure (Figure 4.2).

The simplicity of the freeze-spot method compared to other commercial sprayers makes the technique easy to adapt. In our initial experiments, the freeze-spot method was investigated using 3 μL of DHB at 20 mg/mL in ACN:H₂O (4:1, v/v) onto a cryo-section of wheat seed. Although the volume of matrix was sufficient to cover the entire surface of the seed, the MSI image generated had reduced spatial information. A concern with spotting-based application is always the possibility of analyte delocalization. However, the time from application of the liquid matrix to freezing is on a sub-second time-frame and delocalisation needs to occur during this brief moment. To estimate the magnitude of delocalization, the increase in the spotting volume directly deposited onto the seed section was measured. Increasing the freeze-spot volume to 5 μL not only ensures the complete coverage of the seed section to be acquired but also the increased diameter was measured from extracted ion images of DHB (m/z 585) as an

assessment of analyte spread from the origin. As shown in Figure 4.3, a slight broadening of the spot boundary was observed with both spot volumes. The measured delocalization is within the raster size for these images, suggesting that analyte redistribution should not affect image quality at the current image resolution. The 5 μL DHB solution at 20 mg/mL was ultimately selected in this application, as this composition provided the best spatial resolution for the assessment of surface metabolites on wheat seed sections. Typically, after matrix application, samples are dehydrated to prevent solvent/metabolite evaporation (Li *et al.*, 2016).

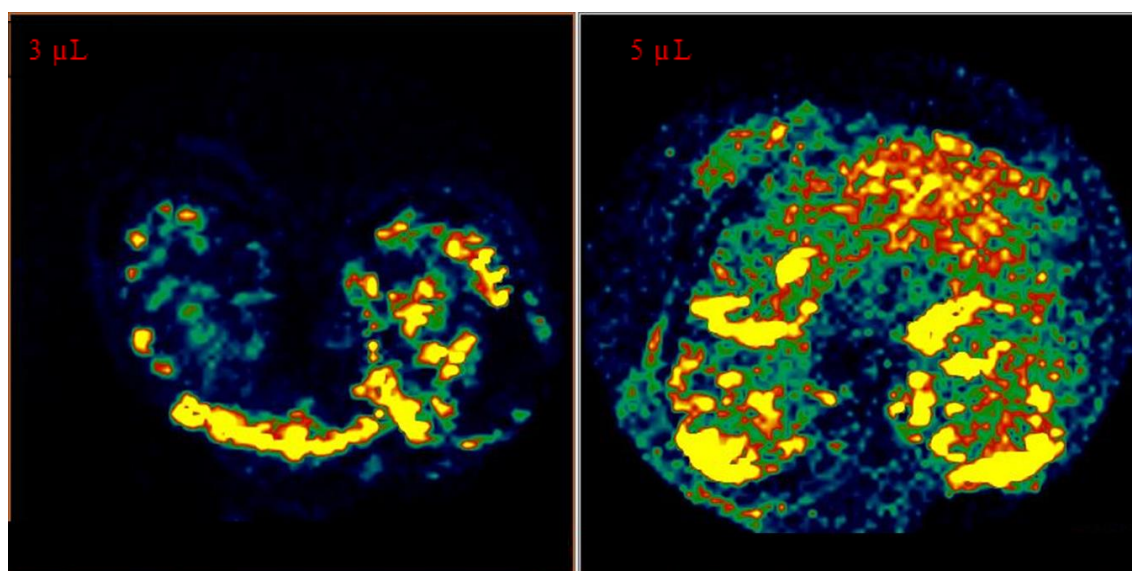


Figure 4.3 MALDI-MSI images comparing the signal intensity of m/z 585 ions found on seed sections when extracted using 3 μL (left) and 5 μL (right) of DHB solution at 20 mg/mL.

The formation of salt adducts upon ionisation in MALDI-MSI can present a challenge to the analyst (Schaiberger and Moss, 2008; Keller *et al.*, 2018); however, it can also provide benefit to efforts of metabolite identification (Petković *et al.*, 2009; Lai and Wang, 2017). Some molecules undergoing ionization in the positive ion mode, will form adduct ions as $[M+Na]^+$, $[M+K]^+$ or $[M+NH_4]^+$ (Mortier *et al.*, 2004) rather than formation of a pseudomolecular ion $[M+H]^+$. Sodium and potassium are abundant in biological systems, such that $[M+Na]^+$ and $[M+K]^+$ cations of metabolite species are commonly observed in MALDI-MSI analyses (Berry *et al.*, 2011). Petkovic *et al.* (2009) have demonstrated adduct formation with sodiated DHB as well as adding complexity to spectral interpretation. Berry *et al.* (2011) also observed both $[M+Na]^+$ and $[M+K]^+$ ions of lipids in their analyses. In the described freeze-spot approach, sodiated and potassiated adduct formation was promoted by addition of sodium and potassium salts to the matrix solution. The resultant effects on measured signal intensities were observed (Figure 4.4). Sucrose was applied to the centre of the sample followed by freeze-spot application of the DHB matrix (10 mM of NaOAc and/or KOAc). The overall signal intensity was at its highest when the DHB solution was potassiated, as demonstrated for the extracted ion image of sucrose (Figure 4.4). The sodiated adduct was also more pronounced than the protonated. The spatial resolving power also looked to improve with inclusion of KOAc; however, it is unclear if this is artefactual to the improved signal of the ion images.

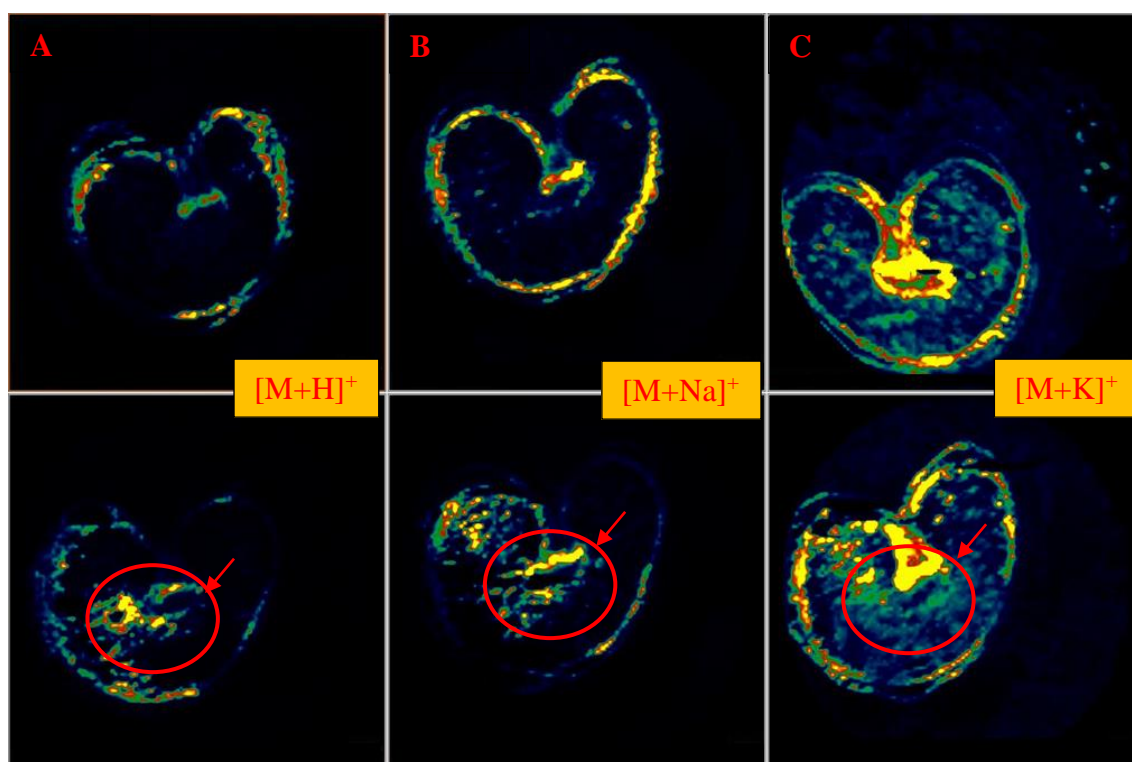


Figure 4.4 MALDI-MSI images comparing the signal intensities of sucrose (m/z 343, m/z 365 and m/z 381) when extracted with the different variations of matrix: DHB only (A), DHB+NaOAc (B), and DHB+KOAc (C). The ion maps illustrated in the top row are from controls whilst images in the second row show a comparison with sections spotted with sucrose standard (1 mg/mL).

The addition of potassium to the matrix prior to freeze-spot application proved particularly well suited to the spatial measurement of more complex sugars of 12 carbons or greater, which readily form sodiated and potassiated adducts. Extracted ion images were generated for sugars up to and including the hexasaccharides (Figure 4.5). Whilst this demonstrated method was successful at providing comparable ion images for complex sugars including tetrasaccharide, pentasaccharide and the lesser complex disaccharides and trisaccharides, no signal was observed for the monosaccharides. Both sucrose (m/z 381) and 1-kestose (m/z 543) were also identified and well-resolved along with their region-specific spatial distributions, which is consistent with the fructan metabolism of barley (Peukert *et al.*, 2014). These analyses demonstrated the freeze-

spot approach to be particularly well suited to small sample sections such as these, with all of the anticipated benefits already described.

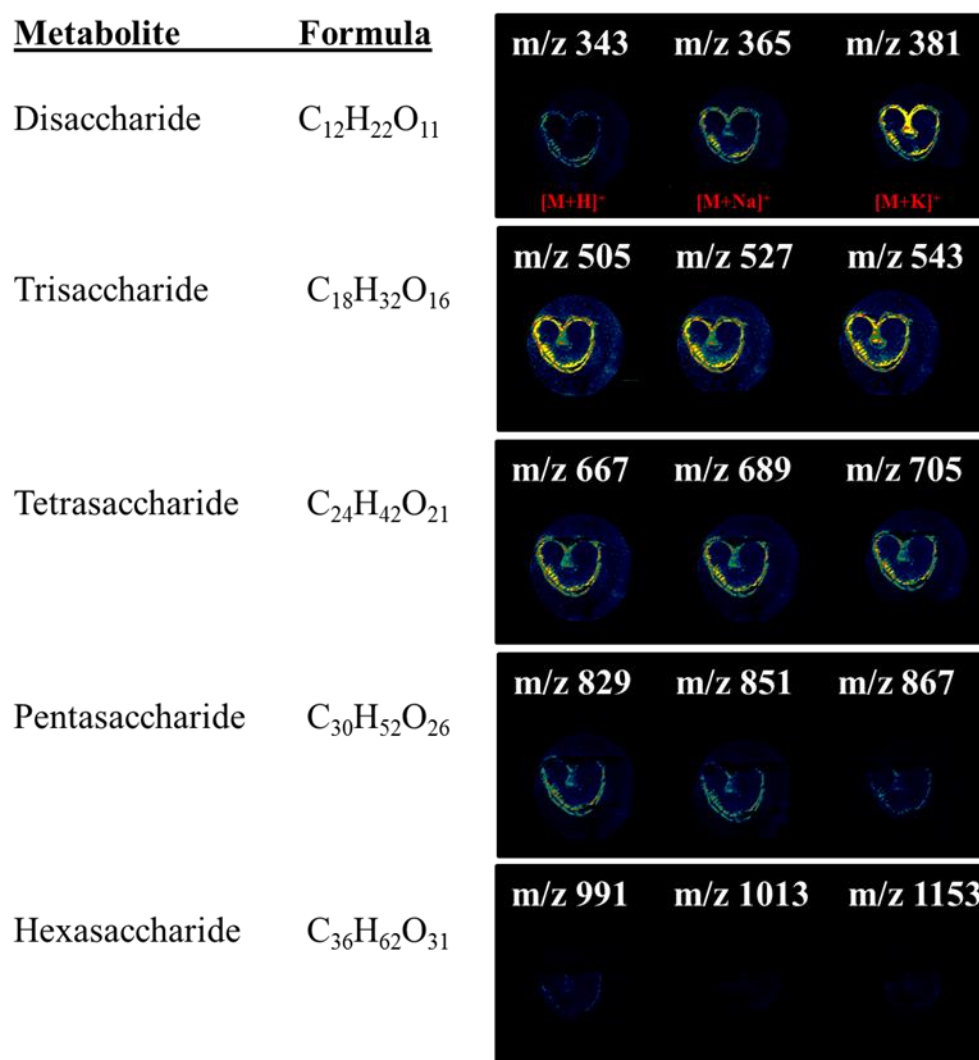


Figure 4.5 Wheat saccharide distribution across the surface of the cryo-sections using the developed MALDI-MSI method. The figure outlines the various sugars present with their associated adduct formation.

The freeze-spot approach was initially conceived as a low-resource intensive approach to matrix-application for MALDI-MSI acquisitions. It was to be a matrix-application intermediate between precipitation of a dry matrix by sublimation and other common methods whereby the sample makes contact with the liquid matrix solution. The chilled stage permits higher freezing point solvents (or aqueous dilutions of), including

acetonitrile, to freeze rapidly, such that the sample is only exposed to the liquid solvent for a sub-second period of time. From a method development standpoint, the choice of and composition of chemical matrices for any given sample type can be easily determined and optimised using these described methods, whilst maintaining the spatial distribution that other pipette spotting approaches fail to accomplish. We also propose here that traditional MALDI may benefit substantially from use of the freeze-spot approach and/or the simple use of drying the applied matrix by lyophilisation, because it prevents hot-spot formation and therefore will likely improve the quantitation which can be achieved by MALDI. A more thorough assessment of the benefit of freeze-spot over application by sublimation in terms of the momentary contact of solvent with the sample surface will be determined in future studies. The resulting desorption of metabolites to the sample surface and the risk of metabolite losses will also warrant further investigation.

4.5 Conclusion

The described simple and robust freeze-spot method for MALDI-MSI is cost effective, requiring substantially less chemical matrix, eliminating the requirement for large volumes of matrix solution or the need for sophisticated automated sprayers for matrix application to small sample sections. The delocalization of analytes was successfully minimised by the rapid freezing of the matrix, and lyophilisation to maintain the native spatial dimensionality of metabolites in the sample, whilst also forming a fine crystal structure for efficient ionisation without the formation of hotspots. The affordability and simplicity of this method makes the approach practical and readily adaptable by other users for various matrices.

4.6 References

- Addie, R. D., B. Balluff, J. V. M. G. Bovée, H. Morreau and L. A. McDonnell (2015). "Current State and Future Challenges of Mass Spectrometry Imaging for Clinical Research." Analytical Chemistry **87**(13): 6426-6433.
- Amstalden van Hove, E. R., D. F. Smith and R. M. A. Heeren (2010). "A concise review of mass spectrometry imaging." Journal of Chromatography A **1217**(25): 3946-3954.
- Baluya, D. L., T. J. Garrett and R. A. Yost (2007). "Automated MALDI Matrix Deposition Method with Inkjet Printing for Imaging Mass Spectrometry." Analytical Chemistry **79**(17): 6862-6867.
- Berry, K. A. Z., J. A. Hankin, R. M. Barkley, J. M. Spraggins, R. M. Caprioli and R. C. Murphy (2011). "MALDI Imaging of Lipid Biochemistry in Tissues by Mass Spectrometry." Chemical reviews **111**(10): 6491-6512.
- Bøgeskov Schmidt, F., A. M. Heskes, D. Thinakaran, B. Lindberg Møller, K. Jørgensen and B. A. Boughton (2018). "Mass Spectrometry Based Imaging of Labile Glucosides in Plants." Frontiers in Plant Science **9**(892).
- Boughton, B. A. and B. Hamilton (2017). Spatial Metabolite Profiling by Matrix-Assisted Laser Desorption Ionization Mass Spectrometry Imaging. Metabolomics: From Fundamentals to Clinical Applications. A. Sussulini. Cham, Springer International Publishing: 291-321.
- Boughton, B. A., D. Thinakaran, D. Sarabia, A. Bacic and U. Roessner (2016). "Mass spectrometry imaging for plant biology: a review." Phytochemistry Reviews **15**(3): 445-488.

- Dai, Y., R. M. Whittal and L. Li (1996). "Confocal Fluorescence Microscopic Imaging for Investigating the Analyte Distribution in MALDI Matrices." Analytical Chemistry **68**(15): 2494-2500.
- Fukuyama, Y. (2015). "MALDI Matrix Research for Biopolymers." Mass Spectrometry **4**(1): A0037.
- Gabriel, S. J., C. Schwarzinger, B. Schwarzinger, U. Panne and S. M. Weidner (2014). "Matrix Segregation as the Major Cause for Sample Inhomogeneity in MALDI Dried Droplet Spots." Journal of The American Society for Mass Spectrometry **25**(8): 1356-1363.
- Gemperline, E., S. Rawson and L. Li (2014). "Optimization and Comparison of Multiple MALDI Matrix Application Methods for Small Molecule Mass Spectrometric Imaging." Analytical Chemistry **86**(20): 10030-10035.
- Goodwin, R. J., A. M. Lang, H. Allingham, M. Boren and A. R. Pitt (2010). "Stopping the clock on proteomic degradation by heat treatment at the point of tissue excision." Proteomics **10**(9): 1751-1761.
- Grove, K. J., S. L. Frappier and R. M. Caprioli (2011). "Matrix Pre-Coated MALDI MS Targets for Small Molecule Imaging in Tissues." Journal of the American Society for Mass Spectrometry **22**(1): 192-195.
- Keller, C., J. Maeda, D. Jayaraman, S. Chakraborty, M. R. Sussman, J. M. Harris, J.-M. Ané and L. Li (2018). "Comparison of Vacuum MALDI and AP-MALDI Platforms for the Mass Spectrometry Imaging of Metabolites Involved in Salt Stress in *Medicago truncatula*." Frontiers in Plant Science **9**(1238).
- Lai, Y.-H. and Y.-S. Wang (2017). "Matrix-Assisted Laser Desorption/Ionization Mass Spectrometry: Mechanistic Studies and Methods for Improving the Structural Identification of Carbohydrates." Mass spectrometry (Tokyo, Japan) **6**(Spec Iss 2): S0072-S0072.

- Li, B., T. J. Comi, T. Si, S. J. B. Dunham and J. V. Sweedler (2016). "A one-step matrix application method for MALDI mass spectrometry imaging of bacterial colony biofilms." Journal of mass spectrometry: JMS **51**(11): 1030-1035.
- Li, S., Y. Zhang, J. a. Liu, J. Han, M. Guan, H. Yang, Y. Lin, S. Xiong and Z. Zhao (2016). "Electrospray deposition device used to precisely control the matrix crystal to improve the performance of MALDI MSI." Scientific Reports **6**: 37903.
- Liu, J. and Z. Ouyang (2013). "Mass spectrometry imaging for biomedical applications." Anal Bioanal Chem **405**(17): 5645-5653.
- McDonnell, L. A. and R. M.A. Heeren (2007). "Imaging mass spectrometry." Mass Spectrometry Reviews **26**(4): 606-643.
- Mortier, K. A., G.-F. Zhang, C. H. Van Peteghem and W. E. Lambert (2004). "Adduct formation in quantitative bioanalysis: effect of ionization conditions on paclitaxel." Journal of the American Society for Mass Spectrometry **15**(4): 585-592.
- Mounfield, W. P., 3rd and T. J. Garrett (2012). "Automated MALDI matrix coating system for multiple tissue samples for imaging mass spectrometry." Journal of American Society of Mass Spectrometry **23**(3): 563-569.
- Murphy, R. C., J. A. Hankin, R. M. Barkley and K. A. Zemski Berry (2011). "MALDI Imaging of Lipids after Matrix Sublimation/Deposition." Biochimica et biophysica acta **1811**(11): 970-975.
- Norris, J. L., D. B. Gutierrez and R. M. Caprioli (2017). Chapter 40 - Imaging Mass Spectrometry in Clinical Pathology A2 - Coleman, William B. Diagnostic Molecular Pathology. G. J. Tsongalis, Academic Press: 517-529.
- Petković, M., J. Schiller, M. Müller, R. Süß, K. Arnold and J. Arnhold (2009). "Detection of Adducts with Matrix Clusters in the Positive and Negative Ion

- Mode MALDI-TOF Mass Spectra of Phospholipids." Z. Naturforsch **64**(b): 331-334.
- Peukert, M., J. Thiel, D. Peshev, W. Weschke, W. Van den Ende, H.-P. Mock and A. Matros (2014). "Spatio-Temporal Dynamics of Fructan Metabolism in Developing Barley Grains." The Plant Cell **26**(9): 3728.
- Rompp, A., J. P. Both, A. Brunelle, R. M. Heeren, O. Laprevote, B. Prideaux, A. Seyer, B. Spengler, M. Stoeckli and D. F. Smith (2015). "Mass spectrometry imaging of biological tissue: an approach for multicenter studies." Analytical and Bioanalytical Chemistry **407**(8): 2329-2335.
- Schaiberger, A. M. and J. A. Moss (2008). "Optimized Sample Preparation for MALDI Mass Spectrometry Analysis of Protected Synthetic Peptides." Journal of the American Society for Mass Spectrometry **19**(4): 614-619.
- Schlosser, G., A. Jakab, G. Pocsfalvi, K. Vékey, F. Hudecz and G. Mező (2009). "Matrix/analyte ratio influencing polymer molecular weight distribution in matrix-assisted laser desorption/ionization time-of-flight mass spectrometry." Rapid Communications in Mass Spectrometry **23**(9): 1249-1254.
- Shariatgorji, M., P. Svenningsson and P. E. Andrén (2014). "Mass Spectrometry Imaging, an Emerging Technology in Neuropsychopharmacology." Neuropsychopharmacology **39**(1): 34-49.
- Van Nuffel, S., N. Elie, E. Yang, J. Nouet, D. Touboul, P. Chaurand and A. Brunelle (2018). "Insights into the MALDI Process after Matrix Deposition by Sublimation Using 3D ToF-SIMS Imaging." Analytical Chemistry **90**(3): 1907-1914.
- Vergeiner, S., L. Schafferer, H. Haas and T. Müller (2014). "Improved MALDI-TOF Microbial Mass Spectrometry Imaging by Application of a Dispersed Solid

- Matrix." Journal of The American Society for Mass Spectrometry **25**(8): 1498-1501.
- Weishaupt, N., S. Caughlin, K. K. Yeung and S. N. Whitehead (2015). "Differential Anatomical Expression of Ganglioside GM1 Species Containing d18:1 or d20:1 Sphingosine Detected by MALDI Imaging Mass Spectrometry in Mature Rat Brain." Frontiers in Neuroanatomy **9**: 155.
- Xu, X., Z. Li, L. Cai, S. Calve and C. P. Neu (2016). "Mapping the Nonreciprocal Micromechanics of Individual Cells and the Surrounding Matrix Within Living Tissues." Scientific Reports **6**: 24272.
- Yang, E., M. Dufresne and P. Chaurand (2017). "Enhancing ganglioside species detection for MALDI-TOF imaging mass spectrometry in negative reflectron mode." International Journal of Mass Spectrometry.
- Ye, H., E. Gemperline and L. Li (2013). "A vision for better health: Mass spectrometry imaging for clinical diagnostics." Clinica Chimica Acta **420**: 11-22.
- Yin, Z., T. Kanade and M. Chen (2012). "Understanding the Phase Contrast Optics to Restore Artifact-free Microscopy Images for Segmentation." Medical Image Analysis **16**(5): 1047-1062.

Optimisation of MALDI-MSI matrix improves spatial resolution of lipid species in fibrotic lung tissue

Adapted from **Nambiar, S.**; Trengove, R. D.; Gummer, J. P. A.; Moodley, Y.; and Bong, S. H. (2018) “Optimisation of MALDI-MSI matrix improves spatial resolution of lipid species in fibrotic lung tissue” *Ready for submission to Progress in Lipid Research*

5.1 Abstract

Idiopathic pulmonary fibrosis (IPF) is an irreversible, chronic and progressive lung disease with unresolved aetiology. Lipids present promising targets for diagnostic and therapeutic intervention due to their role in signalling and as critical determinants in cellular energetics. A number of studies have recently highlighted the pathophysiology of lipid dysregulation in chronic lung diseases, such as chronic obstructive pulmonary disease (COPD; Telenga *et al.*, 2014; t’Kindt *et al.*, 2015) and asthma (Berry *et al.*, 2017; Hough *et al.*, 2018). Mass spectrometry imaging (MSI) provides the means to spatially resolve the distribution of biomolecules, pharmaceuticals and xenobiotics in tissue sections without the use of labels, tags or reporters (Schultz *et al.*, 2019). This approach promises to offer fresh insights into the biochemistry of complex interstitial lung diseases like IPF. Specifically, we employed MSI to characterize changes in lipid signatures between IPF and healthy control tissues and identify putative biomarkers associated with IPF. It is well-known that the addition of ammonium salts can lead to suppression of matrix-assisted laser desorption ionisation (MALDI) matrix clusters; the salt dissociates potential matrix adducts and decreases matrix cluster formation (Ucal and Ozpinar, 2018). We further refined the MSI technique by optimising the amount of inorganic salts in MALDI matrix to improve the intensity and spatial resolution of lipid

species such as ceramides, lysophosphatidylcholines, phosphatidylcholines, phosphatidylethanolamines, sphingomyelins and triglycerides. The lipids in healthy and IPF tissue sections (20 μ m) were then resolved using MALDI-quadrupole time-of-flight (Q-TOF) MSI and data were interrogated by High Definition Imaging (HDI) software by Waters to generate ion intensity maps. Putative identification of lipids was achieved by accurate mass measurement and matched against lipid databases including LIPID MAPS and LipidBlast. This optimised method provides a new approach to enhance the visualisation of lipid distribution in IPF and may provide users with additional metabolite information that can complement existing histopathological assessments, as well as aid in the diagnosis of disease.

Keywords: MALDI, imaging, lung, lipids, IPF

5.2 Introduction

Idiopathic pulmonary fibrosis is a chronic, progressive and fibrosing interstitial pneumonia with unresolved aetiology (Diamantopoulos *et al.*, 2018). The underlying histopathological pattern is one of interstitial pneumonia in the absence of secondary causes or associations (Raghu *et al.*, 2011). Idiopathic pulmonary fibrosis has a poor prognosis with a median survival of three to five years from diagnosis (Raghu *et al.*, 2011; Fabrellas *et al.*, 2018); however, there is considerable heterogeneity among patients in disease course (Poletti *et al.*, 2013). At present, there are limited therapeutic interventions available to patients.

Clinicians and researchers currently rely on clinical data such as patient history, physical examinations including radiology, pulmonary function tests and

histopathological identifications to diagnose patients with IPF (Nakamura and Suda, 2015; Fabrellas *et al.*, 2018). These tests, however, do not reflect the underlying pathophysiological mechanisms of disease and does not adequately allow for the subphenotyping of patients with IPF. This presents a major limitation for both clinical care and research.

Lipidomics is a promising strategy for disease-specific biomarker discovery as there is growing evidence to suggest a role of cellular energy metabolism in lung fibrogenesis (Dautel *et al.*, 2017). Lipids are key cell membrane constituents (Pöyry and Vattulainen, 2016) and serve critical physiological roles including regulation of energy metabolism (Dautel *et al.*, 2017), cellular signalling (Kyle *et al.*, 2018) and trafficking of immune cells (Hubler and Kennedy, 2016). Dysregulated lipid (Carter *et al.*, 2017) and energy (Kang *et al.*, 2016) metabolism have been shown to influence fibrosis. Current methods for chemical localisation of metabolites such as staining with Ehrlich's reagent (Jarman *et al.*, 2014) and Nile Red (Sunaga *et al.*, 2013) can be applied to frozen diseased lung sections. However, these can only reveal the distribution of a defined number of biomolecules. Mass spectrometry imaging (MSI) techniques, on the other hand, offer a means of mapping thousands of ionised lipid signatures within different tissue subtypes, and can potentially generate a global profile of disease based on metabolite distribution and abundance.

A number of studies have applied MSI to spatially resolve small molecules in lung diseases. Römpp and Spengler (2013) identified region-specific phospholipids and peptides in lung carcinoma samples showing high correlation with histological assessment, while Baijnath *et al.* (2016) used MSI to explore the distribution of small molecules and drug metabolites in inflated lungs of a rat model. More recent advances

in global lipidomic approaches have shown lipid compositional changes in post-natal lung development (Dautel *et al.*, 2017) and in radiation-injured lung (Carter *et al.*, 2017). MALDI-MSI is the most widely used method applied to lipids (Bowman *et al.*, 2018). Sectioned tissues coated with MALDI matrix are rastered by a laser beam across the tissue surface while the MS measures the ionised lipids at each coordinate (Walch *et al.*, 2008; Carter *et al.*, 2016). This technique is appealing because the distribution and composition of many analytes can be assessed in a single experiment. Image generation is achieved by plotting the intensities of analyte ions as a function of the x-y coordinates of the sample section (Prentice *et al.*, 2015). MALDI-MSI has been commonly used to investigate spatial distribution of intact proteins and peptides on various mammalian tissues (Berry *et al.*, 2011; Prentice *et al.*, 2015). The high mass resolution of the technique has also been found to resolve isobaric lipid distribution in tissue (Carter *et al.*, 2017). Studies by Desbenoit *et al.* (2014) and Carter *et al.* (2017) further demonstrated that the abundance of lipid signatures in MALDI images strongly correlates with lipid accumulation within specific regions of the tissue.

Here, we utilized a recently optimised matrix application technique termed “freeze-spot” to address the optimisation requirements associated with MSI-based sample preparation including the amount of matrix required and, matrix uniformity (Nambiar *et al.*, unpublished). To improve the sensitivity of the method, we optimised the formation of adducts using various salts such as sodium, potassium and ammonium acetate. In particular, the addition of potassium acetate resulted in improved mass spectra quality as well as feature intensities of MALDI images. We then applied this technique to spatially-resolve the changes in lipid composition and distribution in IPF as well as healthy control tissue samples.

5.3 Materials and Methods

5.3.1 Chemicals

Ultra-pure LC-MS grade solvents including acetonitrile (ACN), isopropanol (IPA), water (H₂O) and trifluoroacetic acid (TFA) were purchased from Thermo Fisher Scientific (Massachusetts, USA). Sodium acetate (NaOAc), potassium acetate (KOAc), ammonium acetate (NH₄OAc) and MALDI matrix 2,5-dihydroxybenzoic acid (DHB) were obtained from Sigma-Aldrich (Castle Hill, Australia). Lipid standards including ceramide (Cer d18:1/17:0), phosphatidylethanolamine (PE 15:0), phosphatidylcholine (PC 15:0) and sphingomyelin (SM d18:1/17:0) were purchased from Avanti Polar Lipids (Alabaster, USA) while lysophosphatidylcholine (LysoPC 15:0) and triglyceride (TG 15:0) standards were sourced from Sigma-Aldrich. Stock lipid standards were prepared in methanol (MeOH) and the working concentrations of all lipids at 1 µg/mL were prepared by dilution in IPA.

5.3.2 Biological samples

A total of 20 frozen lung biopsied samples (10 from IPF patients and 10 healthy controls) were obtained from the Alfred Lung Fibrosis Biobank (Alfred Health, Victoria, Australia) and stored at -80 °C until further analysis. Sample handling and material transfer was approved by The Alfred Ethics Committee (Approval number: 336/13) and the experimental protocol used for this work was approved by the Murdoch University Human Research Ethics Committee (Approval number: 2017/253).

5.3.3 Sample preparation

All microscopy glass slides were thoroughly rinsed with IPA and placed in the cryotome at -17 °C prior to being used. Frozen biopsied lung sample were mounted to a chuck by placing the tissue immediately on a drop of water (on the chuck) upon transfer into the cryotome. Each tissue sample was then cryo-sectioned to 20 µm thickness and subsequently transferred onto a clean, pre-chilled glass slides. This was achieved by gently warming the rear of the slide with a finger to allow the section to thaw and attach to the slide. All prepared sections were stored at -80 °C until matrix application.

5.3.4 Freeze-spot matrix application

An acidified hydroxyl matrix DHB was chosen as the matrix of choice as it has been shown to be suitable for the detection of lipids (Stoyanovsky *et al.*, 2014; Dowlatshahi *et al.*, 2016). The DHB matrix was prepared at a concentration of 20 mg/mL in 80 % ACN (0.1 % TFA). To promote sodium ($[M+Na]^+$), potassium ($[M+K]^+$) or ammonium ($[M+NH_4]^+$) adduct formation, the DHB matrix solution was prepared with 10 mM of either NaOAc, KOAc or NH₄OAc, respectively.

Application of the DHB matrix solution was performed using the freeze-spot approach (Nambiar *et al.*, manuscript in preparation). Briefly, the mounted sample sections were placed onto a stainless-steel stage, pre-chilled on dry ice and 5 µL DHB (20 mg/ml) matrix was transferred onto the sample section by pipette. The solvent immediately froze upon contact with the sample. The glass slides were transferred to a polypropylene 50-mL centrifuge tube, which was sealed, submerged in liquid nitrogen and the solvent

removed by lyophilisation with a Labconco Freezone 2.5 Plus freeze-dryer that is depressurized with a JLT-10 JAVAC high vacuum pump.

5.3.5 MALDI-MSI acquisition

All MALDI-MSI analyses were performed using the Water Synapt G2S mass spectrometer equipped with an orthogonal MALDI ion source and an Nd:YAG laser (Waters Corporation, Manchester, U.K.). Prior to analytical acquisition, digital scans of the tissue sections were obtained using an Epson WorkForce Pro WP-4540 scanner (Epson America, Inc.) and then imported into MALDI Imaging Pattern Creator software. All data were acquired in positive mode operating with a 1,000 Hz firing rate and 350 J laser energy over a mass range of m/z 50 to 1200. From each irradiated spot, a full mass spectrum consisting of signals from protonated molecular species from the desorbed tissue region was noted. The spectra generated were then processed in MassLynx (Waters Corporation, Manchester, UK) to allow for signal intensities of the corresponding ions to be determined. The MSI images were acquired at a spatial resolution at 600 laser shots per position and ion images were generated with High Definition Imaging (HDI) software (Waters Corporation, Manchester, U.K.). The heat maps of specific ions generated corresponded to the relative abundance of ions present over the entire imaged surface.

5.4 Results and Discussion

5.4.1 Potassium adducts enhanced MALDI-MSI intensities of lipids

The formation of adducts during ionisation can potentially compromise the quality of the mass spectra generated (Leite *et al.*, 2004; Bauer *et al.*, 2018). The unintended formation of salt adducts due to exposure from the storage vials, pipette tips or even the glass slides used can present difficulties for the detection and identification of molecules at low abundances. The resulting adducts reduce signal intensities by splitting the ions into multiple mass peaks and suppress the ionisation of low abundance peaks (Leite *et al.*, 2004). The presence of these inorganic lipid adducts are inevitable in MALDI-based techniques and its formation upon ionisation have been reported by Angel *et al.* (2012), and Wang *et al.* (2017). Studies by Zhu and Papayannopoulos (2003) and Leite *et al.* (2004) showed that the reduction or removal of these adduct ions can improve the detection of peptides at low concentration. However, mobile-phase additives such as ammonium acetate is commonly used to improve both LC separation and detection of lipids (Cajka and Fiehn, 2014). Due to their strong affinity for alkali metals, various adducts of alkali metals and ammonium cations have been used to improve the intensity of lipids such as triacylglycerols (Hsu and Turk, 1999; Lin and Arcinas, 2008) and phospholipids (Knittelfelder *et al.*, 2014) using electrospray ionisation (ESI) techniques.

Angel *et al.* (2012), Wang *et al.* (2017) and Rush and Breemen (2018) used DHB as the matrix of choice for lipid extraction and promotion of ionisation. In this study we encouraged the formation of lipid $[M+Na]^+$, $[M+K]^+$ and $[M+NH_4]^+$ adducts using DHB prepared with inorganic salts that consists of a metal cation to investigate their effects on lipid resolution and intensity. Figure 5.1 shows the total ion chromatogram (TIC) of

lipid standard mixture extracted with DHB and DHB spiked with NaOAc, KOAc and NH₄OAc. The TIC from DHB spiked with KOAc showed the highest intensity at approximately 2×10^6 counts. This was consistent with the observations of Birdsall *et al.* (2016) where the intensities of the $[M+K]^+$ ions were two-fold the intensity of $[M+Na]^+$ ions generated by ESI. Wang *et al.* (2017) also reported increase in $[M+K]^+$ ions of phospholipid species from MALDI imaging using DHB. These studies utilised matrices prepared in solvents without salt additives. Rush and Breemen (2018) were also unable to selectively reduce the formation of both $[M+K]^+$ and $[M+Na]^+$ adducts using ammonium salts; however, they were successful at suppressing the ionisation of PCs.

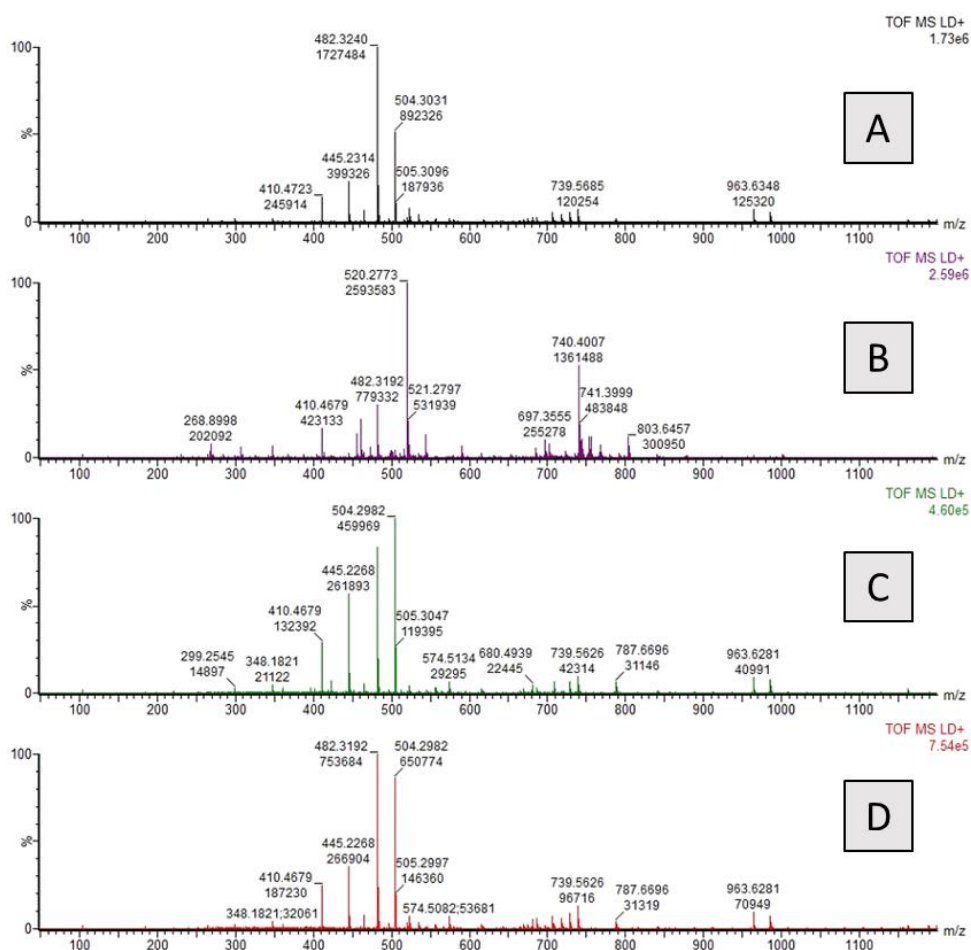


Figure 5.1 The total ion chromatograms (TIC) of the lipid standards mixture spotted on a glass slide at $1 \mu\text{g/mL}$ and extracted with (A) DHB with NH₄OAc ($[M+\text{NH}_4]^+$), (B) DHB with KOAc ($[M+K]^+$), (C) DHB with NaOAc ($[M+Na]^+$) and (D) DHB only ($[M+H]^+$).

To further demonstrate the effects of adduct formation, six lipid classes including LysoPC, Cer, PE, PC, SM and TG were examined. The ions corresponding to each of the four adducts were extracted from the TIC. The proton adduct $[M+H]^+$ has previously been found to be the dominant ion formed during ESI (Dudkowska *et al.*, 2018) while $[M+Na]^+$ and $[M+K]^+$ are the most common when using MALDI (Jovanovic *et al.*, 2018). While $[M+NH_4]^+$ ions are routinely generated due to the addition of solvent buffers and during metabolite extraction, these results showed poor formation of $[M+NH_4]^+$ lipid adducts during ionisation by DHB containing NH_4OAc . This further confirmed the observations of Rush and Breemen (2018) who showed the suppression of PC ionisation when ammonium additives were applied.

Interestingly, the addition of $NaOAc$ resulted in the formation of the $[M+H]^+$, $[M+Na]^+$ and $[M+NH_4]^+$ adducts, with the $[M+NH_4]^+$ adduct showing the highest intensities for all six lipids tested. This finding is potentially indicative of impurities in the salt additive but this observation is still relevant since the NH_4 was in excess relative to the other species been demonstrated. Figure 5.2 shows the extracted ion chromatograms (XICs) of each of the four adducts for each lipid when ionised using DHB containing $NaOAc$. The peak quality of all adducts were comparable to each other except for the potassium adduct where the associated $[M+K]^+$ ions for CE and PE were not evident. In addition, the $[M+K]^+$ spectra for PC, SM and TG showed increased background. This is consistent with the observations of Rush and Breemen (2018) who also demonstrated that the use of ammonium buffers affected the relative abundance of $[M+H]^+$, $[M+Na]^+$ and $[M+K]^+$. We therefore hypothesise that the ion signal of $[M+NH_4]^+$ species were improved when ammonium buffers were used in combination with the DHB matrix. To the authors' knowledge the exact mechanism by which sodium promoted the formation of ammonium adducts is yet to be reported. However, we speculate that by increasing

competition for ionisation sites on the lipid molecule in favour of the ammonium cation, the lesser-abundant cations are less likely to adduct unless they were usually the most preferentially formed. For lipids, the $[M+H]^+$ was less readily formed during ionisation, and as such the ammonium addition decreases the adduction. However $[M+Na]^+$ and $[M+K]^+$ which were more readily formed were still observed as they were conceived to be more favourable than $[M+NH_4]^+$ formation.

Of note, the use of KOAc to encourage adduct formation of these lipids was shown to have improved the relative abundance of $[M+K]^+$ compared to $[M+H]^+$, $[M+Na]^+$ and $[M+NH_4]^+$ ions by at least two orders of magnitude. All four adduct species were identified for LysoPC. For PC, SM and TG, $[M+K]^+$ showed improved abundance while $[M+H]^+$ and $[M+NH_4]^+$ showed poor ion spectra (Figure 5.3). For Cer and PE, only the $[M+K]^+$ ions were detected. In summary, $[M+K]^+$ ions were the only adduct type that were well-resolved in all six lipids whilst suppressing the signal of $[M+H]^+$, $[M+K]^+$ and $[M+NH_4]^+$ ions. Figure 5.3 illustrates the MALDI-MSI ion intensity maps which showed the abundance of these adduct species within the extracted lipids.

The addition of cations was clearly important in MALDI-MSI experiments for the detection of lipid species. Sugiura and Setau (2009) and Griffiths and Bunch (2012) have reported that the addition of either NaOAc or KOAc to the matrix led to reduced signal intensities of the protonated adducts of lipids by MALDI. However, Griffiths and Bunch (2012) showed increased $[M+K]^+$ formation of PCs in rat brain homogenate by the addition of KOAc but with a suppression of the ion counts, in agreement with Sugiura and Setau (2009). Other additives such as caesium chloride and lithium nitrate have also been applied to MALDI matrices. These appeared to reduce the spectral complexity and improved identification of unidentified metabolites by allowing

unambiguous assignment of caesium-lipid and lithium-lipid adducts (Griffiths and Bunch, 2012; Griffiths *et al.*, 2013).

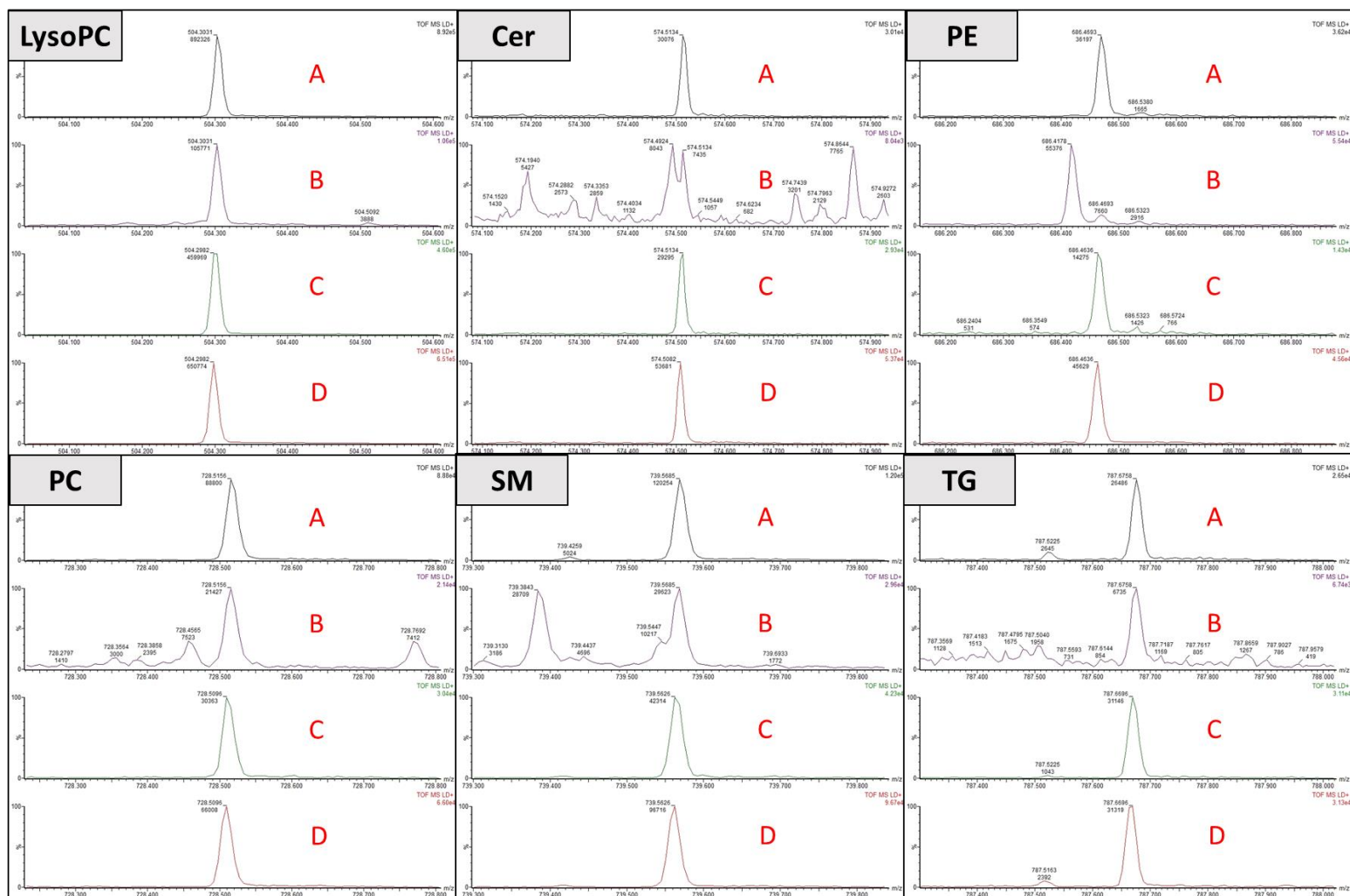


Figure 5.2 Extracted ion chromatograms of the lipid adducts $[M+NH_4]^+$, $[M+K]^+$, $[M+Na]^+$ and $[M+H]^+$ denoted by A, B, C and D, respectively. All six lipid standards were extracted with DHB containing NaOAc.

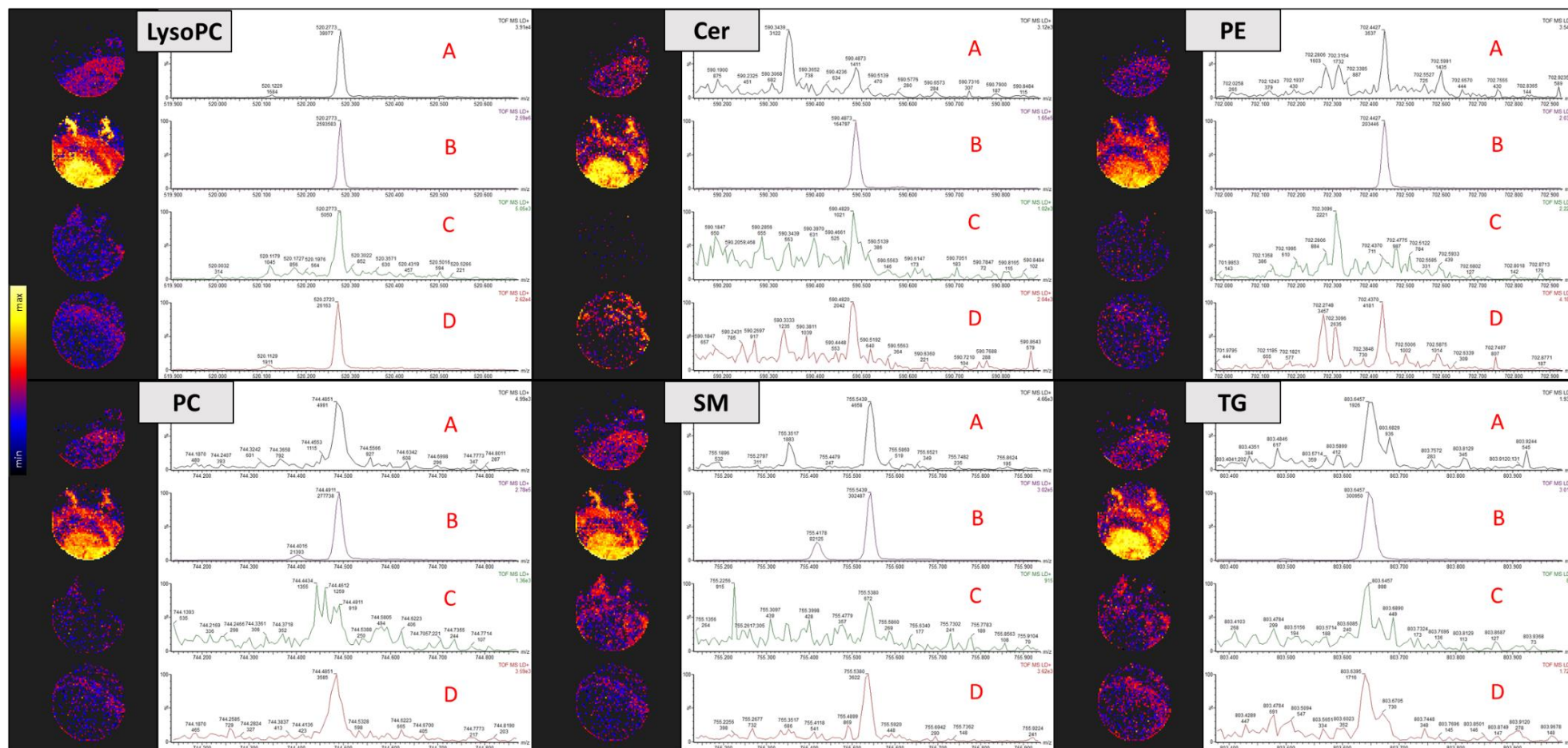
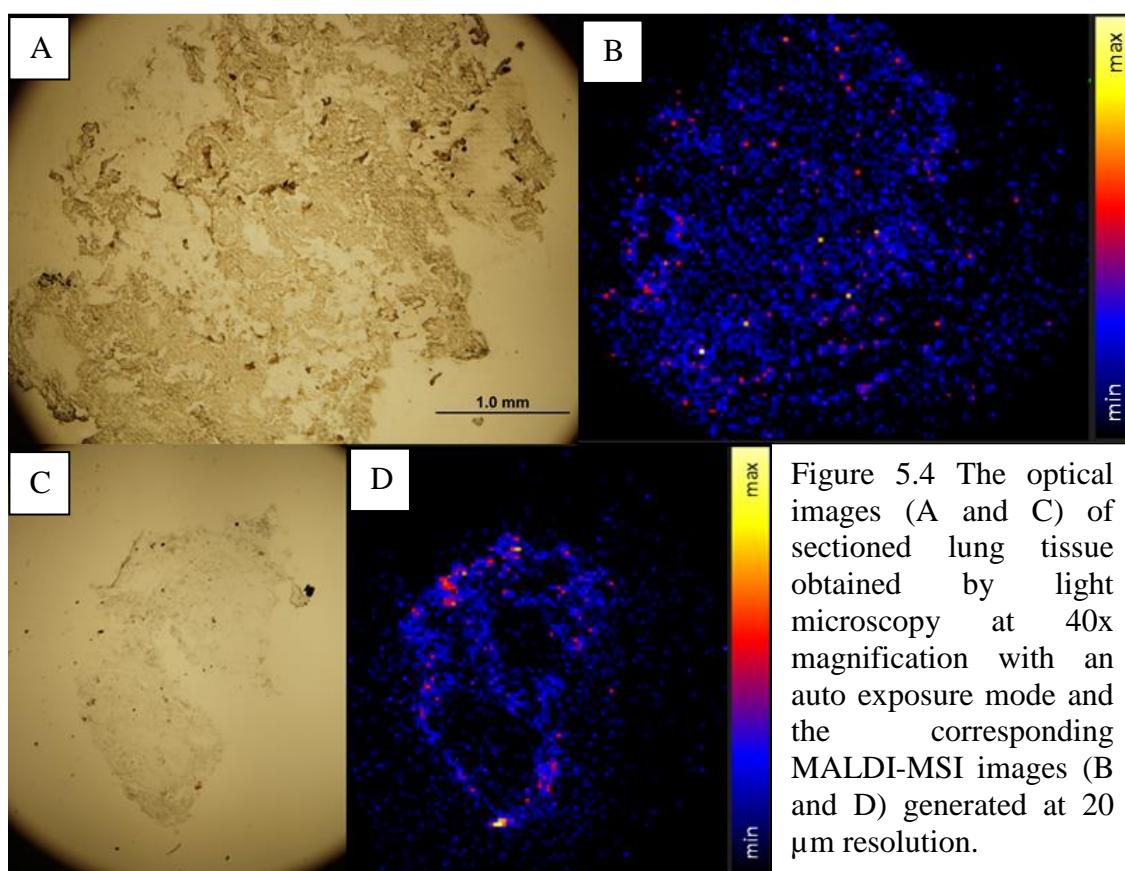


Figure 5.3 Extracted ion chromatograms and ion intensity maps of the lipid adducts generated by MassLynx and HD Imaging software, respectively. All six lipid standards were extracted with DHB containing KOAc and their associated adducts $[M+NH_4]^+$, $[M+K]^+$, $[M+Na]^+$ and $[M+H]^+$ are denoted by A, B, C and D, respectively.

5.4.2 MALDI images of biopsied lung sections

This study builds on the published research of Carter *et al.* (2015 and 2017) which focused on the characterisation of lipids in lung parenchyma using MALDI-MSI. Here, we optimised the addition of KOAc in DHB matrix to promote $[M+K]^+$ adduct formation to investigate the spatial distribution of various lipid species including sphingolipids, phospholipids and triglycerides in IPF and healthy tissue biopsies.

Figure 5.4 shows the spatial resolution of two ions m/z 494.24 and m/z 897.75 compared to optimal light microscopy images obtained at 40x objective magnification. The extracted ion m/z 494.24 was shown to be well-distributed within the rastered tissue region, whereas ions of m/z 897.75 were distributed along the tissue periphery. A closer inspection of both the optical image and ion intensity map revealed that m/z 897.75 was likely to be a matrix-related ion and not a lipid-specific ion. The m/z value did not match any of the calculated theoretical masses of the lipid adducts of interest and the ion was peripherally distributed around the rastered tissue. This was important as it demonstrated the ability of the method to discriminate between lipid-specific ion and matrix ions in cryo-sectioned lung tissues.



One of the challenges of MALDI ionisation is the high matrix background resulting from the use of organic matrices like DHB (Fujimura and Miura, 2014). Studies by Le *et al.* (2013), Fujimura and Miura (2014) and Lee *et al.* (2016) recognised that some background matrix ions can have similar intensities to analyte ions and can interfere with detection and identification of the target analytes. In this study, the enhanced signal intensities resulting from the addition of KOAc was advantageous as it allowed for the improved discrimination of lipid analytes from the background ions. Of note, features with m/z 520.29, m/z 744.38 and m/z 702.33 were identified as LysoPC, PC and PE based on their $[M+K]^+$ adduct accurate mass. Figure 5.5 illustrates a loss of signal intensities for LysoPC, PC and PE ions in IPF tissue sections compared to healthy control tissues.

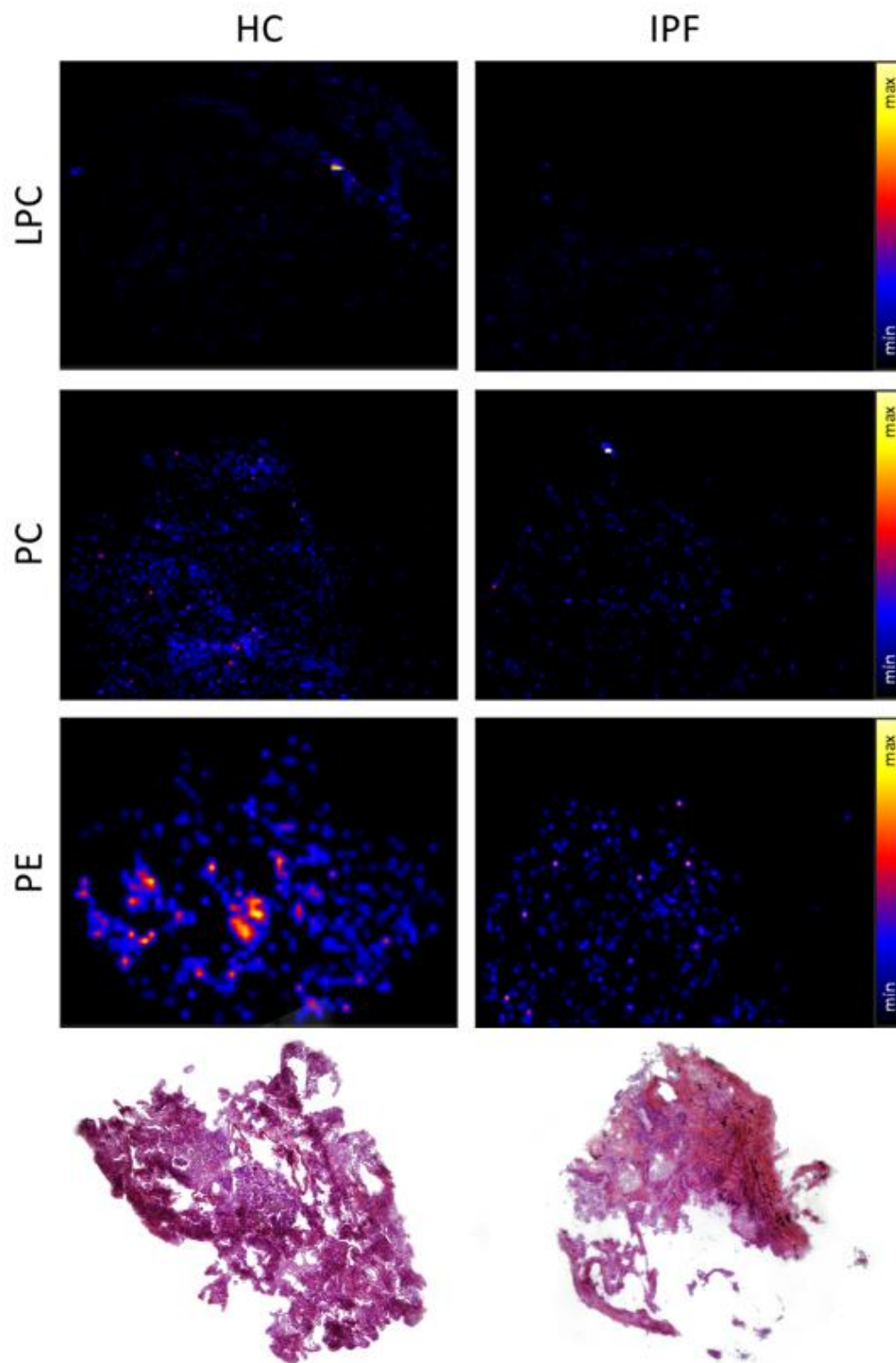


Figure 5.5 MALDI-MSI images showing decreased signal intensities of LysoPC, PC and PE ions in IPF tissues compared to healthy control samples. Representative hemotoxylin and eosin (H&E) stained IPF and healthy tissues were also shown for comparison.

The changes in lipid profiles of diseased lung tissues are well-studied. Naz *et al.* (2017) used LC-Orbitrap MS to elucidate the role of lysophosphatidic acid (LysoPA) in lung function, specifically forced expiratory volume in 1s (FEV₁), from COPD patients, smokers with normal lung functions and healthy (never-smoked) individuals. In this study, we showed that LysoPC, which is a precursor of LysoPA, was down-regulated in IPF compared to health control tissues. This suggested that the LysoPA signalling pathway may be involved in disease mechanism or symptoms. LysoPA, a bioactive glycerophospholipid, has been shown to be associated with asthma (Ackerman *et al.*, 2016), atherosclerosis (Gu *et al.*, 2017), cancer (Ha *et al.*, 2018) and fibrosis (Rancoule *et al.*, 2017). LysoPA is produced through the hydrolysis of phosphatidic acids by phospholipase which are located in cell membranes. The majority of LysoPA is produced by the enzymatic cleavage of LysoPC and lysophosphatidylserine by lysophospholipase D activity. In IPF, type 2 alveolar epithelial cell injury is believed to initiate the fibrotic process. Following an injury, dipalmitoylphosphatidylcholine (DPPC), a major surfactant lipid component, is degraded to LysoPC by phospholipase A2 activity in the type 2 alveolar epithelial cells. However, our study appeared to contradict this as the IPF tissue sections showed reduced intensities of LysoPC compared to healthy samples. The precise reduction in LysoPC levels in IPF tissue has not been determined as the current method was unable to quantitate lipid abundance. Further quantitative work has been envisioned where known concentrations of lipid standards will be spiked to generate calibration curves based on MSI spectral intensities.

Lung surfactant consists of type 2 alveolar cells and is a complex mixture of phospholipids, with PCs accounting for approximately 90% of surfactant composition. The PCs play an important role in reducing surface tension at the air-water interface of the alveolus. Compared to healthy tissues, IPF tissues have a lower composition of PCs

and this appeared to be consistent with our observations of PC intensities in Figure 5.5. A loss or reduction of PCs has adverse effects on the surface tension of the lungs and can lead to alveolar collapse. In lung diseases such as acute respiratory distress syndrome (ARDS; Fessler and Summer, 2016), pneumonia (Facco *et al.*, 2014), sarcoidosis (Devendra and Spragg, 2002) and IPF (Schmidt *et al.*, 2002; Tan *et al.*, 2016), a decrease in PCs and large surface aggregates have been associated with impairment of the surface tension-lowering properties of surfactant. Pulmonary surfactant also plays a key role in protecting the underlying epithelium from toxins and microbes that are inhaled into the lungs. Fessler and Summer (2016) noted that pathogens may drive some of these changes in lipids since *Pseudomonas aeruginosa* (Agassandian *et al.*, 2007) and human adenovirus type 5 (Miakotina *et al.*, 2007) were both reported to reduce PC secretion from the type 2 alveolar cells.

We observed a reduction in PC intensities in IPF tissue sections and this agreed with the published research of Schmidt *et al.* (2002) and Sunaga *et al.* (2013) on altered fatty acid (FA) composition of surfactant lipids. Pathway analysis conducted by Yin *et al.* (2017) and Menon *et al.* (2017) revealed that PCs and FAs such as palmitoleic acid and oleic acid are involved in mTOR signalling pathway. Tan *et al.* (2016) showed that the mTOR complex was a highly conserved intracellular serine/threonine kinase and mTOR expression in pulmonary fibrosis patients were significantly correlated with fibrosis and decreased lung function. This suggested that PC may be conceived as a prognostic marker of pulmonary fibrosis as hypothesised by Park *et al.* (2014). Phosphatidic acid interacts directly with the binding domain in mTOR, and this interaction affects the mTOR's ability to activate downstream effectors such as PCs (Menon *et al.*, 2017).

PE is the second most abundant phospholipid found in biological membranes. The reduction in intensities of PE in the IPF tissue compared to healthy control supported the observations of Hu *et al.* (2015) where the hepatic PE levels were significantly reduced in a bleomycin-induced mice model. Hu *et al.* (2015) suggested that the reduction of PE species was due to the compartmental effects of phosphatidylserine (PS) biosynthesis which occurs in the mitochondria. Farine *et al.* (2015) and Leithner *et al.* (2018) further reported significant reductions in both PC and PE levels in cancer cells as a consequences of increased PS biosynthesis. A recent study by Vazquez-de-Lara *et al.* (2018) demonstrated that PE induced an anti-fibrotic phenotype in an experimental model of lung fibrosis. The study showed that PE contributes to the inhibition of collagen expression and that early administration of PE diminishes lung fibrosis *in vivo*.

MSI is a rapidly emerging application of mass spectrometry that allows for the analysis and spatial visualisation of thousands of analytes without the need for tissue labelling. It is clear that more research is required to develop methods that can provide absolute quantitation as a function of ionisation intensity. While recent work by Hansen and Janfelt (2016), Nishimura *et al.* (2017) and Nazari *et al.* (2018) has introduced internal standards for quantitative MSI, such efforts needs further refinement due to matrix inhomogeneity, ion suppression or analyte extraction efficiencies that can result in suppressed signal (Gemperline *et al.*, 2014). Bergman *et al.* (2016) and Duncan *et al.* (2018) further demonstrated that the addition of deuterated standards to a nano-desorption electrospray ionisation (DESI) solvent beam enabled compensation of sample-matrix effects, which enhanced visualisation and interpretation of the ion images. Bergman *et al.* (2016) and Duncan *et al.* (2018) also performed tandem mass spectrometry (MS/MS) on both deuterated standards and endogenous compounds such

as neurotransmitters and eicosanoids to determine the ratio of analyte intensity to standard intensity as the basis of quantitation. These present promising avenues for future work.

5.5 Conclusion

Here, we demonstrated the utilization of a new matrix application technique, termed the “freeze-spot” method, and successfully promoted potassium adduct formation for MSI of lung tissues. The improvement in mass spectral quality and enhanced signal intensities resulted in the generation of high-quality images with the resolution of six lipid species of interest. The MALDI-MSI method allowed for the visualisation of the lipids and demonstrated the differences in relative intensities and abundances of PC, PE and LysoPC between diseases and healthy control tissue biopsies. Significant differences were observed in lipid species involved in LysoPA and mTOR signalling pathways, as well as surfactant PCs. Further studies are envisioned using quantitative MSI approaches and potential further co-registration of ion maps to conventional hematoxylin and eosin stained sections to allow for a deeper investigation of lung pathology.

5.6 References

- Ackerman, S. J., G. Y. Park, J. W. Christman, S. Nyenhuis, E. Berdyshev and V. Natarajan (2016). "Polyunsaturated lysophosphatidic acid as a potential asthma biomarker." Biomarkers in medicine 10(2): 123-135.
- Agassandian, M., O. L. Miakotina, M. Andrews, S. N. Mathur and R. K. Mallampalli (2007). "Pseudomonas aeruginosa and sPLA2 IB stimulate ABCA1-mediated phospholipid efflux via ERK-activation of PPARalpha-RXR." Biochemical Journal 403(3): 409-420.
- Angel, P. M., J. M. Spraggins, H. S. Baldwin and R. Caprioli (2012). "Enhanced sensitivity for high spatial resolution lipid analysis by negative ion mode matrix assisted laser desorption ionization imaging mass spectrometry." Analytical Chemistry 84(3): 1557-1564.
- Bajjnath, S., A. Shobo, L. A. Bester, S. D. Singh, G. Kruger, T. Naicker and T. Govender (2016). "Small molecule distribution in rat lung: a comparison of various cryoprotectants as inflation media and their applicability to MSI." Journal of Molecular Histology 47(2): 213-219.
- Bauer, A., J. Kuballa, S. Rohn, E. Jantzen and J. Luetjohann (2018). "Evaluation and validation of an ion mobility quadrupole time-of-flight mass spectrometry pesticide screening approach." Journal of Separation Science 41(10): 2178-2187.
- Bergman, H.-M., E. Lundin, M. Andersson and I. Lanekoff (2016). "Quantitative mass spectrometry imaging of small-molecule neurotransmitters in rat brain tissue sections using nanospray desorption electrospray ionization." Analyst 141(12): 3686-3695.

- Berry, K. A. Z., B. Li, S. D. Reynolds, R. M. Barkley, M. A. Gijón, J. A. Hankin, P. M. Henson and R. C. Murphy (2011). "MALDI imaging MS of phospholipids in the mouse lung." Journal of lipid research 52(8): 1551-1560.
- Berry, K. A., R. C. Murphy, B. Kosmider and R. J. Mason (2017). "Lipidomic characterization and localization of phospholipids in the human lung." Journal of lipid research 58(5): 926-933.
- Birdsall, R. E., M. Gilar, H. Shion, Y. Q. Yu and W. Chen (2016). "Reduction of metal adducts in oligonucleotide mass spectra in ion - pair reversed - phase chromatography/mass spectrometry analysis." Rapid Communications in Mass Spectrometry 30(14): 1667-1679.
- Bowman, A. P., R. M. A. Heeren and S. R. Ellis (2018). "Advances in mass spectrometry imaging enabling observation of localised lipid biochemistry within tissues." TrAC Trends in Analytical Chemistry.
- Cajka, T. and O. Fiehn (2014). "Comprehensive analysis of lipids in biological systems by liquid chromatography-mass spectrometry." Trends in analytical chemistry: TRAC 61: 192-206.
- Carter, C. L., J. W. Jones, A. M. Farese, T. J. MacVittie and M. A. Kane (2017). "Lipidomic dysregulation within the lung parenchyma following whole-thorax lung irradiation: Markers of injury, inflammation and fibrosis detected by MALDI-MSI." Scientific Reports 7: 10343.
- Carter, C. L., J. W. Jones, A. M. Farese, T. J. MacVittie and M. A. Kane (2016). "Inflation-Fixation Method for Lipidomic Mapping of Lung Biopsies by Matrix Assisted Laser Desorption/Ionization–Mass Spectrometry Imaging." Analytical Chemistry 88(9): 4788-4794.

- Dautel, S. E., J. E. Kyle, G. Clair, R. L. Sontag, K. K. Weitz, A. K. Shukla, S. N. Nguyen, Y.-M. Kim, E. M. Zink, T. Luders, C. W. Frevert, S. A. Gharib, J. Laskin, J. P. Carson, T. O. Metz, R. A. Corley and C. Ansong (2017). "Lipidomics reveals dramatic lipid compositional changes in the maturing postnatal lung." Scientific Reports 7: 40555.
- Desbenoit, N., E. Saussereau, C. Bich, M. Bourderioux, J. Fritsch, A. Edelman, A. Brunelle and M. Ollero (2014). "Localized lipidomics in cystic fibrosis: TOF-SIMS imaging of lungs from *Pseudomonas aeruginosa*-infected mice." International Journal of Biochemistry & Cell Biology 52: 77-82.
- Devendra, G. and R. G. Spragg (2002). "Lung surfactant in subacute pulmonary disease." Respiratory Research 3(1): 11.
- Diamantopoulos, A., E. Wright, K. Vlahopoulou, L. Cornic, N. Schoof and T. M. Maher (2018). "The Burden of Illness of Idiopathic Pulmonary Fibrosis: A Comprehensive Evidence Review." Pharmacoeconomics 36(7): 779-807.
- Dudkowska, J., M. Frańska and R. Frański (2018). "Detection of the iron complexes with hydrolysis products of cephalexin and cefradine upon high-performance liquid chromatography/electrospray ionization mass spectrometry analysis." Rapid Communications in Mass Spectrometry 32(7): 576-582.
- Duncan, K. D., R. Fang, J. Yuan, R. K. Chu, S. K. Dey, K. E. Burnum-Johnson and I. Lanekoff (2018). "Quantitative Mass Spectrometry Imaging of Prostaglandins as Silver Ion Adducts with Nanospray Desorption Electrospray Ionization." Analytical Chemistry 90(12): 7246-7252.
- Fabrellas, E., R. Peris Sánchez, C. Sabater Abad and G. Juan Samper (2018). "Prognosis and Follow-Up of Idiopathic Pulmonary Fibrosis." Medical Sciences 6(2): 51.
- Facco, M., M. Nespeca, M. Simonato, I. Isak, G. Verlato, G. Ciambra, C. Giorgetti, V. P. Carnielli and P. E. Cogo (2015). "In Vivo Effect of Pneumonia on Surfactant

- Disaturated-Phosphatidylcholine Kinetics in Newborn Infants." PLOS ONE 9(12): e93612.
- Farine, L., M. Niemann, A. Schneider and P. Bütikofer (2015). "Phosphatidylethanolamine and phosphatidylcholine biosynthesis by the Kennedy pathway occurs at different sites in *Trypanosoma brucei*." Scientific Reports 5: 16787.
- Fessler, M. B. and R. S. Summer (2016). "Surfactant Lipids at the Host-Environment Interface. Metabolic Sensors, Suppressors, and Effectors of Inflammatory Lung Disease." American journal of respiratory cell and molecular biology 54(5): 624-635.
- Fujimura, Y. and D. Miura (2014). "MALDI Mass Spectrometry Imaging for Visualizing In Situ Metabolism of Endogenous Metabolites and Dietary Phytochemicals." Metabolites 4(2): 319-346.
- Gemperline, E., B. Chen and L. Li (2014). "Challenges and recent advances in mass spectrometric imaging of neurotransmitters." Bioanalysis 6(4): 525-540.
- Griffiths, R. L. and J. Bunch (2012). "A survey of useful salt additives in matrix-assisted laser desorption/ionization mass spectrometry and tandem mass spectrometry of lipids: introducing nitrates for improved analysis." Rapid Communications in Mass Spectrometry 26(13): 1557-1566.
- Griffiths, R. L., J. Sarsby, E. J. Guggenheim, A. M. Race, R. T. Steven, J. Fear, P. F. Lalor and J. Bunch (2013). "Formal Lithium Fixation Improves Direct Analysis of Lipids in Tissue by Mass Spectrometry." Analytical Chemistry 85(15): 7146-7153.
- Gu, C., F. Wang, Z. Zhao, H. Wang, X. Cong and X. Chen (2017). "Lysophosphatidic Acid Is Associated with Atherosclerotic Plaque Instability by Regulating NF- κ B

- Dependent Matrix Metalloproteinase-9 Expression via LPA (2) in Macrophages." Frontiers in physiology 8: 266-266.
- Guerrera, I. C., G. Astarita, J.-P. Jais, D. Sands, A. Nowakowska, J. Colas, I. Sermet-Gaudelus, M. Schuereberg, D. Piomelli, A. Edelman and M. Ollero (2009). "A Novel Lipidomic Strategy Reveals Plasma Phospholipid Signatures Associated with Respiratory Disease Severity in Cystic Fibrosis Patients." PLOS ONE 4(11): e7735.
- Ha, J. H., R. Radhakrishnan, M. Jayaraman, M. Yan, J. D. Ward, K.-M. Fung, K. Moxley, A. K. Sood, C. Isidoro, P. Mukherjee, Y. S. Song and D. N. Dhanasekaran (2018). "LPA Induces Metabolic Reprogramming in Ovarian Cancer via a Pseudohypoxic Response." Cancer Research 78(8): 1923.
- Hansen, H. T. and C. Janfelt (2016). "Aspects of Quantitation in Mass Spectrometry Imaging Investigated on Cryo-Sections of Spiked Tissue Homogenates." Analytical Chemistry 88(23): 11513-11520.
- Hough, K. P., L. S. Wilson, J. L. Trevor, J. G. Strenkowski, N. Maina, Y.-I. Kim, M. L. Spell, Y. Wang, D. Chanda, J. R. Dager, N. S. Sharma, M. Curtiss, V. B. Antony, M. T. Dransfield, D. D. Chaplin, C. Steele, S. Barnes, S. R. Duncan, J. K. Prasain, V. J. Thannickal and J. S. Deshane (2018). "Unique Lipid Signatures of Extracellular Vesicles from the Airways of Asthmatics." Scientific Reports 8(1): 10340.
- Hsu, F.-F. and J. Turk (1999). "Structural characterization of triacylglycerols as lithiated adducts by electrospray ionization mass spectrometry using low-energy collisionally activated dissociation on a triple stage quadrupole instrument." Journal of the American Society for Mass Spectrometry 10(7): 587-599.
- Hubler, M. J. and A. J. Kennedy (2016). "Role of lipids in the metabolism and activation of immune cells." The Journal of nutritional biochemistry 34: 1-7.

- Jarman, E. R., V. S. Khambata, L. Yun Ye, K. Cheung, M. Thomas, N. Duggan and G. Jarai (2014). "A translational preclinical model of interstitial pulmonary fibrosis and pulmonary hypertension: mechanistic pathways driving disease pathophysiology." Physiological Reports 2(9): e12133.
- Jovanović, J. P., S. B. Novaković, G. A. Bogdanović, A. Minić, A. Pejović, J. Katanić, V. Mihailović, B. Nastasijević, D. Stevanović and I. Damljanović (2018). "Acryloylferrocene as a convenient precursor of tetrahydropyrazolopyrazolones: [3+2] cycloaddition with N,N' -Cyclic azomethine imines." Journal of Organometallic Chemistry 860: 85-97.
- Kang, Y. P., S. B. Lee, J.-m. Lee, H. M. Kim, J. Y. Hong, W. J. Lee, C. W. Choi, H. K. Shin, D.-J. Kim, E. S. Koh, C.-S. Park, S. W. Kwon and S.-W. Park (2016). "Metabolic Profiling Regarding Pathogenesis of Idiopathic Pulmonary Fibrosis." Journal of Proteome Research 15(5): 1717-1724.
- Knittelfelder, O. L., B. P. Weberhofer, T. O. Eichmann, S. D. Kohlwein and G. N. Rechberger (2014). "A versatile ultra-high performance LC-MS method for lipid profiling." Journal of chromatography. B, Analytical technologies in the biomedical and life sciences 951-952(100): 119-128.
- Kyle, J. E., G. Clair, G. Bandyopadhyay, R. S. Misra, E. M. Zink, K. J. Bloodsworth, A. K. Shukla, Y. Du, J. Lillis, J. R. Myers, J. Ashton, T. Bushnell, M. Cochran, G. Deutsch, E. S. Baker, J. P. Carson, T. J. Mariani, Y. Xu, J. A. Whitsett, G. Pryhuber and C. Ansong (2018). "Cell type-resolved human lung lipidome reveals cellular cooperation in lung function." Scientific Reports 8(1): 13455.
- Le, C. H., J. Han and C. H. Borchers (2013). "Dithranol as a matrix for matrix assisted laser desorption/ionization imaging on a fourier transform ion cyclotron

- resonance mass spectrometer." Journal of visualized experiments: JoVE(81): e50733-e50733.
- Lee, C., I. C. Lu, H. C. Hsu, H.-Y. Lin, S.-P. Liang, Y.-T. Lee and C.-K. Ni (2016). "Formation of Metal-Related Ions in Matrix-Assisted Laser Desorption Ionization." Journal of The American Society for Mass Spectrometry 27(9): 1491-1498.
- Leite, J. F., M. R. Hajivandi, T. Diller and R. M. Pope (2004). "Removal of sodium and potassium adducts using a matrix additive during matrix-associated laser desorption/ionization time-of-flight mass spectrometric analysis of peptides." Rapid Communications in Mass Spectrometry 18(23): 2953-2959.
- Leithner, K., A. Triebel, M. Trötz Müller, B. Hinteregger, P. Leko, B. I. Wieser, G. Grasmann, A. L. Bertsch, T. Züllig, E. Stacher, A. Valli, R. Prassl, A. Olschewski, A. L. Harris, H. C. Köfeler, H. Olschewski and A. Hrzenjak (2018). "The glycerol backbone of phospholipids derives from noncarbohydrate precursors in starved lung cancer cells." Proceedings of the National Academy of Sciences 115(24): 6225.
- Lin, J.-T. and A. Arcinas (2008). "Analysis of Regiospecific Triacylglycerols by Electrospray Ionization–Mass Spectrometry³ of Lithiated Adducts." Journal of Agricultural and Food Chemistry 56(13): 4909-4915.
- Menon, D., D. Salloum, E. Bernfeld, E. Gorodetsky, A. Akselrod, M. A. Frias, J. Sudderth, P.-H. Chen, R. DeBerardinis and D. A. Foster (2017). "Lipid Sensing by mTOR via de novo Synthesis of Phosphatidic Acid." Journal of Biological Chemistry.
- Miakotina, O. L., D. M. McCoy, L. Shi, D. C. Look and R. K. Mallampalli (2007). "Human Adenovirus Modulates Surfactant Phospholipid Trafficking." Traffic 8(12): 1765-1777.

- Nakamura, Y. and T. Suda (2015). "Idiopathic Pulmonary Fibrosis: Diagnosis and Clinical Manifestations." Clinical Medicine Insights. Circulatory, Respiratory and Pulmonary Medicine 9(Suppl 1): 163-171.
- Naz, S., J. Kolmert, M. Yang, S. N. Reinke, M. A. Kamleh, S. Snowden, T. Heyder, B. Levanen, D. J. Erle, C. M. Skold, A. M. Wheelock and C. E. Wheelock (2017). "Metabolomics analysis identifies sex-associated metabotypes of oxidative stress and the autotaxin-lysoPA axis in COPD." European Respiratory Journal 49(6).
- Nazari, M., M. T. Bokhart, P. L. Loziuk and D. C. Muddiman (2018). "Quantitative mass spectrometry imaging of glutathione in healthy and cancerous hen ovarian tissue sections by infrared matrix-assisted laser desorption electrospray ionization (IR-MALDESI)." Analyst 143(3): 654-661.
- Nishimura, M., H. Aikawa, M. Hayashi, Y. Mizutani, K. Takenaka, Y. Imamura, N. Chayahara, M. Toyoda, N. Kiyota, T. Mukohara, A. Hamada and H. Minami (2017). "Abstract 2872: Quantitative mass spectrometry imaging of erlotinib in skin rashes of cancer patients receiving erlotinib." Cancer Research 77(13 Supplement): 2872.
- Park, J. S., H. J. Park, Y. S. Park, S. M. Lee, J. J. Yim, C. G. Yoo, S. K. Han and Y. W. Kim (2014). "Clinical significance of mTOR, ZEB1, ROCK1 expression in lung tissues of pulmonary fibrosis patients." BMC Pulmonary Medicine 14: 168.
- Poletti, V., C. Ravaglia, M. Buccioli, P. Tantalocco, S. Piciucchi, A. Dubini, A. Carloni, M. Chilosi and S. Tomassetti (2013). "Idiopathic Pulmonary Fibrosis: Diagnosis and Prognostic Evaluation." Respiration 86(1): 5-12.
- Pöyry, S. and I. Vattulainen (2016). "Role of charged lipids in membrane structures — Insight given by simulations." Biochimica et Biophysica Acta (BBA) - Biomembranes 1858(10): 2322-2333.

- Prentice, B. M., C. W. Chumbley and R. M. Caprioli (2015). "High-speed MALDI MS/MS imaging mass spectrometry using continuous raster sampling." Journal of mass spectrometry: JMS 50(4): 703-710.
- Raghu, G., H. R. Collard, J. J. Egan, F. J. Martinez, J. Behr, K. K. Brown, T. V. Colby, J. F. Cordier, K. R. Flaherty, J. A. Lasky, D. A. Lynch, J. H. Ryu, J. J. Swigris, A. U. Wells, J. Ancochea, D. Bouros, C. Carvalho, U. Costabel, M. Ebina, D. M. Hansell, T. Johkoh, D. S. Kim, T. E. King, Jr., Y. Kondoh, J. Myers, N. L. Muller, A. G. Nicholson, L. Richeldi, M. Selman, R. F. Dudden, B. S. Griss, S. L. Protzko and H. J. Schunemann (2011). "An official ATS/ERS/JRS/ALAT statement: idiopathic pulmonary fibrosis: evidence-based guidelines for diagnosis and management." American Journal of Respiratory Critical Care Medicine 183(6): 788-824.
- Rancoule, C., S. Espenel, J.-C. Trone, J. Langrand-Escure, A. Vallard, A. Rehailla-Blanchard, A. El Meddeb Hamrouni, Y. Xia, J.-B. Guy, M. Ben-Mrad and N. Magné (2017). "Lysophosphatidic acid (LPA) as a pro-fibrotic and pro-oncogenic factor: a pivotal target to improve the radiotherapy therapeutic index." Oncotarget 8(26): 43543-43554.
- Renzoni, E., V. Srihari and P. Sestini (2014). "Pathogenesis of idiopathic pulmonary fibrosis: review of recent findings." F1000Prime Rep 6: 69.
- Rompp, A. and B. Spengler (2013). "Mass spectrometry imaging with high resolution in mass and space." Histochemistry and Cell Biology 139(6): 759-783.
- Rush, M. D. and R. B. van Breemen (2017). "Role of ammonium in the ionization of phosphatidylcholines during electrospray mass spectrometry." Rapid Communications in Mass Spectrometry 31(3): 264-268.
- Schmidt, R., U. Meier, P. Markart, F. Grimminger, H. G. Velcovsky, H. Morr, W. Seeger and A. Günther (2002). "Altered fatty acid composition of lung

- surfactant phospholipids in interstitial lung disease." American Journal of Physiology-Lung Cellular and Molecular Physiology 283(5): L1079-L1085.
- Schulz, S., M. Becker, M. R. Groseclose, S. Schadt and C. Hopf (2019). "Advanced MALDI mass spectrometry imaging in pharmaceutical research and drug development." Current Opinion in Biotechnology 55: 51-59.
- Selman, M., T. E. King and A. Pardo (2001). "Idiopathic pulmonary fibrosis: prevailing and evolving hypotheses about its pathogenesis and implications for therapy." Annals of Internal Medicine 134(2): 136-151.
- Sugiura, Y. and M. Setou (2009). "Selective imaging of positively charged polar and nonpolar lipids by optimizing matrix solution composition." Rapid Communications in Mass Spectrometry 23(20): 3269-3278.
- Sunaga, H., H. Matsui, M. Ueno, T. Maeno, T. Iso, M. R. A. A. Syamsunarno, S. Anjo, T. Matsuzaka, H. Shimano, T. Yokoyama and M. Kurabayashi (2013). "Deranged fatty acid composition causes pulmonary fibrosis in Elovl6-deficient mice." Nature Communications 4: 2563.
- t'Kindt, R., E. D. Telenga, L. Jorge, A. J. M. Van Oosterhout, P. Sandra, N. H. T. Ten Hacken and K. Sandra (2015). "Profiling over 1500 Lipids in Induced Lung Sputum and the Implications in Studying Lung Diseases." Analytical Chemistry 87(9): 4957-4964.
- Tan, Y., D. Jia, Z. Lin, B. Guo, B. He, C. Lu, C. Xiao, Z. Liu, N. Zhao, Z. Bian, G. Zhang, W. Zhang, X. Liu and A. Lu (2016). "Potential Metabolic Biomarkers to Identify Interstitial Lung Abnormalities." International Journal of Molecular Sciences 17(7): 1148.
- Telenga, E. D., R. F. Hoffmann, t. K. Ruben, S. J. Hoonhorst, B. W. Willemse, A. J. van Oosterhout, I. H. Heijink, M. van den Berge, L. Jorge, P. Sandra, D. S. Postma, K. Sandra and N. H. ten Hacken (2014). "Untargeted lipidomic analysis in

- chronic obstructive pulmonary disease. Uncovering sphingolipids." American Journal of Respiratory and Critical Care Medicine 190(2): 155-164.
- Ucal, Y. and A. Ozpinar (2018). "Improved spectra for MALDI MSI of peptides using ammonium phosphate monobasic in MALDI matrix." Journal of Mass Spectrometry 53(8): 635-648.
- Vazquez-de-Lara, L. G., B. Tlatelpa-Romero, Y. Romero, N. Fernández-Tamayo, F. Vazquez-de-Lara, J. M. Justo-Janeiro, M. Garcia-Carrasco, R. de-la-Rosa Paredes, J. G. Cisneros-Lira, C. Mendoza-Milla, F. Moccia and R. Berra-Romani (2018). "Phosphatidylethanolamine Induces an Antifibrotic Phenotype in Normal Human Lung Fibroblasts and Ameliorates Bleomycin-Induced Lung Fibrosis in Mice." International journal of molecular sciences 19(9): 2758.
- Walch, A., S. Rauser, S.-O. Deininger and H. Höfler (2008). "MALDI imaging mass spectrometry for direct tissue analysis: a new frontier for molecular histology." Histochemistry and Cell Biology 130(3): 421-434.
- Wang, Z., Y. Cai, Y. Wang, X. Zhou, Y. Zhang and H. Lu (2017). "Improved MALDI imaging MS analysis of phospholipids using graphene oxide as new matrix." Scientific Reports 7: 44466.
- Yin, G., Y. Wang, X. M. Cen, Y. Yang, M. Yang and Q. B. Xie (2017). "Identification of Palmitoleic Acid Controlled by mTOR Signaling as a Biomarker of Polymyositis." Journal of Immunology Research 2017: 3262384.
- Zhu, X. and I. A. Papayannopoulos (2003). "Improvement in the detection of low concentration protein digests on a MALDI TOF/TOF workstation by reducing alpha-cyano-4-hydroxycinnamic acid adduct ions." Journal of biomolecular techniques: JBT 14(4): 298-307.

6.1 General Discussion

This PhD project has demonstrated the effectiveness of using UPLC-QTOF-MS and MALDI-MSI to deliver improved resolution, specificity and dimensionality for the lipid profiling of plasma and tissue samples of chronic lung diseases. Chapter 1, entitled “Metabolomics in chronic lung diseases: a practical review for clinicians”, presented a comprehensive examination of experimental strategies and its utility in improving the understanding of biochemical changes associated with diseases such as COPD, asthma and IPF. This chapter provided a critical review of recent published outcomes, highlighting the major metabolic pathways associated with pathogenesis as well as identifying potential biomarkers of interest that can aid in the diagnosis, prognosis and, ultimately, treatment of disease.

Chapter 2 is focused on the application of untargeted metabolomics to provide global, unbiased profiling of COPD and IPF. A total of 65 clinical plasma samples were assessed using UPLC-QTOF-MS, of which 21 were obtained from COPD patients, 24 from IPF diagnosed patients and 20 from healthy control subjects. The aim of this study was to use metabolomics to further the understanding of changes that underpinned both chronic lung conditions. The use of multivariate statistics including PCA and OPLS-DA showed distinct differences in the metabolomic profiles of plasma from COPD and IPF patients compared to healthy individuals. This study identified unique lipid mediators such as linoleic, palmitoleic and oleic acids which suggested a dysregulated lipid metabolism indicative of severe lung inflammation and progression of fibrosis (Sunaga *et al.*, 2013; Daabis *et al.*, 2016). This study also revealed significant down-regulation of arachidonoyl tyrosine, bilirubin, dihydrotestosterone and lysoPC in both COPD and

IPF samples that implied increased oxidative stress within the lung (Brown *et al.*, 2017; Zhao *et al.*, 2017).

Chapter 3 involved the application of a data independent acquisition method, termed SONAR, to complement the UPLC-QTOF-MS resolution of lipid species between “stable versus progressor” IPF patient groups. The availability of two diseased groups of IPF were important as it allowed for the characterisation of global lipid changes associated with disease progression. SONAR DIA technique facilitated improved lipid identification of a number of spiked deuterium-labelled lipid standards that were representative of lipids found in human plasma. The isolation of the molecular ions prior to fragmentation allowed fragment ions to be readily assigned to its relevant precursors for specific lipid identification using LIPID MAPS for structural elucidation and confirmation. In addition, the lipid profiles from 30 patients diagnosed with progressive IPF showed changes in lipid plasma composition when compared to the 30 stable subjects. A number of triglycerides and glycerolipids that were unique lipid markers of IPF progression were identified. These lipids were found to be intermediates of key signalling pathways associated with lung inflammation and fibrosis (Yui *et al.*, 2015; Yan *et al.*, 2017; Kulkarni *et al.*, 2018) and hold considerable promise as biomarkers for IPF. While the current sensitivity of SONAR was lower than conventional TOF-MS acquisition, the generation of quantitative MS/MS data with reduced background interferences were highly advantageous. In addition, SONAR-acquired data were significantly smaller in size compared to the DIA methods such as MS^E and were comparable in performance in terms of identification precision and quantitation accuracy (Meyer and Schilling, 2017).

In Chapter 4, a novel and cost-effective preparative method for MALDI referred to as “freeze-spot” was demonstrated. The deposition of matrix in MALDI-MSI was important to enable simultaneous extraction of metabolites from tissue sections as well as maintain the spatial dimensionality of endogenous metabolites (Fujimura and Miura, 2014; Gemperline and Li, 2014). The study used wheat seed sections to demonstrate extraction efficiency and reliability, whilst maintaining the spatial resolution of the acquired MALDI-MSI images. This freeze-spot approach utilized a chilled stage which permitted rapid freezing of matrix followed by a lyophilisation step to prevent hot-spot formation and further improve image quality. The addition of sodium and potassium acetate to the matrix prior to freeze-spot application resulted in improved spatial measurement of complex sugars of 12 carbons or greater, which readily form sodium and potassium adducts. Both sucrose (m/z 381) and 1-kestose (m/z 543) were identified and well-resolved along with their region-specific spatial distributions, which was consistent with the fructan metabolism of barley (Peukert *et al.*, 2014). These analyses demonstrated that the freeze-spot approach using DHB matrix prepared with inorganic salts resulted in increased spatial resolving power of small molecules such as oligosaccharides in seed sections.

In the final study, 10 healthy and 10 fibrotic tissues were profiled using MALDI-MSI previously optimised with the freeze-spot methodology. The MSI technique developed was further enriched by promoting potassium adduct formation to improve spatial resolution of lipid species such as triglycerides, sphingolipids and glycerophospholipids. The results of this study showed a number of interesting changes in lipid composition of IPF tissues compared to healthy controls. MALDI-MSI of tissues were achieved using DHB matrix spiked with sodium and potassium acetate salts for the visualisation of a number of lipids of interest. The method showed differences in relative intensities and

abundances of PC, PE and LysoPC between diseases and healthy control tissue biopsies. Significant differences were also observed in lipid species involved in LysoPA and mTOR signalling pathways, as well as surfactant PCs. Of note, both SONAR DIA acquisition (Chapter 3) and MSI analysis (Chapter 5) identified similar classes of lipids (TG, PE, LysoPC and PC) that were potential determinants in the pathophysiology of the IPF lipidome.

6.2 Current challenges

As an emergent sub-discipline of metabolomics, lipidomic profiling is generating considerable interest due to the ubiquity of lipids as functional building blocks and its roles in health and disease. Nonetheless, a number of technical challenges remain.

In particular, current lipidomic pipelines are unable to resolve more than fifty percent of lipid species that constitute the lipidome (Lydic and Goo, 2018). The existing analytical limits of detection mean that the analysis of some classes of lipids such as eicosanoids require specialised analysis using targeted methodologies (Sorgi *et al.*, 2018). Additional derivatisation or hydrolysis may also be required for total lipids in some cases (De Paola *et al.*, 2017; McDonald *et al.*, 2012). Moreover, the large number of isobaric species may require bespoke chromatographic separation unique to the lipids of interest. Some of these limitations can be overcome by the improvements in MS platforms and modalities which continue to improve in sensitivity, specificity and resolving power. Next-generation MS instrumentation with more effective chromatography and sample ionisation, such as nano-ESI or gas-phase separation techniques such as ion-mobility, show promise (Keating and Glish, 2018). Indeed, the application of ion-mobility MS has the potential to enhance the separation of lipids and

improve isomer resolution due to its ability to exact cross-collisional information (Hinz *et al.*, 2017).

6.3 Future Work

The work presented herein highlighted the importance of lipids as potential indicators of disease and presents a pipeline to assess compositional changes of lipids in a number of disease states. Future work will immediately focus on larger sample cohorts to increase statistical significance and validation of lipids identified in this study, as well as evaluate their utility as clinical diagnostics using targeted methodologies such as tandem LC-MS or enzyme-linked immunosorbent assay (ELISA).

An important aspect of future work will be the correlation of clinical metadata (such as age, sex, disease state, smoking history and lung function tests) against the lipidomic profile of the sampled individual or groups. Observational data, when used to complement the findings of metabolomics analyses, can offer additional means to phenotype disease (Trivedi *et al.*, 2017). This is especially evident where complementary metabolite and clinical metadata can contribute to the effectiveness of subsequent lines of inquiries such as chemometrics (Trivedi *et al.*, 2017).

Additional lipidomic profiling of other chronic lung diseases such as asthma and sarcoidosis will also be interesting to determine if the biochemical changes encountered in this work prevails across a larger spectrum of chronic lung conditions. Future work can also be performed to measure lipid kinetic and flux using stable isotope-labelled standards in diseased *versus* healthy samples. In-depth fluxomics analyses is expected to

provide additional insights into the rate of lipid metabolism at the molecular level and can facilitate a deeper understanding of their roles in IPF.

Future work will also be focused on the development of new quantitative approaches to MSI. This will involve the generation of calibration curves by spiking of isotopically-labelled internal standards directly onto the tissue section followed by MALDI-MSI acquisition. Gentler, ambient ionisation techniques including desorption electrospray ionisation (DESI) and atmospheric pressure (AP)-MALDI can also be evaluated directly on untreated histological samples and has the potential to provide *in situ* analysis in clinical settings.

6.4 Conclusion

The application of untargeted metabolomics and imaging mass spectrometry in combination with multivariate statistical approaches were successful at revealing unique markers which can be used to correlate metabolic mechanisms and pathways fundamental to disease development. The application of a unique DIA mode such as SONAR can potentially enhance the specificity of data acquired using UPLC-QTOF-MS. Finally, the use of the freeze-spot approach optimised with potassium adduct formation for MSI acquisition provides a new avenue to improve the visualisation of lipid distribution in IPF tissues and may provide users with additional metabolite information that can complement existing histopathological assessments, and aid in the diagnostic of the disease.

6.5 References

- Brown, K. E., D. D. Sin, H. Voelker, J. E. Connett, D. E. Niewoehner, K. M. Kunisaki and C. C. R. Network (2017). "Serum bilirubin and the risk of chronic obstructive pulmonary disease exacerbations." Respiratory research 18(1): 179-179.
- Daabis, R. G., R. N. Abdel Rehem, M. M. Hassan and G. I. Khalil (2016). "Hypogonadism in patients with chronic obstructive pulmonary disease: relationship with airflow limitation, muscle weakness and systemic inflammation." Alexandria Journal of Medicine 52(1): 27-33.
- De Paola, E. L., G. Montevecchi, F. Masino, A. Antonelli and D. P. Lo Fiego (2017). "Single step extraction and derivatization of intramuscular lipids for fatty acid Ultra Fast GC analysis: application on pig thigh." Journal of food science and technology 54(3): 601-610.
- Fujimura, Y. and D. Miura (2014). "MALDI Mass Spectrometry Imaging for Visualizing In Situ Metabolism of Endogenous Metabolites and Dietary Phytochemicals." Metabolites 4(2): 319-346.
- Gemperline, E. and L. Li (2014). "MALDI-mass spectrometric imaging for the investigation of metabolites in *Medicago truncatula* root nodules." Journal of visualized experiments: JoVE(85): 51434.
- Hinz, C., S. Liggi and J. L. Griffin (2018). "The potential of Ion Mobility Mass Spectrometry for high-throughput and high-resolution lipidomics." Current Opinion in Chemical Biology 42: 42-50.
- Keating, J. E. and G. L. Glish (2018). "Dual Emitter Nano-Electrospray Ionization Coupled to Differential Ion Mobility Spectrometry-Mass Spectrometry for Shotgun Lipidomics." Analytical Chemistry 90(15): 9117-9124.

- Kulkarni, Y. M., S. Dutta, A. K. V. Iyer, C. A. Wright, V. Ramesh, V. Kaushik, O. J. Semmes and N. Azad (2018). "A Lipidomics Approach to Identifying Key Lipid Species Involved in VEGF-Inhibitor Mediated Attenuation of Bleomycin-Induced Pulmonary Fibrosis." Proteomics Clinical Applications 12(3): e1700086.
- Lydic, T. A. and Y.-H. Goo (2018). "Lipidomics unveils the complexity of the lipidome in metabolic diseases." Clinical and translational medicine 7(1): 4-4.
- McDonald, J. G., D. D. Smith, A. R. Stiles and D. W. Russell (2012). "A comprehensive method for extraction and quantitative analysis of sterols and secosteroids from human plasma." Journal of lipid research 53(7): 1399-1409.
- Meyer, J. G. and B. Schilling (2017). "Clinical applications of quantitative proteomics using targeted and untargeted data-independent acquisition techniques." Expert review of proteomics 14(5): 419-429.
- Peukert, M., J. Thiel, D. Peshev, W. Weschke, W. Van den Ende, H.-P. Mock and A. Matros (2014). "Spatio-Temporal Dynamics of Fructan Metabolism in Developing Barley Grains." The Plant Cell 26(9): 3728.
- Sorgi, C. A., A. P. F. Peti, T. Petta, A. F. G. Meirelles, C. Fontanari, L. A. B. d. Moraes and L. H. Faccioli (2018). "Comprehensive high-resolution multiple-reaction monitoring mass spectrometry for targeted eicosanoid assays." Scientific Data 5: 180167.
- Sunaga, H., H. Matsui, M. Ueno, T. Maeno, T. Iso, M. R. A. A. Syamsunarno, S. Anjo, T. Matsuzaka, H. Shimano, T. Yokoyama and M. Kurabayashi (2013). "Deranged fatty acid composition causes pulmonary fibrosis in Elov16-deficient mice." Nature Communications 4: 2563.
- Trivedi, D. K., K. A. Hollywood and R. Goodacre (2017). "Metabolomics for the masses: The future of metabolomics in a personalized world." New horizons in translational medicine 3(6): 294-305.

- Yan, F., Z. Wen, R. Wang, W. Luo, Y. Du, W. Wang and X. Chen (2017). "Identification of the lipid biomarkers from plasma in idiopathic pulmonary fibrosis by Lipidomics." BMC Pulmonary Medicine 17: 174.
- Yui, K., G. Imataka, H. Nakamura, N. Ohara and Y. Naito (2015). "Eicosanoids Derived From Arachidonic Acid and Their Family Prostaglandins and Cyclooxygenase in Psychiatric Disorders." Current neuropharmacology 13(6): 776-785.
- Zhao, Y. D., L. Yin, S. Archer, C. Lu, G. Zhao, Y. Yao, L. Wu, M. Hsin, T. K. Waddell, S. Keshavjee, J. Granton and M. de Perrot (2017). "Metabolic heterogeneity of idiopathic pulmonary fibrosis: a metabolomic study." BMJ Open Respiratory Research 4(1).

... and looks like I've hit my lipid.